L_2-Gain Based Control of a Flexible Parameter-Varying Robot Link

Jochen M. Rieber

(cand. kyb.)

Diplomarbeit

Prof. D. G. Taylor, PhD, Georgia Institute of Technology
Prof. Dr.-Ing. F. Allgöwer, Universität Stuttgart

Institut für Systemtheorie Technischer Prozesse
Universität Stuttgart

August 2001

Acknowledgements

I would like to thank Professor David Taylor for being an outstanding advisor during my research. I am very grateful for his support, his patience and his most valuable suggestions during many discussions. His deep knowledge and overview on control theory and applications enriched my education at Georgia Tech significantly.

My special gratitude goes to Professor Laurence Jacobs. He gave very valuable suggestions for my research. Moreover, he enabled my stay at Georgia Tech in part, and contributed to the great experience of living in the U.S.

I would also like to thank Professor Wayne Book, who supported this work with very valuable suggestions.

Furthermore, I would like to express my gratitude to Professor Lothar Gaul from University of Stuttgart for giving me the opportunity to study at Georgia Tech, and also to the DAAD (German Academic Exchange Service) for providing generous financial support.

I am moreover grateful to Professor Frank Allgöwer, who acknowledged the results of this research on behalf of University of Stuttgart.

Siemens AG made the experimental results possible by providing a prototype gantry robot and technical assistance.

Finally, I am deeply grateful to my family for their continuing support, encouragement, and love.

Contents

List of Tables

List of Figures

Summary

This thesis addresses planar motion control of a two-axis gantry robot. The considered positioning mechanism consists of a rigid body, called the head, sliding on a beam with linear elastic flexibility, and a compliant belt-drive transmission system. Due to movement of the head along the beam, a varying mass distribution is given. Since the flexible beam exhibits bending displacement, structural vibrations are excited by rapid beam motion. The two-axis mechanism can be modeled as a linear parameter-varying system, where the head position represents the parameter. Main challenges for motion control are nonlinearly varying dynamics, excitation of bending vibrations, friction disturbances, and transmission resonance.

L_2-gain based control methodology is applied, based on a flexible beam model. A linear time-invariant H_∞ controller as well as three different linear parameter-varying H_∞ controllers, scheduled with respect to head position, are designed and implemented on a prototype gantry robot. These controllers are divided into an inner loop for compensation of transmission compliance and an outer loop for motion control. To speed up online computations of the control algorithm, a modification of existing procedures is proposed. Positioning experiments are conducted, with full utilization of available motor power, in order to verify applicability and performance of the controllers. Steady-state errors of less than one micrometer are achieved, together with suppression of bending vibrations and attenuation of friction disturbances. An investigation into the influence of reference command shapes on controller performance and vibration excitation is included. Furthermore it is shown how positioning times may be improved by modifications in beam design.

Zusammenfassung

Präzisions-Fertigungsprozesse wie die Bestückung von Leiterplatten werden oft mit Hilfe von kartesischen Mehrachs-Mechanismen, sogenannten "Gantry Robots", ausgeführt. Solche industriellen Prozesse erfordern eine äußerst genaue Positionierung der Bestückungseinheit mittels Hochgeschwindigkeits-Bewegungen, um hohe Effizienz und Zuverlässigkeit zu erreichen. Deshalb ist das Regelungssystem für die Bewegung der mechanischen Maschinenteile eine Schlüsselkomponente eines Bestückungsroboters.

Eine weit verbreitete Art von Mehrachs-Mechanismen erlaubt die Positionierung in der horizontalen Ebene und besteht aus einem elastischen Ausleger oder Balken, der über zwei Schienen gleitet (Bewegung in y-Richtung), und aus einem Bestückungskopf, der sich entlang des Auslegers bewegt (Bewegung in x-Richtung). Da der Ausleger eine begrenzte Steifigkeit besitzt, ruft eine schnelle Positionierung möglicherweise Strukturschwingungen im elastischen Balken hervor, was zu hohen Positionierzeiten oder sogar Instabilität führen kann. Die Position des Bestückungskopfes bezüglich der x-Koordinate bestimmt die Massenverteilung der Anordnung, weshalb das dynamische Verhalten in y-Richtung stark von der aktuellen Lage dieses Kopfes beeinflusst wird. Im Gegensatz dazu kann der Kopf selbst als starrer Körper betrachtet werden, dessen Bewegung entlang des Auslegers von zeitgleicher Bewegung in y-Richtung entkoppelt ist. Deshalb stellt die Positionierung des Auslegers entlang der y-Achse größere Herausforderungen an ein Regelungssytem und muss als Hauptproblem angesehen werden.

Die sogenannte ± 10 μm-Einschwingzeit wird als ein Maß für die Güte der Bewegungsregelung herangezogen. Dies ist die Zeit, innerhalb derer der Bestückungskopf von einem Startpunkt bis auf ± 10 μm an die gewünschte Position bezüglich x- und y-Koordinaten herangeführt wird, ohne diesen Zielkorridor wieder zu verlassen. Diese Grenze wurde ausgewählt, da das eigentliche Platzieren von Bauteilen durch den schließlichen Eintritt in besagten Korridor ausgelöst wird. Es sei betont, dass die y-Koordinate der Kopfposition nicht gemessen werden kann, sondern nur deren x-Koordinate entlang des Auslegers. Positionsmessungen an beiden Enden des Balkens sind jedoch verfügbar. Es ist daher von großer Wichtigkeit, dass die Einschwingzeiten an beiden Enden des Auslegers zur Überprüfung der Regelgüte herangezogen werden.

Um eine erfolgreiche Unterdrückung von Strukturschwingungen zu gewährleisten, sollten diese beiden Werte nahe beieinander liegen.

Die soeben beschriebene Klasse von Zwei-Achs-Robotern kann mit für Regelungszwecke ausreichender Genauigkeit durch ein System mit verteilten Parametern modelliert werden, das eine nichtlineare Abhängigkeit von der Kopf-Position aufweist (Yang [45], Yang et al. [49]). Mit der Anwendung von Diskretisierungsmethoden, wie Bestimmung der Moden, kann dieses Modell in ein lineares gewöhnliches Differential-Gleichungs-System mit veränderlichen Parametern (engl. linear parameter-varying (LPV) system) überführt werden. Darin ist die Kopf-Position, gemessen in Echtzeit, der veränderliche Parameter.

Während der letzten 20 Jahre hat sich die sogenannte H_∞-Regelungstheorie entwickelt und als ein Hauptgegenstand der regelungstechnischen Forschung etabliert. Die Beschränkung des sogenannten L_2-Gain oder der H_∞-Norm der Übertragungsfunktion des geschlossenen Regelkreises zwischen exogenen Eingängen (z.B. Führungsgrößen, Störungen) und exogenen Ausgängen (z.B. Regelfehler, Stellgrößen, Zustandsvariablen) ist wesentlicher Bestandteil dieser Methodik. Für linear zeit-invariante Systeme (engl. linear time-invariant (LTI) systems) sind vor allem Ansätze interessant, die auf der Lösung von linearen Matrizenungleichungen (engl. linear matrix inequalities (LMIs)) beruhen, siehe Gahinet und Apkarian [22], Iwasaki und Skelton [28], Scherer et al. [40]. Diese LMIs können durch flexible und effiziente Programme für konvexe Optimierung numerisch gelöst werden, siehe Nesterov und Nemirovski [33], Boyd et al. [11], Gahinet et al. [24].

Neue Forschungsergebnisse auf dem Gebiet der H_∞-Regelungstheorie für LPV Systeme stellen verschiedene Ansätze für den Reglerentwurf bereit. Das Ziel dieser Methodik ist der systematische Entwurf von sogenannten “gain-scheduled” (GS) LPV H_∞-Reglern. Diese Regler sind für entsprechende Anwendungsfälle weniger konservativ als robuste LTI Regler, da sie Veränderungen des zu regelnden Systems direkt einbeziehen. Im Rahmen von konvexer Optimierung und LMIs wurden Ansätze mittels konstanter Lyapunov-Funktionen (Becker und Packard [8], Helmersson [26], Apkarian und Gahinet [3]) und mittels parameter-abhängiger Lyapunov-Funktionen (Apkarian und Adams [2], Apkarian und Tuan [5], Gahinet et al. [23], Scherer [39]) entwickelt.

Bisherige Forschung mit Blick auf die oben beschriebene Klasse von Zwei-Achs-Robotern umfasste die Modellbildung des Zwei-Achs-Mechansimus und weiterer Komponenten wie Zahnriemenantrieb und Motoren (Yang [45], Yang et al. [49]). Es wurde eine Regelkreisstruktur zur ebenen Bewegungsregelung des Bestückungskopfes vorgeschlagen. Diese besteht aus einem inneren Kreis zur Kompensierung von Resonanzeffekten in den Antriebselementen sowie aus einem äußeren Kreis zur Positionsregelung. Unter Zuhilfenahme dieser Struktur wurden Regler, basierend auf Starrkörper-Annahmen (Yang and Taylor [47]) sowie auf linear elastischen Annahmen für den Ausleger (Yang und Taylor [46], [48]), entwickelt. Im zweiten Fall wurden LTI H_∞- und GS LPV H_∞-Regler untersucht. Die Regelgüte im geschlossenen Kreis wurde durch Experimente auf einem Roboter-Prototyp überprüft, wobei "Bang-Bang"-Referenzsignale für die gewünschte Beschleunigung vorgegeben wurden. Es wurde gezeigt, dass H_∞-Methoden, basierend auf einem elastischen Balkenmodell, klassische Methoden wie PID-Regler übertreffen.

Die Ergebnisse von Yang [45] lassen einige Fragen offen. Zuerst erstaunt der fehlende Erfolg bei der Entwicklung eines einzelnen LTI H_∞-Reglers, der sowohl Stabilität als auch eine hohe Regelgüte über den Bereich aller betrachteten Kopfpositionen erzielt. Außerdem sollte das Design von GS LPV H_∞-Reglern nochmals untersucht werden. Durch die Verwendung von variablen Lyapunov-Funktionen, durch Einbeziehung der Maximalwerte für Parameter-Variationsraten sowie durch volle Berücksichtigung der nichtlinearen Parameterabhängigkeit des Balken-Modells kann möglicherweise die erreichbare Regelgüte gesteigert und der Konservatismus gesenkt werden. Drittens wurde der Einfluss von verschiedenen Referenzsignalen nicht diskutiert, im Besonderen das Verhalten unter weniger aggressiven Führgrößen. Schließlich ist das Erreichen einer hohen Regelgüte nur für Kopfbeschleunigungen bis zu 15 m/s^2 eine wesentlicher Nachteil in Yangs Dissertation. Es kann damit der Fall eintreten, dass der Bestückungskopf seine Zielposition hinsichtlich der x-Achse noch nicht erreicht hat, obwohl dies hinsichtlich der y-Achse schon eingetreten ist. Damit wäre die erreichte Regelgüte für Positionierung in y-Richtung von untergeordneter Bedeutung.

In dieser Arbeit werden L_2-Gain basierte Methoden zur Bewegungsregelung eines elastischen Roboterarms mit bewegtem Bestückungskopf eingesetzt. Dabei werden sowohl ein robuster LTI H_∞-Regler (Gahinet und Apkarian [22]) als auch eine GS LPV H_∞-Methode mit variabler Lyapunov-Funktion (Apkarian und Adams [2]) betrachtet. Die Verfügbarkeit von direkten Messungen der Kopfposition sowie Vorwissen über die maximalen Kopfgeschwindigkeiten werden im zweiten Fall in den Prozess der Regler-Entwicklung mit einbezogen. Weiterhin wird die Benutzung von verschiedenen Feedback-Signalen diskutiert. Um die Online-Berechnungen des Regelungsalgorithmus zu vereinfachen und zu beschleunigen, wird eine Modifikation des bisher verfügbaren Algorithmus präsentiert.

Der Reglerentwurf basiert auf einem elastischen Balkenmodell. Der Entwurf bedient sich der Kaskadenstruktur aus Yang [45]. Das übergeordnete Ziel ist die Bewegung des Bestückungskopfes zu einer Zielposition mit Mikrometer-Genauigkeit in minimaler Zeit. Dies soll sowohl für lange als auch für kurze Auslegerbewegungen realisiert werden. Die besonderen Herausforderungen werden durch die nichtlinear veränderliche Dynamik des Balkens, durch Erregung von Strukturschwingungen, durch Resonanz in den Antriebselementen sowie durch mechanische Reibung gestellt.

Der Reglerentwurf benutzt "Loop shaping"-Methoden, zusammen mit der Unterdrückung von Strukturschwingungen und Störungen. Über den Bereich typischer Kopfpositionen des parameterabhängigen Balkenmodells wird ein Gitterverfahren angewandt, um die volle Bandbreite der veränderlichen Dynamik zu erfassen. Der Reglerentwurf garantiert interne Stabilität des geschlossenen Regelkreises für beliebige

Kopfbewegungen innerhalb der definierten Grenzen, und setzt eine obere Grenze für den L_2-Gain von den Eingangssignalen zum Regelfehler und zur Schwingungserregung im geschlossenen Kreis.

Der Einfluss von Kopf- und Ausleger-Führungsgrößen verschiedener Form auf die Erregung von Strukturschwingungen wird angesprochen. Aus praktischen Überlegungen ist es wünschenswert, möglichst glatte, wenig aggressive Referenzsignale vorzugeben, um solche Schwingungen zu vermeiden. Von einem akademischen Forschungsstandpunkt aus gesehen kann gerade die Vorgabe von aggressiven Trajektorien Strukturschwingungen erregen und wertvolle Informationen über Dämpfungsfähigkeiten der Regler geben.

Experimente auf einem Roboter-Prototyp zeigen die erreichbare Güte und Leistung des geschlossenen Regelkreises für verschiedene Auslegerbewegungen mit feststehendem oder bewegtem Bestückungskopf. Ausleger- und Kopfbewegungen werden mit Beschleunigungen bis 32 m/s^2 und Geschwindigkeiten bis 2.5 m/s vorgegeben. Bleibende Regelabweichungen von weniger als 1 μm sind erreichbar. Strukturschwingungen des Auslegers und Störungen durch Reibung werden größtenteils unterdrückt. Eine Auslegerbewegung von 0.5 m mit zeitgleicher Kopfbewegung wird vom entwickelten LTI H_∞-Regler in 372 ms bewältigt, während der GS H_∞-Regler 366 ms benötigt. Wird ein aggressiveres Bang-Bang Beschleunigungsprofil vorgegeben, kann der GS H_∞-Regler seine Leistung halten, während der LTI H_∞-Regler deutlich länger für die Positionierung benötigt. Bei der Betrachtung von kurzen Auslegerbewegungen zeigt sich, dass weniger aggressive Referenztrajektorien vorzuziehen sind. Hier zeigen LTI H_∞- und GS H_∞-Regler etwa gleiche Leistung.

Um die Vorzüge von integriertem Design des Auslegers und des Regelsystems zu zeigen, wird eine Simulationsstudie ausgeführt. Sie untersucht, wie gesteigerte Positioniergeschwindigkeit und reduzierte Balkenmasse gegeneinander abgewägt werden können. Durch Reduzierung der Balkenmasse kann der Ausleger bei gleichbleibender Motorleistung theoretisch schneller positioniert werden. Bei gleichzeitiger Reduzierung der Balken-Steifigkeit werden aber stärkere Strukturschwingungen erregt, die durch das Regelsystem gedämpft werden müssen. Es wird gezeigt, dass die Positionierung des Auslegers von einem neuen Balken-Design profitieren kann, wenn angemessene Regelungstechnik angewandt wird.

Die Arbeit ist wie folgt organisiert. Kapital 2 fasst die Modellbildung des Zwei-Achs-Roboters zusammen. Kapitel 3 präsentiert einige dem Reglerentwurf vorausgehende oder untergeordnete Punkte wie die Reglerstruktur, die Kompensierung der Antriebsdynamik, die Wahl der Regler-Entwurfsmodelle, Diskretisierung von Reglern, Geschwindigkeitsschätzung, und die experimentellen Rahmenbedingungen. Kapitel 4 beinhaltet die Hauptergebnisse dieser Arbeit. Verschiedene Ansätze zum Reglerentwurf und ihre Anwendung auf den Zwei-Achs-Roboter werden erläutert. Die Verwendung verschiedener Sensor-Signale als Feedback wird verglichen, und eine Modifikation der verwendeten Regleralgorithmen wird vorgestellt. Experimentelle Resultate zeigen die erreichte Regelgüte auf. Kapitel 5 diskutiert den Einfluss von Modifikationen des Ausleger-Designs auf die Positionierzeiten als einen zweiten wichtigen Beitrag dieser Arbeit. Schliesslich gibt Kapitel 6 Schlussfolgerungen aus dieser Arbeit und Anregungen zu weitergehender Forschung.

Chapter 1

Introduction

High-precision manufacturing tasks such as circuit-board assembly are often carried out with the use of gantry robots. Industry applications of this type require very accurate positioning of the part placement device via high-speed movements in order to achieve high efficiency and reliability of the process. Therefore, a key component of such a gantry robot is the motion control system, which causes the motor and transmission system to generate appropriate forces for movement of the mechanical parts.

A widely used design for gantry robots allows motion in the horizontal plane, in particular a flexible beam moving along two rails (y-axis motion), and a head for placement of parts sliding along the beam (x-axis motion). Due to the finite beam stiffness, rapid positioning may excite structural vibrations in the beam, thus leading to unacceptably large positioning times or even instability. Since the x-position of the placement head determines the mass distribution of the configuration, the dynamical behavior of the beam-head combination along the y-axis is significantly influenced by the (x-axis) head position. In contrast, the placement head can be viewed as a rigid body, whose motion along the beam is not influenced by a simultaneous y-axis beam motion. Therefore the beam positioning part of the problem poses greater challenges to control than head positioning and has to be viewed as the main focus of control system design. Moreover, mechanical friction has to be considered as a major disturbance to beam and head movements.

A measure of performance for motion control is given by the so-called ± 10 μm settling time. This is the time interval after which the head has been moved from some starting point into a corridor within ± 10 μm of the desired final location with respect to both axes, without leaving this corridor again. This limit is chosen since the actual part placement is triggered by finally entering the described corridor. It has to be emphasized that the y-coordinate of head position cannot be measured, but only its x-coordinate along the beam. However, y-coordinate measurements at both ends of the beam are available. Therefore, it is of major importance that settling times of both beam ends are observed for evaluation of controller performance. These two values should be close to each other for succesful vibration suppression.

The type of two-axis robot described above is accurately modeled as a distributed parameter system with nonlinear dependence on head position (Yang [45], Yang et al. [49]). Applying discretization methods like mode shape determination, this model can be transformed into a linear parameter-varying (LPV) system with lumped parameters, i.e. a finite dimensional linear system of parameter-varying ordinary differential equations (ODEs). Therein the head position, which can be measured in real-time, is the time-varying parameter.

During the last 20 years, the so-called H_∞ control theory has evolved and established itself as a main focus in control research. A general framework for different problem classes has been developed. The main idea is to bound the so-called L_2-gain or H_∞-norm of the closed-loop transfer function between exogenous inputs (e.g. reference commands, disturbances) and exogenous outputs (e.g. control error, control energy, state values) by applying feedback and possibly feedforward compensation. For linear time-invariant (LTI) systems, Riccati equation based methods (Doyle et al. [17], Zhou and Khargonekar [51]) or linear matrix inequality (LMI) based methods (Gahinet and Apkarian [22], Iwasaki and Skelton [28], Scherer et al. [40]) can be applied for controller design. LMI-based approaches are very attractive because of the existence of flexible and efficient numerical solvers for convex optimization, see Nesterov and Nemirovski [33], Boyd et al. [11], Gahinet et al. [24]. Well-known techniques such as loop shaping and pole placement can be incorporated into controller design in modified form (Doyle et al. [16], Zhou et al. [50], Chilali and Gahinet [14]).

Recent research on gain-scheduled (GS) H_∞ control theory for LPV systems provides different approaches for control design of low conservatism. Main focus is the systematic design of a GS controller, using convex optimization in an LMI framework. Work based on constant Lyapunov functions includes Becker and Packard [8], Helmersson [26], Apkarian and Gahinet [3], Apkarian et al. [4], Dussy and El Ghaoui [18], Scorletti and El Ghaoui [41], Kajiwara et al. [29]. A possibly less conservative design can be obtained by using parameter-varying Lyapunov functions, as well as general nonlinear dependence on parameters and bounds on parameter variation rates, as in Apkarian and Adams [2], Apkarian and Tuan [5], Gahinet et al. [23], Wu et al. [44], Scherer [39], Feron et al. [19]. Also extensions to descriptor systems have been considered (Rehm and Allgöwer [35]).

Previous work on the described type of gantry robot included extensive modeling of the two-axis mechanism as well as of additional components like belt-drive transmission and motors (Yang [45], Yang et al. [49]). Furthermore, a two-loop control structure, consisting of an inner-loop compensation for actuator compliance and an outer-loop position controller, was proposed for planar motion control of the placement head. Using this structure, controllers based on a rigid beam assumption (Yang and Taylor [47]), and on a linear elastic beam assumption (Yang and Taylor [46], [48]), were developed. In the latter case, H_∞ theory based LTI and GS LPV controllers were designed. Closed-loop performance was validated in experiments on a prototype robot, using bang-bang motion trajectories. It was shown that H_∞ techniques based on a flexible beam model outperform classical approaches like PID control.

Some open questions remain from the results achieved by Yang [45]. Among them is the lack of success in designing a single LTI H_∞ controller achieving stability and good performance over the whole range of considered head positions. As a second point, the design of a GS LPV controller should be revisited. In particular, increased performance and less conservatism may be achieved by establishing a parameter-varying Lyapunov function instead of a constant one, by incorporating parameter variation rate limits, and by accounting for the nonlinear parameter dependence of the beam model instead of having piecewise linear or polytopic approximations. Furthermore, the influence of the reference command shape was not discussed, especially not the behavior for other than bang-bang acceleration references. Finally, a main drawback of Yang's results was the achievement of decent y-positioning performance only for head accelerations up to 15 m/s^2 in x-direction. This could mean that the head has not reached the ± 10 μm corridor with respect to x-direction, even though it has with respect to y-direction, in which case the y-axis performance is of subordinate importance.

In this thesis, L_2-gain based control design methods are applied to motion control of a flexible gantry robot beam with moving head. In particular, a single robust LTI H_∞ controller is considered (Gahinet and Apkarian [22]) as well as a GS H_∞ control technique with parameter-dependent Lyapunov function (Apkarian and Adams [2]). Availability of direct measurements of head position along the beam and knowledge about head velocity limits are incorporated in the control design process in the second case. Also the use of different feedback signals is discussed. In order to simplify and speed up online computations, a modification of the applied control design method is presented.

The control system design is based on a flexible beam model. The design uses the two-loop control structure proposed by Yang [45]. The overall control objective is movement of the placement head to a target position with micrometer accuracy in minimal time. This should be achieved for large beam movements of about 0.5 meters as well as for small movements of several millimeters. The main design challenges are nonlinearly varying dynamics due to head movement, excitation of bending vibrations due to beam flexibility, transmission resonance, and mechanical friction disturbances. The controller uses loop shaping objectives, completed with attenuation of structural vibrations and with disturbance rejection. A gridding procedure is applied over the range of typical head positions of the parameter-dependent plant. The design guarantees closed-loop stability for head motions within the specified limits, while also imposing a bound on the closed-loop L_2-gain from reference signals and disturbances to control error and flexible mode excitation.

To a certain extent, the influence of different reference commands for head and beam motion on excitation of structural vibrations is addressed. From practical considerations it is desirable to have a smooth, non-aggressive commanded motion in order to avoid such vibrations. From an academic research standpoint, the application of aggressive trajectories may excite vibrations and give valuable insights into the damping capabilities of the applied controller.

Experiments on a prototype machine show achievable performance for different motions with either fixed or moving placement head. Beam and head motions are commanded with accelerations of up to 32 m/s^2 and velocities of up to 2.5 m/s. Steady-state errors of less than 1 μm are achieved. Structural vibrations of the beam and friction disturbances are largely attenuated. For a smooth beam motion of 0.5 m with simultaneous head motion, the developed LTI H_∞ controller achieves a settling time of 372 ms, whereas a GS H_∞ controller achieves 366 ms. In the case of bang-bang acceleration command profiles, the GS H_∞ controller maintains its performance level, whereas the LTI H_∞ performance degrades. With respect to small beam movements, smooth reference commands are favorable over bang-bang-like commands. In this case, the LTI H_∞ and the GS H_∞ controllers show equal performance.

Furthermore, a simulation study is carried out in order to show potential benefits of combined control system and beam design. In particular, the trade-off between increased positioning performance and reduced beam mass is investigated. By reduction of beam mass, beam positioning time can be reduced theoretically when keeping the same motor power. Due to reduced beam stiffness, also stronger structural vibrations will be excited, which have to be damped by the control system. It is shown that positioning performance may benefit from beam re-design when applying appropriate control technology. For additional discussions on these topics also see Rieber and Taylor [36], [37].

The thesis is organized as follows. Chapter 2 summarizes the modeling of a two-axis gantry robot. Chapter 3 presents some preliminary issues such as the control system structure, inner-loop compensation, choice of design models and reference trajectories, discretization of controllers, velocity estimation, and the experimental framework. Chapter 4 contains the main contributions of this work. Several control design approaches and their application to the gantry robot are explained, namely LTI H_∞ control and GS H_∞ control. The use of different sensor signals is compared and a modification for optimal online computation of controllers is presented. Experimental results indicate the performance levels achieved by the controllers. Chapter 5 discusses the influence of beam design modifications on positioning performance as a second main contribution. Finally, Chapter 6 gives a conclusion about this work and suggestions for further research.

Chapter 2

The Gantry Robot

In the following sections, the considered gantry robot will be described. A general overview of the configuration as well as mathematical models and parameter data are given in order to provide the necessary basis for obtaining simulation results and applying control design methods.

2.1 Gantry Robot Configuration

The considered gantry robot is designed to perform fast and accurate positioning of a head for part placement in a horizontal plane. This is essentially achieved with a cartesian two-axis mechanism (Figure 2.1), where a beam moves along two rails in y-direction, and the placement head slides along the beam in x-direction perpendicular to the y-axis. The point-to-point motion control task involves repositioning the head with coordinates $(x_H(t), y_H(t))$, from some initial point (x_0, y_0) to some desired final destination (x_d, y_d). Circuit boards are supposed to be delivered in between the two rails by a conveyor belt. A typical work cycle then consists of the following steps:

1. The placement head moves to the feeders by simultaneous x- and y-axis motion to obtain parts. This is usually a motion of about 0.5 meters in the considered setup.

2. After grabbing some parts with several vacuum nozzles, which also involves some small x-axis motions, the placement head moves back to the circuit board location by simultaneous x- and y-axis motion. This is again a motion of about 0.5 meters.

3. The parts are placed onto circuit boards. This is done by several small simultaneous x- and y-axis motions, from a few millimeters up to several centimeters.

After placing all the parts, the cycle restarts with the feeding step 1. It is obvious that high accuracy is necessary in order to correctly place electronic parts. Also a high

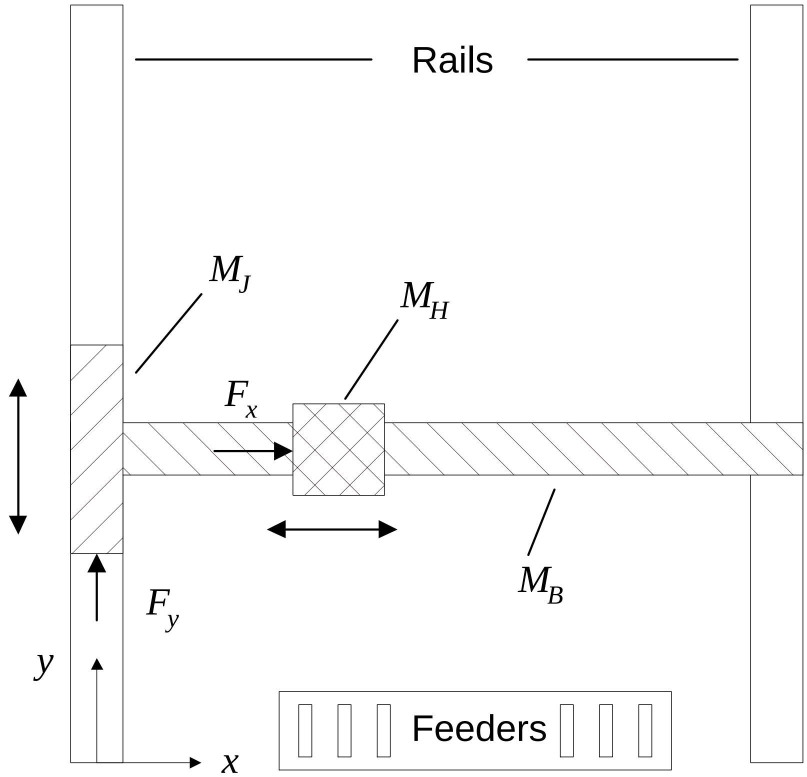

Figure 2.1: Schematic top view of gantry robot configuration. M_J, M_B and M_H denote joint, beam and head masses, respectively, F_x and F_y represent forces applied to joint and head.

speed for the individual motions is desired, such that the time for running a work cycle is as short as possible. The goal is to obtain micrometer positioning accuracy of the two-axis mechanism, for large as well as for small movements, within the shortest possible time span.

Other components of the gantry robot create and control forces for moving this two-axis mechanism. Permanent-magnet synchronous motors generate a torque which is converted to a linear force by means of a belt-drive transmission. For y-axis motion, the force is applied to a joint which is located at one end of the beam. Optical linear position sensors for y-axis position are located at the joint and at the free beam tip which is the end opposite of the joint. For x-axis motion, the force is applied to the placement head whose position along the beam is also measured by an optical linear position sensor. Additional rotary position sensors measure the angular positions of the x- and y-axis motor shafts.

2.2 Modeling

In this section, the main modeling results are presented, closely following Yang [45]. The equations given are important for establishing simulation models and for motivating the proposed control design approaches. Derivations and details can be found in Yang [45] and Yang et al. [49].

2.2.1 Flexible Beam

The most interesting component of the robot for control design is the beam which is moving along the y-axis and which supports the placement head, see Figure 2.1. It is assumed that there is no influence from y-axis beam movement to x-axis head movement. However, the x-position determines the mass distribution of the beam-head configuration and therefore influences the beam dynamics.

The straight flexible beam has been modeled as an Euler-Bernoulli beam, modified to include the effects of concentrated masses representing the fixed joint and the moving head. This formulation describes the bending deflection of the beam in y-direction. The beam is assumed to be homogeneous and uniform, with the cross-sectional dimensions being small compared to the beam length. The characteristic parameters of the beam are length l, mass density ϱ, modulus of elasticity E, and joint mass M_J. The cross section is described by the constant area A and the constant moment of inertia I_z. Then the beam mass is $M_B = \varrho A\, l$. A partial differential equation for the bending displacement $w(x,t)$ (see Figure 2.2) is given by

$$EI_z \frac{\partial^4 w(x,t)}{\partial x^4} + \varrho A \frac{\partial^2 w(x,t)}{\partial t^2} = f(x,t) \qquad x \in (0,l)\ , \quad t > t_0\ , \tag{2.1}$$

where $f(x,t)$ denotes an external distributed load. This external force represents the influence of the moving head. Given the forces $F_0(t)$ and $F_l(t)$ acting in y-direction at $x = 0$ and $x = l$, respectively, the boundary conditions in the gantry robot framework

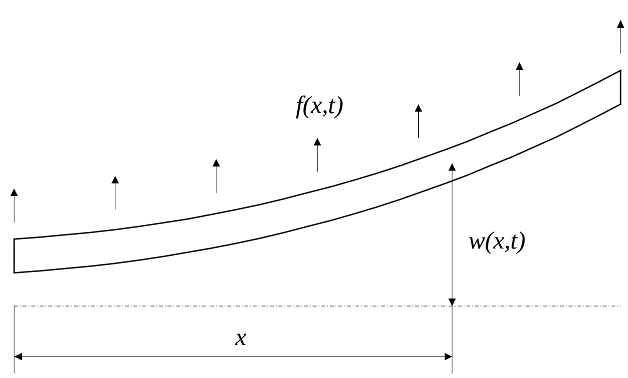

Figure 2.2: Bending displacement $w(x,t)$ of the flexible beam. The distributed load is denoted by $f(x,t)$.

require

$$\begin{aligned} \frac{\partial w(0,t)}{\partial x} &= 0 \\ EI_z \frac{\partial^3 w(0,t)}{\partial x^3} + M_J \frac{\partial^2 w(0,t)}{\partial t^2} &= F_0(t) \\ EI_z \frac{\partial^2 w(l,t)}{\partial x^2} &= 0 \\ -EI_z \frac{\partial^3 w(l,t)}{\partial x^3} &= F_l(t) \qquad\qquad t > t_0 \ . \end{aligned} \tag{2.2}$$

For completeness, the initial conditions are $w(x, t_0) = w_0(x)$ and $\dot{w}(x, t_0) = w_1(x)$, $x \in (0, l)$.

Determination of Mode Shapes

In order to transform this problem into ODEs, consider first the free vibration problem with $f(x,t) \equiv F_0(t) \equiv F_l(t) \equiv 0$. By separation of variables, the bending displacement is assumed to be

$$w(x,t) = W_b(x) q_b(t) \ . \tag{2.3}$$

Substituting this solution structure into (2.1) and (2.2) yields two decoupled ODEs

$$W_b''''(x) - \alpha_b^4 W_b(x) = 0 \tag{2.4}$$

$$\ddot{q}_b(t) + \omega_b^2 q_b(t) = 0 \tag{2.5}$$

together with the constraints

$$\begin{aligned} W_b'(0) &= 0 \\ EI_z W_b'''(0) - M_J \omega_b^2 W_b(0) &= 0 \\ W_b''(l) &= 0 \\ W_b'''(l) &= 0 \ , \end{aligned} \tag{2.6}$$

where $\omega_b^2 := EI_z \alpha_b^4 / \varrho A$. The parameter α_b will be determined as follows. From (2.4), a possible choice for $W_b(x)$ is

$$W_b(x) = c_{b1} \sin(\alpha_b x) + c_{b2} \cos(\alpha_b x) + c_{b3} \sinh(\alpha_b x) + c_{b4} \cosh(\alpha_b x) \ . \tag{2.7}$$

This function is required to satisfy the four constraints (2.6). Substitution of (2.7) into (2.6) leads to an equation for α_b, which can be solved numerically:

$$\sin(\alpha_b l) \cosh(\alpha_b l) + \cos(\alpha_b l) \sinh(\alpha_b l) + \alpha_b l \frac{M_J}{\varrho A l} (1 + \cos(\alpha_b l) \cosh(\alpha_b l)) = 0 \ .$$

There are infinitely many solutions α_i, $i = 0, 1, 2, \ldots$, in particular $\alpha_0 = 0$ for the rigid mode. From relation (2.7), the so-called eigenfunctions or exact mode shapes $W_i(x)$ are obtained:

$$W_i(x) = (k_{i,1}\sin(\alpha_i x) + k_{i,2}\cos(\alpha_i x) + k_{i,3}\sinh(\alpha_i x) + \cosh(\alpha_i x))\, c_{i,4} \qquad i = 0, 1, 2, \ldots \, . \tag{2.8}$$

The coefficients $c_{i,j}$, $j = 1, 2, 3$, have been replaced by $c_{i,j} := k_{i,j}c_{i,4}$, where $k_{i,j}$, $j = 1, 2, 3$ are computed from (2.6) to be

$$\begin{bmatrix} k_{i,1} \\ k_{i,2} \\ k_{i,3} \end{bmatrix} = \begin{bmatrix} 1 & 0 & 1 \\ -1 & -\alpha_i M_J/(\varrho A) & 1 \\ -\sin(\alpha_i l) & -\cos(\alpha_i l) & \sinh(\alpha_i l) \end{bmatrix}^{-1} \begin{bmatrix} 0 \\ \alpha_i M_J/(\varrho A) \\ -\cosh(\alpha_i l) \end{bmatrix} \qquad i = 0, 1, 2, \ldots \, .$$

The remaining coefficients $c_{i,4}$ are to be chosen freely in general. One possible normalization is obtained by applying the orthogonality property of the eigenfunctions:

$$M_J W_i(0) W_j(0) + \int_0^l \varrho A W_i(x) W_j(x) dx = \begin{cases} 0 & , \ i \neq j \\ 1 & , \ i = j \end{cases} \qquad i, j = 0, 1, 2, \ldots \tag{2.9}$$

In particular, $W_0(x) = \frac{1}{\sqrt{M_J + \varrho A l}}$ is obtained for the rigid mode. Thus a solution to the free vibration problem is given by the infinite series

$$w(x,t) = \sum_{i=0}^{\infty} W_i(x) q_i(t) \tag{2.10}$$

with mode shapes $W_i(x)$ from (2.8) and solutions $q_i(t)$ of (2.5).

Galerkin Method

In order to obtain a solution of the forced vibration problem (2.1)–(2.2), Galerkin's method is used. By this method, $w(x,t)$ is represented as a finite series consisting of the mode shapes $W_i(x)$ and generalized coordinates $q_i(t)$, using just the rigid mode $i = 0$ and N flexible modes, i.e.

$$w(x,t) = \sum_{i=0}^{N} W_i(x) q_i(t) \, . \tag{2.11}$$

The dynamics of the generalized coordinates are selected such that the residual error integrated over the spatial domain with weighting functions $W_i(x)$ will be zero, i.e.

$$\int_0^l \varepsilon_1(x,t) W_i(x) dx + \varepsilon_2(t) W_i(0) + \varepsilon_3(t) W_i(l) = 0 \qquad i = 0, 1, \ldots, N \, , \tag{2.12}$$

where, from (2.1) and (2.2), the residual errors are defined as

$$\begin{aligned}
\varepsilon_1(x,t) &:= EI_z\frac{\partial^4 w(x,t)}{\partial x^4} + \varrho A\frac{\partial^2 w(x,t)}{\partial t^2} - f(x,t) \\
\varepsilon_2(t) &:= EI_z\frac{\partial^3 w(0,t)}{\partial x^3} + M_J\frac{\partial^2 w(0,t)}{\partial t^2} - F_0(t) \\
\varepsilon_3(t) &:= -EI_z\frac{\partial^3 w(l,t)}{\partial x^3} - F_l(t)\ . \qquad (2.13)
\end{aligned}$$

Substituting (2.13) and (2.11) in (2.12) and invoking the orthogonality property (2.9) yields the decoupled dynamics of generalized coordinates

$$\ddot{q}_i(t) + \omega_i^2 q_i(t) = \int_0^l W_i(x)f(x,t)dx + W_i(0)F_0(t) + W_i(l)F_l(t)$$
$$i = 0,1,\ldots,N\ . \qquad (2.14)$$

External Force Distribution

As discussed in Yang [45], the effect of the movable head mass M_H may be included in the external distributed force $f(x,t)$ as an inertial reaction force

$$f(x,t) = -M_H\frac{\partial^2 w(x,t)}{\partial t^2}\delta(x - x_H)\ .$$

Here $\delta(\cdot)$ represents the impulse function. Using this expression together with (2.11), the integral in (2.14) can be evaluated as

$$\int_0^l W_i(x)f(x,t)dx = -M_H\sum_{j=0}^{N} W_i(x_H)W_j(x_H)\ddot{q}_j(t)\ . \qquad (2.15)$$

Mechanical Friction

Since friction is a considerable disturbance during beam motion, it has to be included in simulation models and in control system design. A model for the friction force $F_f(t)$ based on Coulomb friction with coefficient F_c, viscous friction with coefficient F_v, and the velocity $v(t)$ is used [6]:

$$F_f(t) = F_c\,\mathrm{sgn}(v(t)) + F_v\,v(t)\ . \qquad (2.16)$$

The signum function is approximated by a saturation function, having a transient region with slope 10^4 s/m.

Complete ODE Beam Model

In order to provide a compact form of the beam dynamics, the vector notations

$$\begin{aligned}
q(t) &:= [q_0(t),\ldots,q_N]^T \\
W(x) &:= [W_0(x),\ldots,W_N(x)]^T
\end{aligned}$$

are introduced. The y-axis beam model (2.14) together with (2.15) thus can be written in the form

$$M(x_H(t))\ddot{q}(t) + C_d\dot{q}(t) + Kq(t) = B_f F(t) \ , \tag{2.17}$$

where the mass, damping, stiffness and input matrices are defined as

$$\begin{aligned} M(x_H(t)) &:= I + M_H W(x_H(t)) W^T(x_H(t)) \\ C_d &:= \operatorname{diag}\{2\zeta_0\omega_0, \ldots, 2\zeta_N\omega_N\} \\ K &:= \operatorname{diag}\{\omega_0^2, \ldots, \omega_N^2\} \\ B_f &:= [W(0),\ W(l)] \ , \end{aligned}$$

and the force vector is given by

$$F(t) := [F_0(t),\ F_l(t)]^T = [F_{ty}(t) - F_{fy0}(t),\ -F_{fyl}(t)]^T \ .$$

The ω_i are computed numerically as given above, whereas the ζ_i are heuristically introduced to account for damping effects not incorporated in the Euler-Bernoulli beam model. F_{ty} denotes the force applied to the joint by the transmission, and F_{fy0} and F_{fyl} represent friction forces at the joint and at the tip, respectively. The initial conditions for this description are given by

$$\begin{aligned} q(t_0) &= M_J W(0) w(0, t_0) + \int_0^l \varrho A W(x) w(x, t_0)\, dx \\ \dot{q}(t_0) &= M_J W(0) \frac{\partial w}{\partial t}(0, t_0) + \int_0^l \varrho A W(x) \frac{\partial w}{\partial t}(x, t_0)\, dx \ . \end{aligned} \tag{2.18}$$

Using output equation (2.11), the y-coordinates of joint, head and tip are obtained as

$$y_J(t) = W^T(0) q(t) \tag{2.19}$$
$$y_H(t) = W^T(x_H(t)) q(t) \tag{2.20}$$
$$y_T(t) = W^T(l) q(t) \ . \tag{2.21}$$

The second-order model (2.17) can be written as a first-order state-space model:

$$\begin{aligned} \dot{x}_B &= A_B(x_H(t))\, x_B + B_B(x_H(t))\, u_B \\ y_B &= C_B\, x_B \ , \end{aligned} \tag{2.22}$$

where

$$\begin{aligned} x_B &:= \begin{bmatrix} q(t) \\ \dot{q}(t) \end{bmatrix} \\ u_B &:= F(t) \\ A_B(x_H(t)) &:= \begin{bmatrix} 0 & I \\ -M^{-1}(x_H(t))K & -M^{-1}(x_H(t))C_d \end{bmatrix} \\ B_B(x_H(t)) &:= \begin{bmatrix} 0 \\ M^{-1}(x_H(t))B_f \end{bmatrix} \ . \end{aligned}$$

The output matrix C_B can be designed according to the desired output of the system. If for example only y_J should constitute the output signal, C_B is defined as

$$C_B \;:=\; \left[W^T(0),\ 0\right] \,.$$

The y-axis model of the gantry robot is thus parameterized by $x_H(t)$, the location of the head along the beam. Since $x_H(t)$ is directly measured, (2.22) may be viewed as an LPV system.

2.2.2 Further Robot Components

The gantry robot under consideration has other components in addition to the beam. The mathematical models of the belt-drive transmission, of the moving placement head, and of the electric motors are described briefly.

Belt-drive Transmission

The belt-drive transmission consists of an elastic belt on two pulleys, see Figure 2.3. One of the pulleys is driven by the motor torque T_1, the other one is passive. The motor torque is transformed into a translating force via the belt and thus transmitted to the beam joint. The complete moving mass, consisting of joint, beam and head, is represented by the mass M here.

For derivation of the transmission model, the belt mass is neglected due to the dominance of pulley and load masses. Furthermore, the mass moment of inertia J_2 of the driven pulley is neglected compared to the mass moment of inertia J_1 of the driving pulley, since the latter one includes the motor inertia, and its value is therefore typically much larger. Assuming the belt to be a spring with constant stiffness k, yields the following simplified transmission model for translation $y(t)$ and rotation $\varphi_1(t)$ by applying force and moment equilibrium:

$$M\ddot{y}(t) \;=\; k(r_1\varphi_1(t) - y(t)) \tag{2.23}$$

$$J_1\ddot{\varphi}_1(t) \;=\; -r_1 k(r_1\varphi_1(t) - y(t)) + T_1(t) \,. \tag{2.24}$$

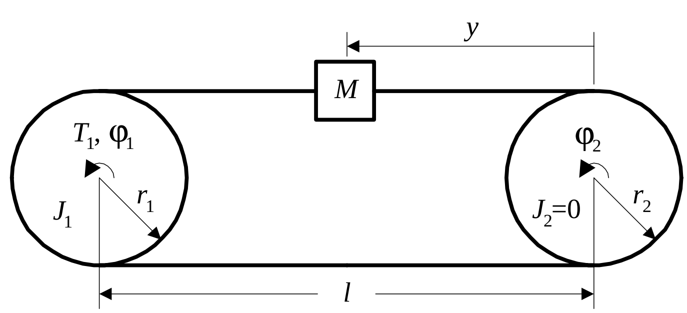

Figure 2.3: Belt-drive transmission with translating load mass M. The driving pulley (left) is subject to a torque T_1.

Placement Head

The placement head is considered as a point mass translating along the x-axis. The head mass is denoted by M_H. F_{tx} denotes the force applied to the head by the transmission, and F_{fx} represents a friction force. Thus a second-order ODE is given by

$$M_H \ddot{x}_H(t) = F_{tx}(t) - F_{fx}(t) \; . \tag{2.25}$$

Electric Motors

Permanent-magnet synchronous motors are used to drive the gantry robot axes. The electromagnetic torque produced is

$$T_m(t) \approx N_p \lambda_m i_q(t) \; ,$$

where N_p is the number of alternately poled permanent magnet pairs on the rotor, and λ_m denotes the magnitude of flux linkage due to permanent magnets. The torque is thus proportional to the q-axis stator current i_q, but is not influenced by the d-axis stator current i_d. The motors are regulated by PI current loops, the so-called motor drives. Reference signals for these motor drives are the commanded values $i_{q,c}$ of i_q, which should be chosen proportional to the desired motor torque $T_{md}(t)$ according to

$$i_{q,c}(t) = \frac{T_{md}(t)}{N_p \lambda_m} \; , \tag{2.26}$$

whereas the commanded value of i_d is zero.

2.3 Parameter Values for Prototype Robot

Numerical parameter values for beam, head, y-axis belt-drive transmission and y-axis friction for the considered prototype gantry robot are summarized in the following tables. One of the entries, z_H, did not appear in any mathematical model in this chapter, but is used in Appendix A. The peak force available from the drive system is about 900 N. The linear position sensors have a resolution of 1 μm, the rotary position sensors $2\pi/40$ mrad. The range of considered head positions is $x_H \in [0.2 \text{ m}, 0.6 \text{ m}]$. Throughout the thesis, numerical values (for software implementation) without specified units are understood to correspond to standard SI units.

Parameter	Symbol	Value	
Beam mass	M_B	8.72	kg
Joint mass	M_J	7.41	kg
Length	l	0.8	m
Moment of inertia of cross section area	I_z	$3.868 \cdot 10^{-7}$	m^4
Modulus of elasticity	E	$2.1 \cdot 10^{11}$	$\mathrm{N/m}^2$
Mass per unit length	ϱA	10.9	kg/m
Mass density	ϱ	7850	$\mathrm{kg/m}^3$
Head mass	M_H	7.57	kg
Head center of gravity z-coordinate with respect to beam neutral axis	z_H	-0.058	m
Driving and driven pulley radii	r_1, r_2	0.0167	m
Driving pulley moment of inertia including motor	J_1	$7.47 \cdot 10^{-4}$	$\mathrm{kg\,m}^2$
Belt spring constant	k	$2.8 \cdot 10^6$	N/m
Torque constant	$N_p\lambda_m$	0.77	Nm/A
Viscous friction coefficient	F_v	≈ 100	N s/m
Coulomb friction coefficient	F_c	≈ 50	N

Table 2.1: Prototype parameter values of beam, placement head, y-axis belt-drive transmission with motor, and mechanical friction for y-axis motion.

Mode i	0	1	2	3	4	5
ω_i	0	579.41	3228.0	8594.5	16593	27250
α_i	0	2.5907	6.1151	9.9779	13.864	17.767
$c_{1,i}$	0	0.1534	0.2677	0.2905	0.3036	0.3111
$c_{2,i}$	0.1245	-0.4043	-0.3915	-0.3764	-0.3680	-0.3626
$c_{3,i}$	0	-0.1534	-0.2677	-0.2905	-0.3036	-0.3111
$c_{4,i}$	0.1245	0.2301	0.2627	0.2908	0.3036	0.3111
ζ_i	0	0.02	0.02	0.02	0.02	0.02

Table 2.2: Numerical values for prototype beam model.

Chapter 3

Preliminary Issues in Controller Design

In this chapter, preliminary issues are addressed before the actual control system design is discussed. They include an overview of the proposed control system structure and specification of the design models. The design of a filter for velocity estimation is shown as well as methods for controller discretization. Finally, the choice of position reference trajectories is motivated.

3.1 Control System Structure

A schematic overview of the gantry robot motion control system for the y-axis is shown in Figure 3.1. The position reference signal $r(t)$ and the error signal are used by the position controller to generate the force command u_K. The transmission, whose behavior is compensated by an inner-loop controller to yield desired actuator dynamics, generates the force u_B. This force is applied to the beam joint and is responsible for beam motion and therefore beam position y. The beam position signal, which is either joint position y_J or a vector containing joint and tip positions y_J and y_T, is fed back to the position controller to generate the error signal. The inner-loop compensation is explained in Section 3.2. The choice of design models for controller construction is motivated in Section 3.3. The details of designing the position controller and the underlying theory are postponed for the next chapter in Sections 4.1 and 4.2.

In the actual implementation, the overall controller is a series connection of the position controller, the gain k^{-1} and the transmission compensator. The overall controller has to send a current command signal to the motor drive. This current command is obtained from the desired motor torque $T_{md}(t)$ via (2.26), where $T_{md}(t)$ can be computed from the controller output $\tilde{u}$ via (3.3) (see next section) by replacing T_1 with T_{md}.

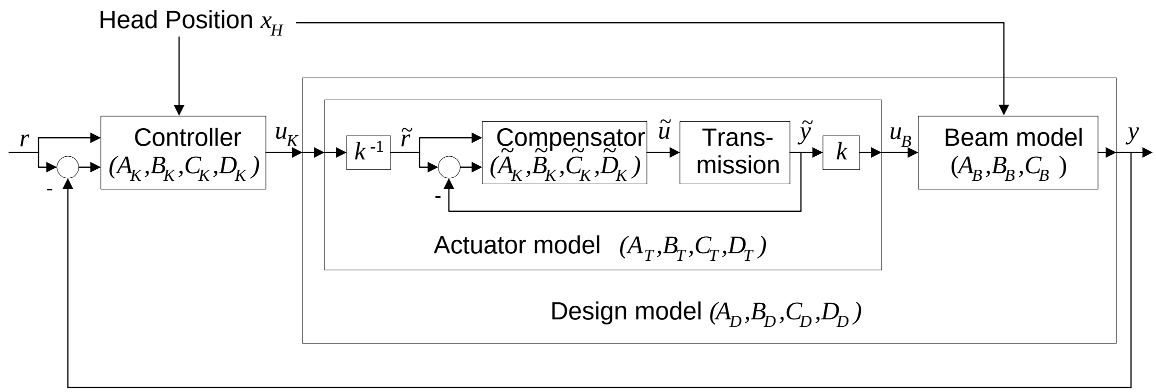

Figure 3.1: Control system structure, as proposed by Yang [45].

3.2 Compensation of Transmission Flexibility

The belt-drive transmission of the considered gantry robot exhibits compliance due to spring effects in the belt, in the belt teeth and in the motor shaft. In reality, the spring coefficient k is time-varying, the motor also exhibits some dynamic behavior which is not modeled here, and belt friction creates a disturbance. In order to generate a predictable and favorable behavior of the transmission system, a compensation of these effects is proposed by Yang [45]. The compensator constitutes an inner-loop controller as shown in Figure 3.1. The main position controller takes the presence of this inner loop into account and builds upon its performance. The position controller is therefore called the outer-loop controller. Here the main results of the inner-loop design are recalled.

A transformation is carried out by performing a change of variables on equations (2.23)–(2.24), using the differential position $\tilde{y}(t) = r_1\varphi_1(t) - y(t)$. This yields

$$\begin{aligned} M\ddot{y}(t) &= k\tilde{y}(t) && (3.1)\\ \tilde{M}\ddot{\tilde{y}}(t) &= -k\tilde{y}(t) + \tilde{u}(t)\ , && (3.2) \end{aligned}$$

where

$$\tilde{M} := \left(\frac{1}{M} + \frac{r_1^2}{J_1}\right)^{-1}\ , \qquad \tilde{u}(t) := \left(1 + \frac{J_1}{r_1^2 M}\right)^{-1} \frac{T_1(t)}{r_1}\ . \tag{3.3}$$

From (3.2), the transfer function of the transmission is

$$\tilde{G}(s) = \frac{\tilde{Y}(s)}{\tilde{U}(s)} = \frac{1}{\tilde{M}s^2 + k}\ .$$

It is desired to have a behavior of

$$\tilde{G}_d(s) = \frac{\tilde{Y}(s)}{\tilde{R}(s)} = \frac{\tilde{\omega}^2}{s^2 + 2\tilde{\zeta}\tilde{\omega} + \tilde{\omega}^2}\ . \tag{3.4}$$

The reference input $\tilde{r}(t)$ to (3.4) has the following meaning. It is clearly visible from (3.1) that the force applied to the mass M is $F_t(t) = k\tilde{y}(t)$. Since the outer-loop controller generates a force command $u_K(t)$ to be applied to the mass M, $k\tilde{y}(t)$ has to be equal to $u_K(t)$. This again requires $\tilde{y}(t) = k^{-1}u_K(t)$. Thus, the reference command for the inner loop has to be $\tilde{r}(t) = k^{-1}u_K(t)$.

In Yang [45] it is shown that a controller with state-space realization

$$\dot{\tilde{x}}_K = \tilde{A}_K\,\tilde{x}_K + \tilde{B}_K\,\tilde{w}\;, \qquad \tilde{u} = \tilde{C}_K\,\tilde{x}_K + \tilde{D}_K\,\tilde{w}\;, \tag{3.5}$$

where

$$\begin{aligned}
\tilde{w} &:= [\tilde{r}\;,\;\tilde{r}-\tilde{y}]^T \\
\tilde{A}_K &:= -(2\tilde{\zeta}\tilde{\omega}+\tilde{\alpha}) \\
\tilde{B}_K &:= \left[2\tilde{\zeta}\tilde{\omega}\tilde{\alpha}(2\tilde{\zeta}\tilde{\omega}+\tilde{\alpha})\;,\;-2\tilde{\zeta}\tilde{\omega}(\tilde{\omega}^2+2\tilde{\zeta}\tilde{\omega}\tilde{\alpha}+\tilde{\alpha}^2)\right] \\
\tilde{C}_K &:= \tilde{M} \\
\tilde{D}_K &:= \left[k-2\tilde{\zeta}\tilde{\omega}\tilde{\alpha}\tilde{M}\;,\;-k+\tilde{M}(\tilde{\omega}^2+2\tilde{\zeta}\tilde{\omega}\tilde{\alpha})\right]\;,
\end{aligned}$$

achieves (3.4). $\tilde{\alpha}$ is an additional design parameter introduced to affect a stable pole-zero cancellation. Note that this inner-loop compensator requires measurements of the position y of the mass as well as of the angular position φ_1 of the driving pulley. The transfer function from u_K to u_B is equal to (3.4) and therefore represents the ideal actuator dynamics with state-space realization

$$\dot{x}_T = A_T\,x_T + B_T\,u_K\;, \qquad u_B = C_T\,x_T + D_T\,u_K\;, \tag{3.6}$$

where

$$A_T := \begin{bmatrix} 0 & 1 \\ -\tilde{\omega}^2 & -2\tilde{\zeta}\tilde{\omega} \end{bmatrix}, \quad B_T := \begin{bmatrix} 0 \\ \tilde{\omega}^2 \end{bmatrix}, \quad C_T := [1\;,\;0]\;, \quad D_T := 0\;.$$

The design parameters are set to $\tilde{\omega} := 2000$, $\tilde{\zeta} := 0.9$, $\tilde{\alpha} := 2000$.

3.3 Models for Controller Design and Simulation

The beam model (A_B, B_B, C_B) given by (2.22) is used for simulation purposes with $N = 5$ flexible bending modes in addition to the rigid mode, thus specifying a twelfth-order model. For controller design only one flexible mode was used, resulting in a fourth-order model. The rigid mode and the first bending mode include the effects of a translating mass as well as beam flexibility and beam deflection. Higher-order modes were neglected because of two reasons. First, these modes represent frequencies above 350 Hz with very low and well-damped amplitudes, and therefore do not provide information as significant as the rigid and the first bending mode. These higher-order modes might even be hindering the design of a high-performance controller if included. Second, certain optimization algorithms used during computation of controllers cannot cope with the badly conditioned matrices which arise when using the higher-order modes.

Since beam joint position only or both beam joint and tip positions are considered for feedback, y and C_B are defined according to (2.22) as

$$\begin{array}{lll} & y := y_J\ , & C_B := \left[W^T(0),\ 0\right] \\ \text{or} & y := [y_J,\ y_T]\ , & C_B := \begin{bmatrix} W^T(0) & 0 \\ W^T(l) & 0 \end{bmatrix}\ . \end{array}$$

Furthermore, friction forces are excluded for controller design, which leaves $u_B(t) := F(t) = F_{ty}(t)$ as a scalar and $B_f := W(0)$ as a column vector.

The simulation and design model for actuator dynamics is taken to be the second-order compensated transmission model (A_T, B_T, C_T, D_T) of (3.6). The overall design model (A_D, B_D, C_D, D_D) is obtained by a series connection of (A_B, B_B, C_B) after (A_T, B_T, C_T, D_T). Note that the beam model and therefore also the overall design model depend nonlinearly on head position $x_H(t)$.

3.4 Estimation of Velocity

In the gantry robot application, the measurements available for motion control include the head position, but not head velocity. Since some of the controllers developed in Chapter 4 require the head velocity signal for scheduling purposes, an estimation filter for head velocity $v_H(t)$ is designed using the head position measurement $x_H(t)$. Although the signal processing electronics used for controlling the robot provide a velocity estimation based on a simple *Backward Euler* scheme (see below), this may not be accurate enough for use in a control algorithm.

The head position measurement is available at certain sample times with a resolution of 1 μm. Due to the highly accurate optical sensor, there is virtually no noise present. Therefore a reliable estimate of head velocity can be obtained through a filter. An overview of several approaches to design such a derivative filter is shown in Brown et al. [12].

Here a dynamic filter is designed on the basis of fitting a polynomial to the current and p preceding position measurements $x_H(t)$. Assume the values $x_H((k-p)T)$, $x_H((k-p+1)T), \ldots, x_H(kT)$ are given, where T is the sampling time. A polynomial of order p

$$x(t) = \sum_{i=0}^{p} c_i \cdot t^i \tag{3.7}$$

with coefficients c_i, $i = 0, \ldots, p$, is fitted to these measurements. This yields $p + 1$ equations

$$\begin{aligned} x_H(kT) &= \sum_{i=0}^{p} c_i \cdot (kT)^i \\ x_H((k-1)T) &= \sum_{i=0}^{p} c_i \cdot ((k-1)T)^i \\ &\vdots \\ x_H((k-p)T) &= \sum_{i=0}^{p} c_i \cdot ((k-p)T)^i \,. \end{aligned} \tag{3.8}$$

The coefficients c_i, dependent on $x_H((k-p)T), \ldots, x_H(kT)$ and on T, are obtained by solving these equations. Inserting the c_i into (3.7) results in an approximation of the position measurement curve over time for $t = kT$:

$$x_H(kT) \approx x(kT) = \sum_{i=0}^{p} c_i \cdot (kT)^i \,. \tag{3.9}$$

The approximation is applicable for $k \geq 0$ if p initial values $x_H(-pT), \ldots, x_H(-T)$ are pre-defined. Then an approximation of velocity over time for $t = kT$ is obtained by differentiation of (3.7), using the already known coefficients c_i:

$$v_H(kT) = \left.\frac{d\,x_H(t)}{dt}\right|_{t=kT} \approx \left.\frac{d\,x(t)}{dt}\right|_{t=kT} = \sum_{i=1}^{p} i\,c_i \cdot (kT)^{i-1} \,. \tag{3.10}$$

This velocity approximation can be established for arbitrary p and T. The choice of p represents a trade-off between high accuracy (large values of p) and small online computational requirements (small values of p). An implementation is realized by a p^{th}-order finite impulse response (FIR) filter. For $p = 1$, the well-known *Backward Euler* approximation

$$v_H(kT) \approx \frac{1}{T}\left(x_H(kT) - x_H((k-1)T)\right) \tag{3.11}$$

follows from (3.10) with coefficients from (3.8). Regarding the short sampling interval of $T = 10^{-4}$ s, the measurement resolution of 1 μm and the virtual lack of noise, a second-order filter provided the necessary accuracy for estimating head velocity from a position measurement. Using (3.10) and (3.8) with $p = 2$, a realization is obtained as

$$v_H(kT) \approx \frac{1}{2T}\left(3x_H(kT) - 4x_H((k-1)T) + x_H((k-2)T)\right) \,. \tag{3.12}$$

In fact, application of this second-order filter provided significant improvement of the closed-loop response in experiments, compared to the Backward Euler approximation. Most important, steady-state oscillations, occuring for Backward Euler velocity estimation, vanished in large part. However, the application of higher-order filters or Least-Squares based techniques (Brown et al. [12]) might give even better accuracy. The velocity estimations reported in this thesis were obtained by the FIR filter (3.12) for head velocity along the beam, and by the built-in Backward Euler estimator of the signal processing equipment for beam joint velocity.

3.5 Discretization of Controllers

The controllers designed for the gantry robot application are obtained as continuous-time dynamic systems. Since they are to be implemented as a computer program running on a digital signal processor, these controllers have to be discretized. The discretized controller is supposed to obtain a new measurement value y_k at every sample time $t = kT$, $k = 0, 1, 2, \ldots$. Likewise, the controller generates a control output u_k at every sample time. For approximations of the continuous-time controller behavior there exist several possibilities, see Franklin et al. [20]. Here the use of zero-order hold (ZOH) discretization is shown.

Consider a continuous-time LPV controller depending on the parameter vector $\theta(t)$:

$$\dot{x} = A(\theta(t))\,x + B(\theta(t))\,y\;, \qquad u = C(\theta(t))\,x + D(\theta(t))\,y\;. \tag{3.13}$$

Assume the input signal $y(t)$ and the parameter signal $\theta(t)$ can be approximated by $y_k := y(kT)$ and $\theta_k := \theta(kT)$ on the interval $t \in [kT, (k+1)T)$ for $k = 0, 1, 2, \ldots$. This constitutes a piecewise-constant approximation. Then the discrete form of (3.13) using ZOH and sampling time T is given by (Apkarian [1], Franklin et al. [20])

$$\xi_{k+1} = \bar{A}(\theta_k)\,\xi_k + \bar{B}(\theta_k)\,y_k\;, \qquad u_k = C(\theta_k)\,\xi_k + D(\theta_k)\,y_k\;, \tag{3.14}$$

where $\xi_k := \xi(kT)$ and

$$\begin{aligned} \bar{A}(\theta_k) &:= e^{A(\theta_k)T} \\ \bar{B}(\theta_k) &:= \int_0^T e^{A(\theta_k)(T-\tau)}\,B(\theta_k)\,d\tau\;. \end{aligned}$$

The matrix exponential of a square matrix M is defined as $e^M := \sum_{k=0}^{\infty} M^k/k!$. It can be obtained exactly via Laplace transform or approximated numerically, see Franklin et al. [20]. The drawback of using this scheme for discretization of an LPV plant is the online computation of the matrix exponential and of an approximation for the integral in $\bar{B}(\theta_k)$, since the parameter value θ_k is time-varying. A solution to this problem is proposed in Section 4.2.2.

For the special case of an LTI system with constant matrices (A, B, C, D), simplified equations can be applied which do not need online computation of matrix gains. Trapezoidal discretization as in Apkarian [1] has also been applied in this work, and showed virtually identical results for the chosen sampling time $T = 10^{-4}$ s.

3.6 Selection of Reference Command

Treatments on reference selection and command shaping are given in Book et al. [9], Meckl and Seering [32], Singer and Seering [42], Dijkstra et al. [15]. Here a more direct and simplified approach is taken.

Planar positioning of the placement head involves motion of the head itself and of the beam supporting the head. If the movable masses were rigid bodies, then a bang-bang profile for acceleration would be a time-optimal choice. However, a bang-bang acceleration profile may lead to excessive excitation of high-frequency modes in flexible robots. Consequently, the chosen motion profile has a symmetric trapezoidal (rather than rectangular) shape of the acceleration curve, as shown in Figure 3.2. The three adjustable parameters are rise time t_r for acceleration, maximum acceleration a_{max} and maximum velocity v_{max}. These parameters could also be defined solely in terms of the acceleration profile. Choosing $t_r > 0$ leads to a finite value for maximum jerk, here $j_{max} = a_{max}/t_r$.

For practical reasons, a sufficiently smooth reference command with reasonable ideal positioning time is desirable, since from such a choice there is less vibration excitation to be expected than from a more "aggressive" trajectory. On the other hand, an aggressive reference command might reveal strengths and weaknesses of controllers regarding bending vibration suppression, and could be used to judge the effectiveness of controller design. By adjusting the parameter t_r in the presented motion profile, the reference command can be altered from near bang-bang behavior to a more smooth non-aggressive shape.

In the gantry robot application, only a finite value of torque or equivalently of force is available. Therefore these parameters have to be chosen such that the absolute value of the applied force, i.e. the force needed for acceleration and overcoming friction, does not exceed the available maximum force according to

$$|F_y(t)| = |Ma(t) + F_v v(t) + F_c \mathrm{sgn}(v(t))| \leq F_{y,max} \ . \tag{3.15}$$

The friction terms follow equation (2.16). An ideal force curve over time corresponding to the motion defined by Figure 3.2 is shown in Figure 3.3.

For experiments on a prototype gantry robot, several motion profiles have been defined for various beam traveling distances between 10 mm and 500 mm. Their parameters are summarized in Table 3.1. Henceforth, the reference commands with $t_r \gg 10^{-7}$ s are called "smooth" motion profiles. The ones with $t_r = 10^{-7}$ s are called "bang-bang" motion profiles, because an acceleration curve with practically bang-bang shape is implied. A "smooth" profile is defined as a profile where $a_{max}/t_r \leq$ 850 m/s^3. In experiments, such smooth motions caused less noise and less hectic controller activity than one where the mentioned ratio is greater than 850 m/s^3. For the 0.5 m motion, the full motor power, just shy of saturation, is utilized.

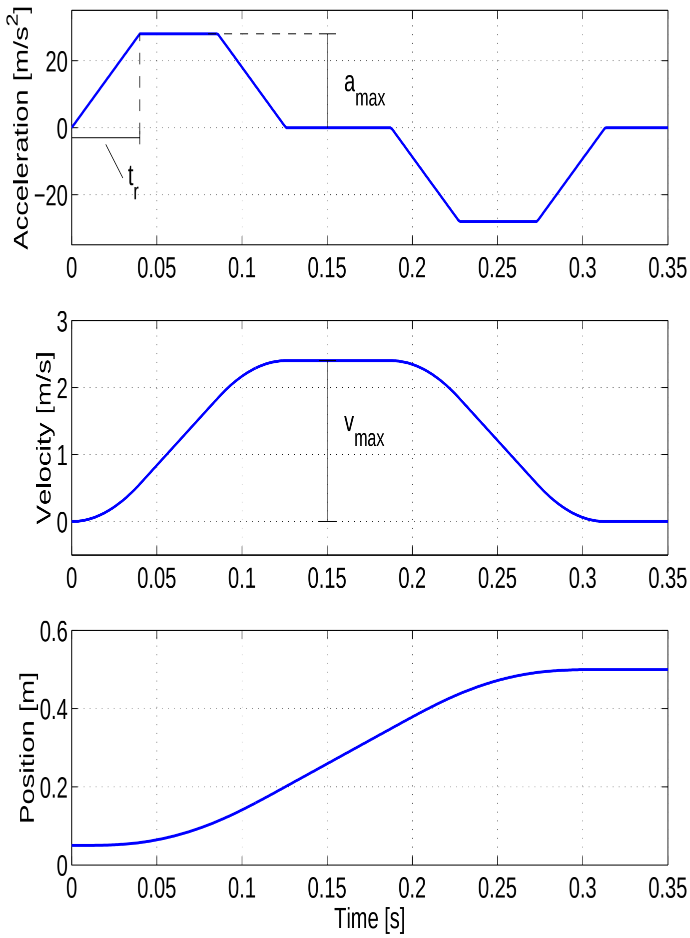

Figure 3.2: Reference motion profile with acceleration rise time t_r, maximum acceleration a_{max} and maximum velocity v_{max} as parameters.

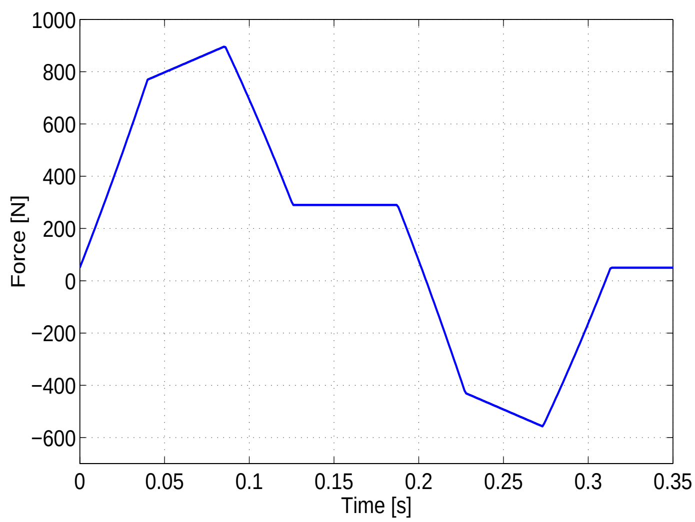

Figure 3.3: Force curve for reference motion profile.

Distance [mm]	Type	v_{max} [m/s]	a_{max} [m/s^2]	t_r [s]	Ideal pos. time [ms]
500	smooth	2.4	32	0.040	319
500	bang-bang	2.4	24	10^{-7}	307
250	smooth	2.3	31	0.037	216
250	bang-bang	2.4	30	10^{-7}	183
100	smooth	1.3	29	0.035	153
100	bang-bang	1.8	30	10^{-7}	115
50	smooth	0.8	26	0.031	120
50	bang-bang	1.3	30	10^{-7}	81
25	smooth	0.5	19	0.023	95
25	bang-bang	0.9	30	10^{-7}	57
10	smooth	0.3	12.5	0.015	69
10	bang-bang	0.6	30	10^{-7}	36

Table 3.1: Reference motion profile parameters including acceleration rise time t_r, maximum acceleration a_{max} and maximum velocity v_{max}.

For head motion along the beam, the parameters are defined as $v_{max} := 2.5$ m/s, $a_{max} := 25$ m/s^2, $t_r := 0.02$ s, when applied simultaneously to a 0.5 m beam motion. In that case, the head moves from $x_{H,0} = 0.2$ m to $x_{H,d} = 0.6$ m. This can be seen as a worst-case experiment, since (i) the full range of head positions is covered, (ii) the head is accelerating and decelerating rapidly, (iii) the head is moving at relatively high speed, and (iv) the head is moving towards the beam tip such that lower frequency/higher amplitude bending vibrations are excited. For y-position control, all controllers considered in this thesis use the position component of the reference motion profile only, due to exclusive joint position feedback.

3.7 Experimental Framework

The prototype gantry robot used for experiments was provided by *Siemens* AG, München, Germany, see `http://www.siemens.com` on the World Wide Web.

For implementation of the developed controllers, a rapid prototyping environment was used. This environment consisted of a *dSPACE* digital signal processing board DS 1103, the *dSPACE* product *ControlDesk*, and the *MATLAB* supplements *Simulink* and *Real-Time Workshop*. The *dSPACE* board provides signal channels, A/D and D/A converters and microprocessors for interaction with the prototype machine and for execution of machine code. *Simulink*, *Real-Time Workshop* and *dSPACE* software provide the functionality to translate *Simulink* block diagrams of even great complexity directly to run-time machine code. *ControlDesk* finally allows monitoring of a real-time experiment and direct interaction with the controlled plant. Information about *dSPACE Inc.*, Paderborn, Germany, can be found at `http://www.dspaceinc.com`. Information about *Mathworks Inc.*, Natick, Massachusetts and *MATLAB* is available at `http://www.mathworks.com`.

Chapter 4

Control System Design

In this chapter, two different controller design methods are presented, namely linear time-invariant robust H_∞ control and gain-scheduled linear parameter-varying H_∞ control. For the latter case several variations, such as different controller structures or use of different measurement signals, are considered. Both control system designs have been implemented on a prototype gantry robot, and experimental results show achievable performance.

Motion control of the placement head along the x-axis basically involves control of an LTI system. In contrast, motion control of the beam along the y-axis has to deal with a distributed LPV system and structural vibrations. Hence, this thesis is concerned only with the more delicate problem of y-axis motion control. For generation of experimental results, a controller for head x-position designed by Yang [45] has been used.

4.1 Linear Time-Invariant H_∞ Control

The first approach to y-axis motion control seeks a single LTI controller using joint position feedback. This controller needs to establish stability and guaranteed performance for the design model. Furthermore, robust stability with respect to the real gantry beam including varying head position has to be achieved. Such a controller would necessarily be somewhat conservative because of the large range of dynamical plant behavior to be considered. The advantage however is the simplicity of design and implementation and the speed of online computations. Performance goals have been achieved by applying loop-shaping techniques as well as by disturbance rejection and attenuation of flexible mode vibrations.

4.1.1 Theoretical Background

The H_∞ optimal control design method used here formulates the problem via LMIs and follows Gahinet and Apkarian [22]. First, a general problem statement is given. Consider an LTI multi-input/multi-output (MIMO) system G with state space equations

$$G \left\{ \begin{array}{rcl} \dot{x} & = & Ax + B_1 w + B_2 u \\ z & = & C_1 x + D_{11} w + D_{12} u \\ y & = & C_2 x + D_{21} w \ . \end{array} \right. \tag{4.1}$$

The variables represent the states $x \in \mathbb{R}^n$, reference signals and disturbances $w \in \mathbb{R}^{m_1}$, control inputs $u \in \mathbb{R}^{m_2}$, outputs $z \in \mathbb{R}^{p_1}$ and measurements $y \in \mathbb{R}^{p_2}$. All matrices are constant and have corresponding dimensions. For this plant, an LTI output-feedback controller K

$$K \left\{ \begin{array}{rcl} \dot{x}_K & = & A_K x_K + B_K y \\ u & = & C_K x_K + D_K y \end{array} \right. \tag{4.2}$$

is designed in order to meet desired specifications on closed-loop behavior. A realization G_{cl} of the closed loop is therefore given by

$$G_{cl} \left\{ \begin{array}{rcl} \dot{x}_{cl} & = & A_{cl} x_{cl} + B_{cl} w \\ z & = & C_{cl} x_{cl} + D_{cl} w \ , \end{array} \right. \tag{4.3}$$

where

$$\begin{array}{ll} A_{cl} := \begin{bmatrix} A + B_2 D_K C_2 & B_2 C_K \\ B_K C_2 & A_K \end{bmatrix} , & B_{cl} := \begin{bmatrix} B_1 + B_2 D_K D_{21} \\ B_K D_{21} \end{bmatrix} \\ C_{cl} := [C_1 + D_{12} D_K C_2 \ , \ D_{12} C_K] \ , & D_{cl} := D_{11} + D_{12} D_K D_{21} \ . \end{array}$$

H_∞ control theory tries to establish an upper bound γ on the closed-loop L_2-gain from w to z according to

$$\int_{t_0}^{t_1} z^T z d\tau \leq \gamma^2 \int_{t_0}^{t_1} w^T w \, d\tau \qquad \forall \ t_1 > t_0 \ . \tag{4.4}$$

This can be interpreted as bounding the effect of a worst-case input w from the set of all finite-energy signals on the output z. For a stable closed loop G_{cl}, the L_2-gain from w to z is equivalent to the H_∞ norm of G_{cl}, see Khalil [31]. The H_∞ norm of $G_{cl}(s) = C_{cl}(sI - A_{cl})^{-1} B_{cl} + D_{cl}$ is defined as

$$\|G_{cl}(s)\|_{H_\infty} := \sup_{\omega \in \mathbb{R}} \bar{\sigma}(G_{cl}(j\omega)) \ .$$

$\bar{\sigma}(M) = \sqrt{\lambda_{max}(M^* M)}$ denotes the maximum singular value of a complex matrix M, where M^* is the complex conjugate transpose of M and $\lambda_{max}(N)$ is the maximum eigenvalue of a matrix N.

The LMI approach to the LTI H_∞ control problem is based on the so-called Bounded Real Lemma, see for example Gahinet and Apkarian [22], Scherer et al. [40]:

Theorem 4.1 *Consider an LTI system described by (4.3). The matrix A_{cl} is stable and $\|G_{cl}(s)\|_{H_\infty} < \gamma$ for some given $\gamma > 0$ if and only if there exists a constant matrix $P = P^T > 0$ such that*

$$\begin{bmatrix} A_{cl}^T P + P A_{cl} & P B_{cl} & C_{cl}^T \\ B_{cl}^T P & -\gamma I & D_{cl}^T \\ C_{cl} & D_{cl} & -\gamma I \end{bmatrix} < 0 \, . \tag{4.5}$$

The notation $M > 0$, where M is a matrix, stands for M being positive definite. By virtue of this theorem, a Lyapunov function $V(t) = x^T(t)\, P\, x(t)$ is established. The unknowns in this formulation are (P, A_K, B_K, C_K, D_K) (see definitions of $A_{cl}, B_{cl}, C_{cl}, D_{cl}$). Since (4.5) implicitly contains products of these variables, it does not constitute an LMI. For controller design purposes, this result can be reformulated by the following theorem just in terms of the given plant G (4.1), see Gahinet and Apkarian [22].

Theorem 4.2 *Consider the LTI plant G (4.1). A controller K (4.2), guaranteeing that A_{cl} of G_{cl} (4.3) is stable and $\|G_{cl}(s)\|_{H_\infty} < \gamma$ for some given $\gamma > 0$, can be found if and only if there exist constant matrices $X = X^T$ and $Y = Y^T$, both $\in \mathbb{R}^{n \times n}$, such that*

$$\begin{aligned}
\begin{bmatrix} \mathcal{N}_{12} & 0 \\ 0 & I \end{bmatrix}^T \begin{bmatrix} AX + XA^T & XC_1^T & B_1 \\ C_1 X & -\gamma I & D_{11} \\ B_1^T & D_{11}^T & -\gamma I \end{bmatrix} \begin{bmatrix} \mathcal{N}_{12} & 0 \\ 0 & I \end{bmatrix} &< 0 \\
\begin{bmatrix} \mathcal{N}_{21} & 0 \\ 0 & I \end{bmatrix}^T \begin{bmatrix} A^T Y + YA & YB_1 & C_1^T \\ B_1^T Y & -\gamma I & D_{11}^T \\ C_1 & D_{11} & -\gamma I \end{bmatrix} \begin{bmatrix} \mathcal{N}_{21} & 0 \\ 0 & I \end{bmatrix} &< 0 \\
\begin{bmatrix} X & I \\ I & Y \end{bmatrix} &\geq 0 \, ,
\end{aligned} \tag{4.6}$$

where $\mathcal{N}_{12}$ and $\mathcal{N}_{21}$ denote bases of the null spaces of (B_2^T, D_{12}^T) and (C_2, D_{21}), respectively.

The unknowns in this formulation are (X, Y). Since they enter linearly into (4.6), this constitutes a system of LMIs and can be solved efficiently with available interior-point polynomial algorithms.

It is often desirable to choose the bound γ as small as possible. Since γ also enters linearly into (4.6), it can be made an unknown of the formulation. The new problem statement then is "Minimize γ over (γ, X, Y) such that (4.6) holds." This is a convex optimization problem and can also be solved by interior-point polynomial algorithms [22]. In Gahinet [21], explicit formulas are given for computing the corresponding LTI H_∞ controller from any solution (γ, X, Y) of this optimization problem. The controller will generally be of the same order n as the plant, unless order reduction techniques are applied. The entire process of controller design following this approach is conveniently implemented by the function `hinflmi` of the LMI Control Toolbox [24]. Furthermore controller order reduction can be performed with this function.

4.1.2 Design Methodology

Motion control of the flexible beam is dealt with in the context of certain loop-shaping techniques as well as of specific usage of weights for vibration damping, disturbance attenuation and robustness considerations. The controller uses joint error feedback and position reference feedforward. Although only a single LTI controller is designed, it has to cope with all practically possible head positions and therefore with changing dynamics. In other words, the controller has to ensure robust stability with respect to the changing dynamics.

The controller synthesis diagram is shown in Figure 4.1, which uses ideas from Yang [45]. The block “Beam Dynamics” represents the LTI beam model (A_B, B_B, C_B) for $x_H = 0.5$ m with joint position feedback, as described in Section 3.3. This model especially includes the effects of the placement head being close to its maximum location $x_H = 0.6$ m. Choosing $x_H = 0.5$ m proved to be well-suited in the sense that the singular value plots

$$\left\{\bar{\sigma}\left(\left.(C_B(sI - A_B)^{-1}B_B)\right|_{x_H=\chi} - \left.(C_B(sI - A_B)^{-1}B_B)\right|_{x_H=\xi}\right)\right\}\Big|_{\xi\in[0.2,0.6]}$$

over frequency were minimal for $\chi \approx 0.5$.

The position sensor has neglectable dynamics. The block “Actuator Dynamics” stands for the compensated belt-drive transmission (A_T, B_T, C_T, D_T). An “Integrator” filter is inserted to achieve zero steady-state error. The input signals are reference command r, input disturbance d_1 (e.g. a friction force), and output disturbance d_2

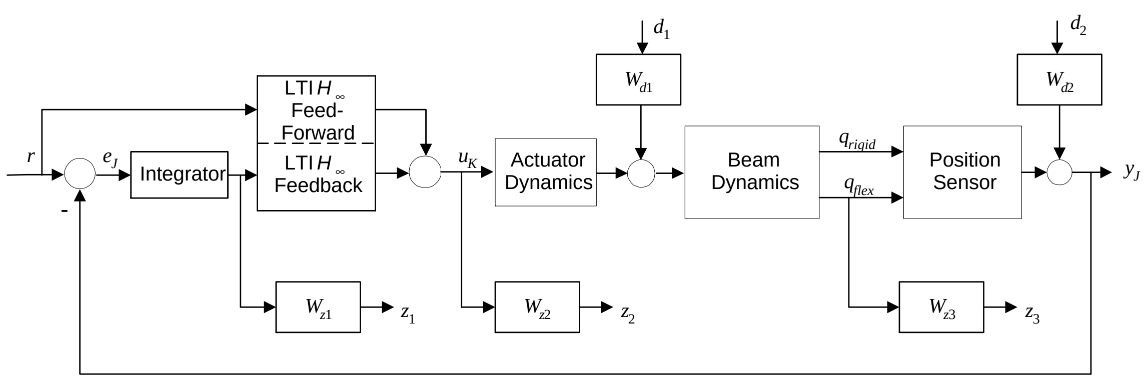

Figure 4.1: Synthesis diagram for LTI H_∞ control, with reference signal r, disturbances d_1, d_2, controller output u_K, generalized coordinates of rigid mode q_{rigid} and of flexible modes q_{flex}, joint position y_J, error signal e_J, and external outputs z_1, z_2, z_3.

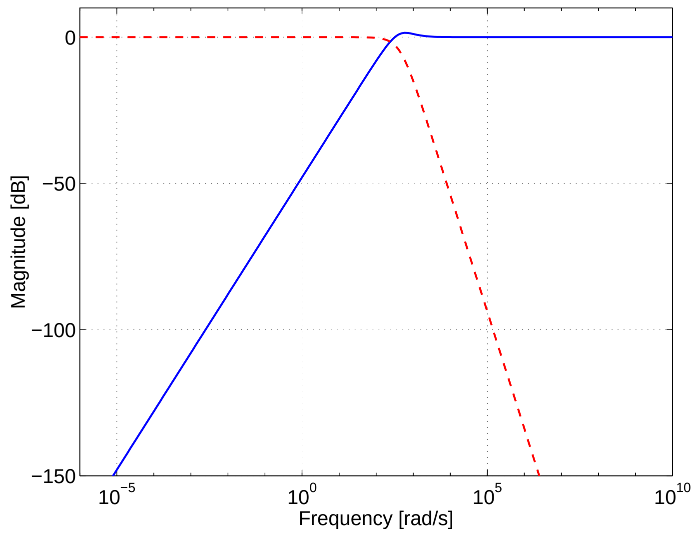

Figure 4.2: Desired second-order closed-loop behavior, expressed as Bode magnitude plots of sensitivity (–) and complimentary sensitivity (- -). Complimentary sensitivity is given by (4.7) with $\omega = 400$, $\zeta = 0.9$.

(e.g. sensor noise or unmodeled dynamics). The output signals are the weighted error z_1, the weighted controller output z_2, and the weighted beam deflection z_3.

The input weight W_{d1} is used to introduce the friction effect into the plant, and improves disturbance attenuation as well as steady-state error. W_{d2} accounts for uncertainties in the beam model, since only one flexible bending mode is considered, and influences the steady-state error. The output weight W_{z1} gives a possibility to shape the behavior of the closed loop and influence performance criteria like steady-state error and bandwidth. W_{z2} is a weight on the controller output u_K and can be used to limit the control energy or to influence performance and robustness. W_{z3} finally provides for vibration damping by penalizing activity of the flexible mode states q_{flex}. All weighting functions except W_{z1} are taken to be constants. This yields a minimal number of tuning parameters as well as a controller of relatively low order.

The weight W_{z1}, applied to the filtered position error, can be used as a loop-shaping or model-matching weight. From the desired complimentary sensitivity function, chosen as

$$T_d(s) = \frac{\omega^2}{s^2 + 2\zeta\omega s + \omega^2} \,, \tag{4.7}$$

the desired sensitivity becomes

$$S_d(s) = 1 - T_d(s) = \frac{s^2 + 2\zeta\omega s}{s^2 + 2\zeta\omega s + \omega^2}$$

with design parameters ζ and ω. For a Bode magnitude plot see Figure 4.2. If the integrator filter with design parameter c_I is defined as

$$G_I(s) := \frac{s + c_I}{s} \ , \tag{4.8}$$

then the choice

$$W_{z1}(s) := \frac{1}{G_I(s)S_d(s)} = \frac{s^2 + 2\zeta\omega s + \omega^2}{(s + c_I)(s + 2\zeta\omega)} \tag{4.9}$$

applies the sensitivity as a loop-shaping weight to the position error e_J. The main reason for this construction is the avoidance of a weighting function with a pole on the imaginary axis, which otherwise may cause problems in LMI optimization.

The external inputs and outputs of the control system are respectively combined into the vectors

$$\begin{aligned} w &:= [r, d_1, d_2]^T \\ z &:= [z_1, z_2, z_3]^T = [W_{z1}(s)\epsilon(s), W_{z2}u_K(s), W_{z3}q_{flex}(s)]^T \ . \end{aligned} \tag{4.10}$$

The controller inputs and outputs are

$$y := [r, \epsilon]^T \ , \qquad u := u_K \ , \tag{4.11}$$

respectively, where $\epsilon(t)$ is the filtered joint position error $e_J(t) := r(t) - y_J(t)$. With these definitions and the interconnections of Figure 4.1, the control system can be easily transformed into the form (4.1). The control goals incorporated into the weights are achieved, if the L_2-gain γ of the closed loop from w to z is $\gamma \approx 1$.

The choice of design parameters was determined through an iterative process. When a controller was constructed for a certain set of design parameter values, it was tested via closed-loop simulations and experiments on the prototype machine. Stability and the best achievable settling times for a 0.5 m beam motion with simultaneous 0.4 m head motion along the beam were the criteria for choosing the final values for design parameters. These motions were chosen (i) to allow comparisons to Yang's work [45] and (ii) to actually have strong vibration excitation in the relatively stiff prototype beam. It has to be emphasized that the experimental settling times for small beam movements of only some millimeters may have been better if controller tuning were done for these small movements instead.

For simulations and experiments, the design parameters were set to $\omega := 400$, $\zeta := 0.9$, $c_I := 1000$, $W_{d1} := 9 \cdot 10^4$, $W_{d2} := 0.1$, $W_{z2} := 10^{-10}$, $W_{z3} := 6$. After LMI optimization, a value of $\gamma = 1.67$ was obtained. This γ-value is only meaningful for the design model, where $x_H = 0.5$ m. Robust stability with respect to varying head positions and to the unmodeled modes of a twelfth-order beam model was shown via simulations. A theoretical investigation on robust stability with small-gain arguments (see for example Zhou et al. [50]) was not found very expressive, mainly because of the heavy impact of mechanical friction.

Controller Implementation

Given the controller obtained by LMI optimization, the final controller matrices (A_K, B_K, C_K, D_K) are obtained after multiplying the error input channel by the integrator filter $G_I(s)$. This controller then has an order of 10. For digital implementation, it has been discretized using the ZOH approach (3.14) with a sample time of $T = 10^{-4}$ s.

Since reference command feedforward is included, the controller initial condition ξ_0 has to be chosen appropriately. Here ξ_0 was computed as the vector of states resulting in $u_K(t_0) = 0$ and $\xi_1 \approx \xi_0$, given the initial controller input $y_0 := [r(t_0), 0]^T$. This works correctly only if the beam joint is indeed located at $y_J = r(t_0)$ at the start of the experiment.

4.1.3 Experimental Results

In this section, experimental results for a beam motion of 0.5 m are presented. Figure 4.3 shows an overview of the closed-loop response with simultaneous head movement for the smooth motion profile, including joint position, joint velocity estimation, applied current, and position error of joint and tip. From the joint position response, it can be seen that the controller does not achieve perfect tracking of the reference command. This can be explained by (i) the punishment of the position error filtered by the weight W_{z1} instead of the position error itself in the controller, (ii) the influence of mechanical friction and unmodeled compliant effects of motor and belt-drive transmission, and (iii) the lack of predictive or anticipatory controller behavior, as would be provided by a derivative action on joint position. See Yang [45] for more detailed discussion of these effects. The velocity profile is lagging its reference for the same reasons. The current waveform exhibits large-amplitude low-frequency variations due to the outer-loop motion control, and small-amplitude high-frequency features caused by the inner-loop transmission compensation. The current curve also shows the influence of Coulomb friction between $t = 0.15$ s and 0.2 s, where a non-zero (in the mean) current is applied, although no acceleration takes place. Due to the smoothness of the motion, the effect of viscous friction is not visible. The position error plot shows an error of up to 1.75 cm during motion.

A zoomed view of the position error, now for fixed head at three locations as well as for the moving-head case, is shown in Figure 4.4. For all four cases, zero steady-state error up to measurement accuracy is achieved finally. Structural vibrations along the beam are well damped, indicated by the nearly equal run of the joint and tip curves. In Figure 4.5, the position error plots for the 0.5 m bang-bang motion are given. In the plots for $x_H = 0.2$ m and in the moving-head case, either significant deviations between joint and tip curves are present or oscillations around the desired location occur. In contrast, the position error curves look more favorable as in the smooth-motion case for $x_H = 0.4$ m and for $x_H = 0.6$ m. This had to be expected, since the LTI H_∞ controller was designed for $x_H = 0.5$ m. It has to be remarked that tip position usually deviated from joint position by about 20 μm in average. This offset is an effect of joint clearance, and was removed in all position error plots shown in this thesis.

It has to be emphasized again that all experimental results in this chapter were obtained through the use of a *single*, robustly stable LTI H_∞ controller. This is in contrast to Yang [45] and Yang and Taylor [46]. There, results were obtained through a family of LTI H_∞ controllers, where each component controller was optimized for a specific head position x_H. As a main drawback, this family of controllers cannot be applied for the practically relevant moving-head case.

To complete the experimental data, the closed-loop response of head movement along the beam is shown in Figure 4.6. The head positioning achieves zero steady-state error as well. Note that the velocity estimation via the FIR filter (3.12) is just slightly noisy despite the simple design of the filter. A comparative analysis of settling times and vibration suppression is given in Section 4.3.

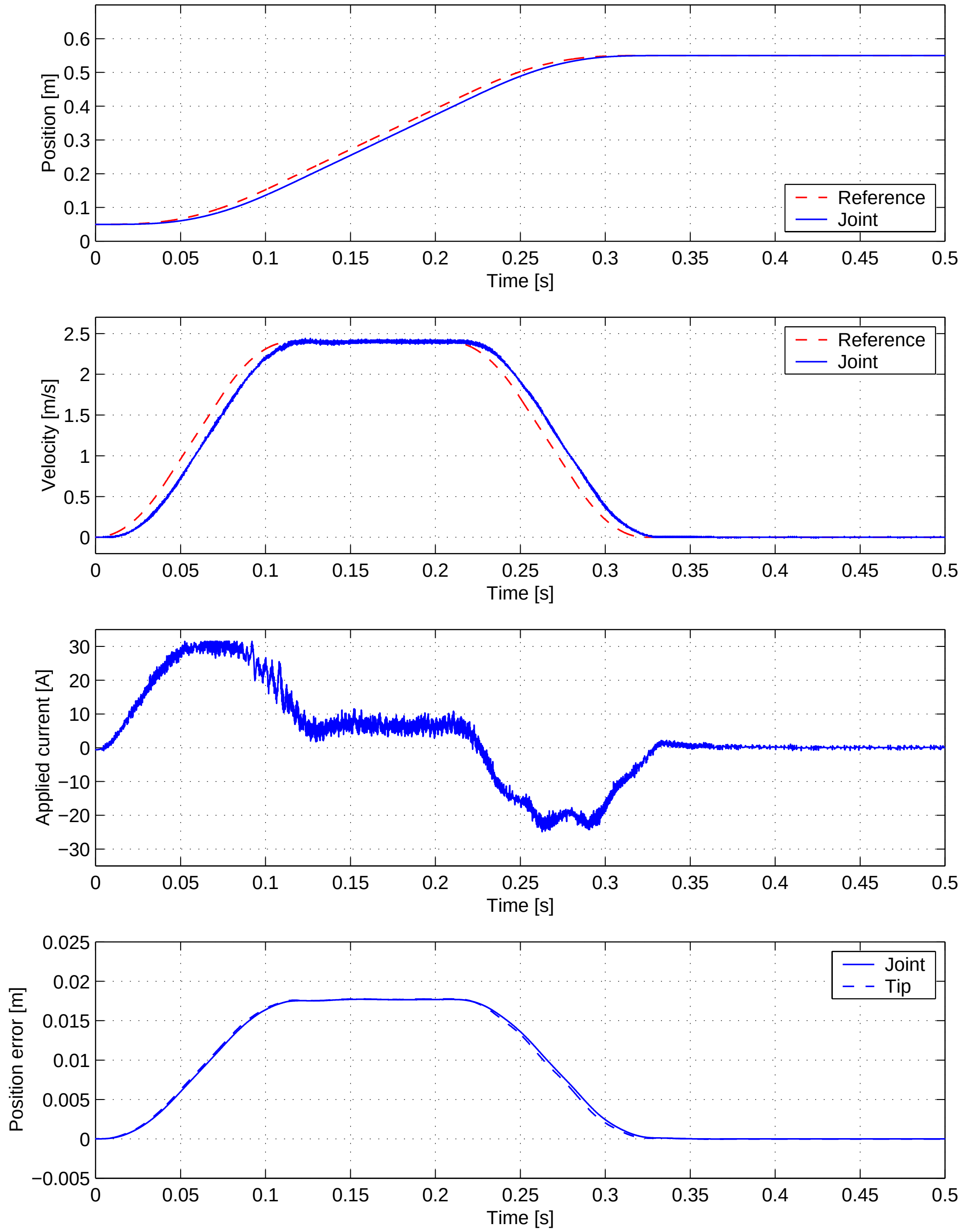

Figure 4.3: Experimental results of 0.5 m y-axis motion for LTI H_∞ controller, moving head from x_H=0.2 $\rightarrow$ 0.6 m. The smooth motion profile is applied.

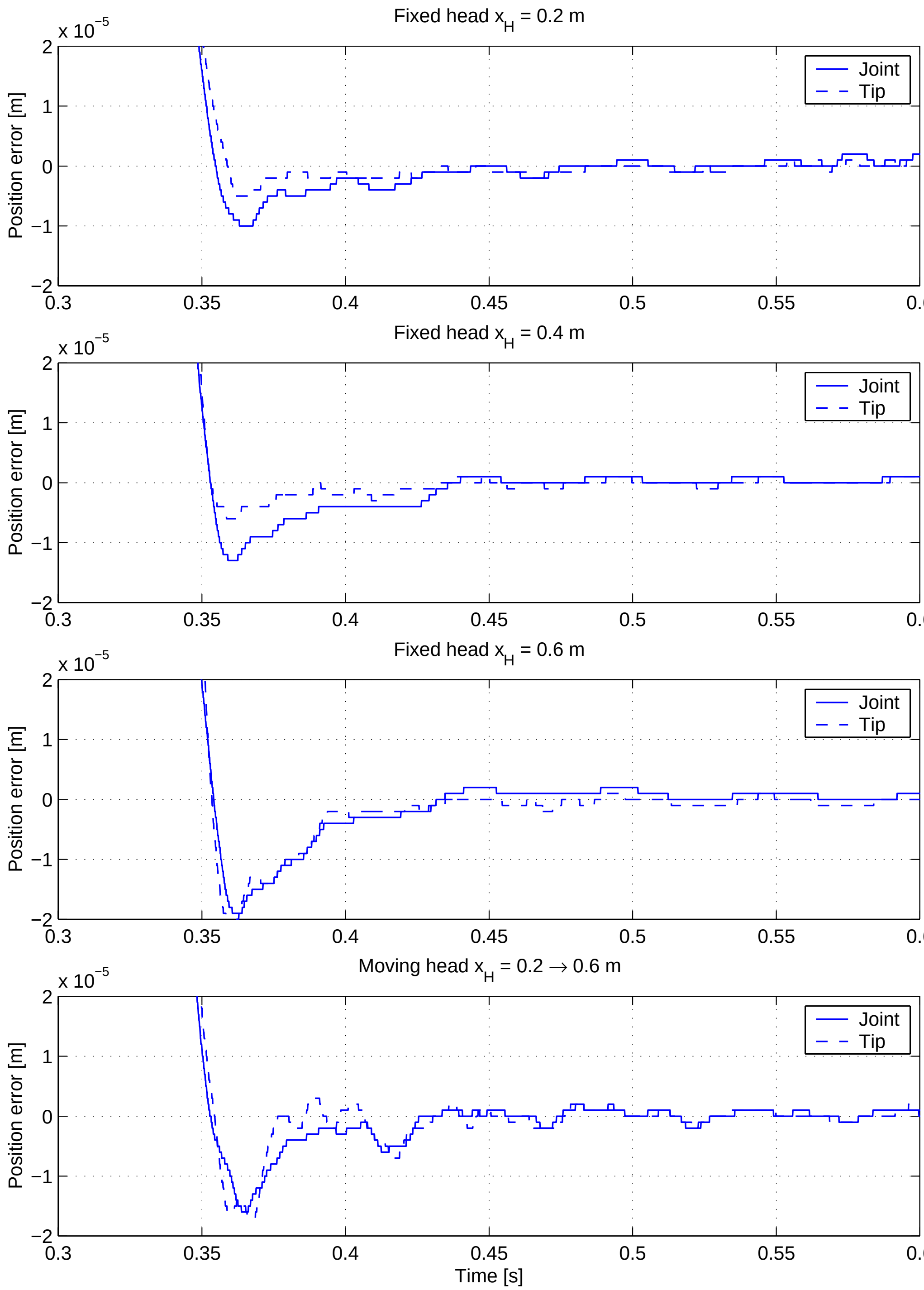

Figure 4.4: Position error of 0.5 m y-axis motion for LTI H_∞ controller, with fixed head at different locations and moving head. The smooth motion profile is applied.

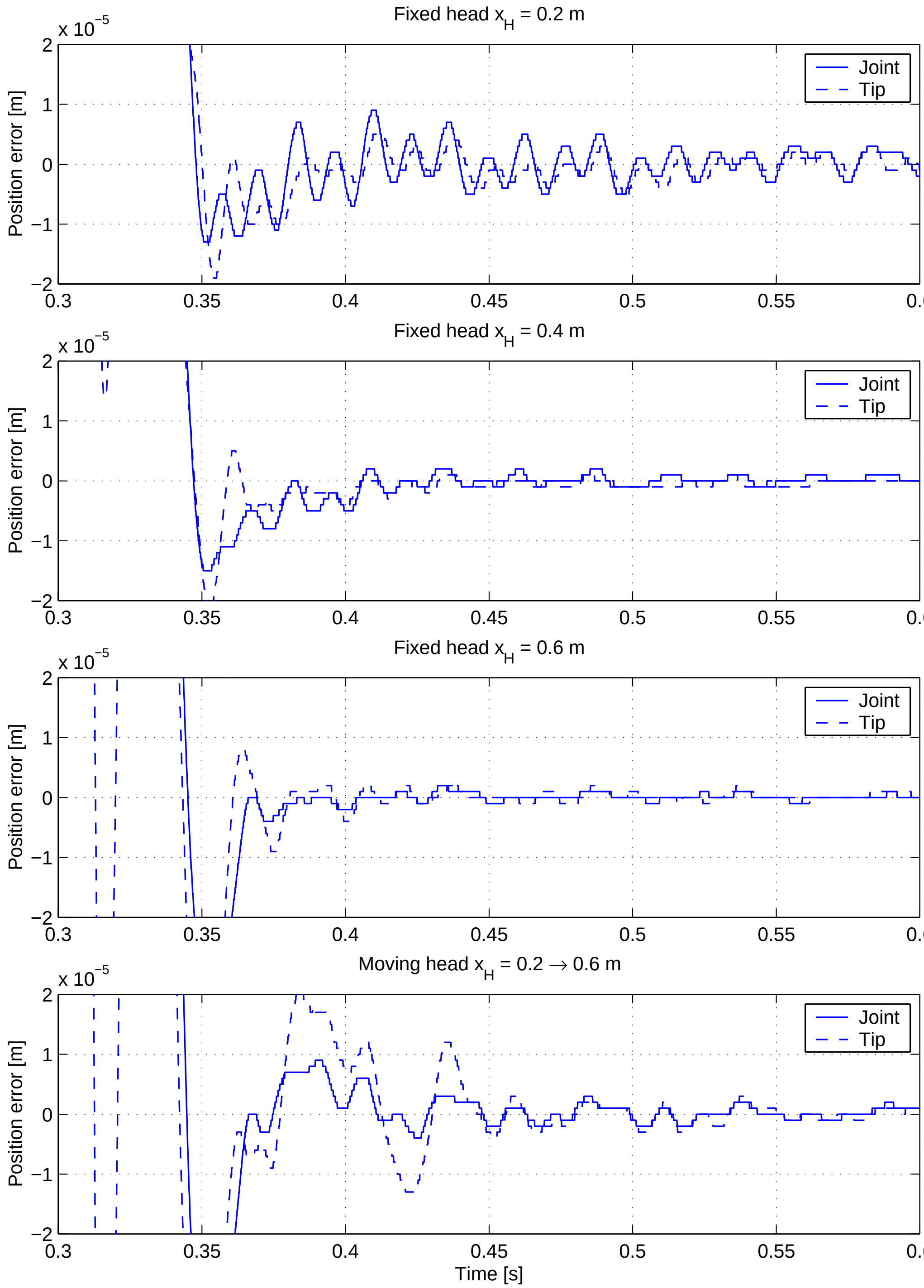

Figure 4.5: Position error of 0.5 m y-axis motion for LTI H_∞ controller, with fixed head at different locations and moving head. The bang-bang motion profile is applied.

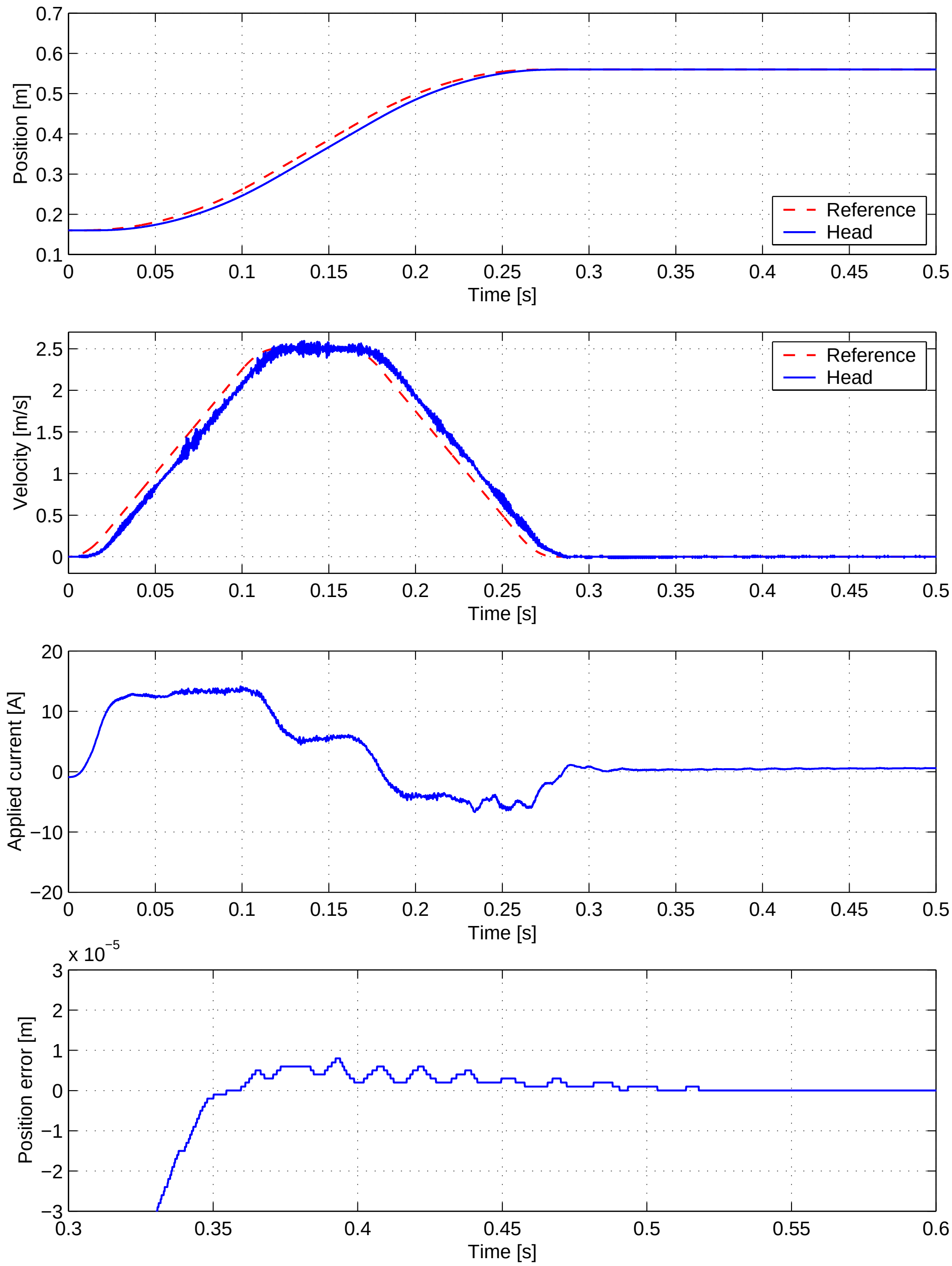

Figure 4.6: Experimental results for x-axis head motion.

4.2 Gain-Scheduled H_∞ Control

In this section, a recently developed controller design method called "Advanced gain-scheduled H_∞ control" (Apkarian and Adams [2]) is applied to y-axis motion control. A parameter-dependent and thus time-varying controller, using real-time measurement of the head position as scheduling parameter, is designed. Closed-loop performance bounds and a parameter-dependent Lyapunov function, guaranteeing closed-loop stability, are established. The large amount of online computation for the resulting controller, indicated in Apkarian and Adams [2], has been considerably reduced by an interpolation technique without changing any controller properties significantly. As in the LTI H_∞ design, performance goals have been achieved by applying loop-shaping techniques as well as by disturbance rejection and attenuation of flexible mode vibrations.

4.2.1 Theoretical Background

In contrast to the LTI H_∞ design, the problem considered now is the control of an LPV MIMO plant $G(\theta)$ with state-space realization

$$G(\theta)\left\{\begin{array}{rcl} \dot{x} & = & A(\theta)x + B_1(\theta)w + B_2(\theta)u \\ z & = & C_1(\theta)x + D_{11}(\theta)w + D_{12}(\theta)u \\ y & = & C_2(\theta)x + D_{21}(\theta)w \ . \end{array}\right. \tag{4.12}$$

The variables represent the states $x \in \mathbb{R}^n$, reference signals and disturbances $w \in \mathbb{R}^{m_1}$, control inputs $u \in \mathbb{R}^{m_2}$, outputs $z \in \mathbb{R}^{p_1}$ and measurements $y \in \mathbb{R}^{p_2}$. The matrices have corresponding dimensions and are allowed to depend on time-varying parameters $\theta(t) := [\theta_1(t), \dots, \theta_q(t)]^T$. The parameter values must be known at every time instant, for example by measurements, estimations or assumptions. The parameter trajectories are constrained only by known bounds $\underline{\theta}_i < \overline{\theta}_i$ on parameter values and known bounds $\underline{\nu}_i < \overline{\nu}_i$ on parameter variation rates according to

$$\theta_i(t) \in [\underline{\theta}_i, \overline{\theta}_i] \ , \qquad \dot{\theta}_i(t) \in [\underline{\nu}_i, \overline{\nu}_i] \qquad t \geq 0 \ , \quad i = 1, 2, \dots, q \ . \tag{4.13}$$

The parameters and parameter variation rates are thus allowed to evolve in hypercubes Θ and Θ_d, respectively. An output-feedback controller $K(\theta, \dot{\theta})$

$$K(\theta,\dot{\theta})\left\{\begin{array}{rcl} \dot{x}_K & = & A_K(\theta,\dot{\theta})x_K + B_K(\theta,\dot{\theta})y \\ u & = & C_K(\theta,\dot{\theta})x_K + D_K(\theta,\dot{\theta})y \ , \end{array}\right. \tag{4.14}$$

called a GS LPV controller, is designed to influence the closed-loop behavior in a desired way.

Controller Characterization

The presented design method for such a controller closely follows Apkarian and Adams [2]. As in LTI H_∞ control theory, the controller should guarantee closed-loop stability and an upper bound γ on the L_2-gain of the closed loop between w and z according to (4.4). But since the plant $G(\theta)$ varies with the parameters, so should the controller in order to generate the best control at every time instant. Therefore the basic idea is to use the current parameter values as scheduling parameters. Furthermore knowledge about limits of parameter variation rates $(\underline{\nu}_i, \overline{\nu}_i)$ is incorporated in the design to reduce conservatism. The controller establishes performance bounds for the closed-loop system and a parameter-varying Lyapunov function guaranteeing internal stability.

The following theorem (Apkarian and Adams [2]) gives sufficient conditions for a characterization of such a gain-scheduled LPV controller. Dependencies on θ are dropped for readability where unmistakable. The symbol $\star$ stands for the transpose of the corresponding matrix block with column and row position interchanged, such that the composite matrix is symmetric.

Theorem 4.3 *Consider the LPV plant (4.12) and parameter trajectories $\theta(t)$ constrained by (4.13). Suppose there exist parameter-dependent matrices $X(\theta) = X^T(\theta)$, $Y(\theta) = Y^T(\theta)$, $\hat{A}_K(\theta)$, $\hat{B}_K(\theta)$, $\hat{C}_K(\theta)$, $\hat{D}_K(\theta)$ such that for all permissible pairs $(\theta, \dot{\theta})$ the LMIs*

$$\left[\begin{array}{c|c|c|c} \dot{X} + XA + A^T X + \hat{B}_K C_2 + C_2^T \hat{B}_K^T & \star & \star & \star \\ \hline \hat{A}_K^T + A + B_2 \hat{D}_K C_2 & -\dot{Y} + AY + YA^T + B_2 \hat{C}_K + \hat{C}_K^T B_2^T & \star & \star \\ \hline (XB_1 + \hat{B}_K D_{21})^T & (B_1 + B_2 \hat{D}_K D_{21})^T & -\gamma I & \star \\ \hline C_1 + D_{12} \hat{D}_K C_2 & C_1 Y + D_{12} \hat{C}_K & D_{11} + D_{12} \hat{D}_K D_{21} & -\gamma I \end{array}\right] < 0$$

$$\begin{bmatrix} X & I \\ I & Y \end{bmatrix} > 0 \qquad (4.15)$$

hold. Then there exists a gain-scheduled LPV output-feedback controller (4.14) enforcing closed-loop stability and an upper bound γ on the L_2-gain of the closed-loop system according to (4.4).

The theorem guarantees the existence of a parameter-varying quadratic Lyapunov function $V(x, \theta) = x^T P(\theta) x$, where $P(\theta)$ can be constructed from $X(\theta)$ and $Y(\theta)$. If the value of γ is subject to minimization under conditions (4.15), the task of computing an LPV controller consists of solving a convex optimization problem with regard to the solution variables

$$\left(\gamma, X(\theta), Y(\theta), \hat{A}_K(\theta), \hat{B}_K(\theta), \hat{C}_K(\theta), \hat{D}_K(\theta)\right) . \qquad (4.16)$$

Note that the LMI conditions (4.15) imply an infinite number of restrictions on the solution variables, since they have to hold for *all* permissible values of θ and $\dot{\theta}$. In order to reduce these conditions to a finite number, two possibilities exist. The first alternative consists of applying so-called multi-convexity concepts, together with an appropriate functional choice of candidates for the solution matrices (4.16), see Apkarian and Tuan [5], Gahinet et al. [23]. Additional constraints ensure multi-convexity in the different coordinate directions of the parameter space. As a consequence, the LMIs (4.15) are satisfied for all permissible values of θ and $\dot{\theta}$, if they hold on the vertices of $\Theta \times \Theta_d$. This yields an augmented but finite number of LMIs.

The second possibility is a gridding procedure of the space $\Theta \times \Theta_d$. The LMIs are just sought to be satisfied at certain grid points, leading to a finite number of LMIs. The resulting values of the solution matrices and of γ may be too optimistic, since the LMIs are not considered for all pairs $(\theta, \dot{\theta})$. Therefore, the conditions (4.15) have to be checked on a very dense grid by inserting the solution (4.16) into LMIs (4.15). This verification on the dense grid typically takes much less time than a solution of the optimization on the same grid. If the verification fails, a new optimal solution has to be computed on a denser grid than the one chosen first. This procedure is repeated until (4.15) holds for some solution variables on a very dense grid.

The dependence of LMIs (4.15) on $\dot{\theta}_i$ via the term

$$\dot{X}(\theta) = \frac{d\,X}{d\,\theta}\dot{\theta}$$

is linear and therefore convex. So it is only necessary to invoke the LMIs for $\Theta \times \{\underline{\nu}_i, \overline{\nu}_i\}$ instead of $\Theta \times \Theta_d$ (Apkarian and Adams [2]).

Computation of Controller Matrices

After obtaining a solution to the convex optimization problem, the construction of controller matrices consists of two steps (Apkarian and Adams [2]). Again, dependencies on θ and $\dot{\theta}$ are omitted. First, solve for N, M the factorization problem

$$I - XY = NM \tag{4.17}$$

such that N and M are smooth, bounded, and have a bounded inverse. For example, the choices $N := I - XY$, $M := I$, or $N := X - Y^{-1}$, $M := -Y$, or $N := -X$, $M := Y - X^{-1}$ are possible (Scherer [39]). Second, compute $A_K(\theta, \dot{\theta})$, $B_K(\theta, \dot{\theta})$, $C_K(\theta, \dot{\theta})$, $D_K(\theta, \dot{\theta})$ via

$$A_K = N^{-1}\Big(X\dot{Y} + N\dot{M} + \hat{A}_K - X(A - B_2\hat{D}_K C_2)Y - \hat{B}_K C_2 Y - XB_2\hat{C}_K\Big)M^{-1} \tag{4.18}$$

$$B_K = N^{-1}\left(\hat{B}_K - XB_2\hat{D}_K\right) \tag{4.19}$$

$$C_K = \left(\hat{C}_K - \hat{D}_K C_2 Y\right)M^{-1} \tag{4.20}$$

$$D_K = \hat{D}_K\,. \tag{4.21}$$

The state-space realization of the gain-scheduled LPV output-feedback controller $K(\theta, \dot{\theta})$ is then given by (4.14).

Note the explicit dependence on the derivative of the parameter trajectory $\dot{\theta}(t)$. Since these derivatives are not always easily available, this dependence may not be desired. A simple way of eliminating the $\dot{\theta}(t)$-dependence consists of choosing either $X(\theta) := X$ or $Y(\theta) := Y$, i.e. defining one of these solution matrices to be constant (Apkarian and Adams [2]). If $Y :=$ constant and $M := I$ in (4.17), then the source of $\dot{\theta}$-dependence, $X\dot{Y} + N\dot{M}$ in (4.18), will be zero. Due to the identity $\dot{X}Y + \dot{N}M = -(X\dot{Y} + N\dot{M})$, which follows from (4.17), this is also true for setting $X :=$ constant and $N := I$ to be the identity matrix. Setting either X or Y constant introduces conservatism, however, and may lead to degraded performance.

4.2.2 Simplified Computation of Controller Matrices

In this approach to gain-scheduling, recommended by Apkarian and Adams [2], the factorization (4.17) as well as the computation of controller matrices (4.18)–(4.21) have to be carried out at each time-step. By choosing either $M := I$ or $N := I$, this can be reduced to one matrix inversion and several matrix multiplications and additions. Moreover, the design plant (4.12) with its parameter-dependence has to be stored in a memory such that it can be reconstructed for any value of θ. These computations are likely to generate quantization errors and require a considerable amount of online computation, which may even not be executable in the available time interval. Discretization of the controller matrices following (3.14) demands additional computation effort at each time-step. To reduce these online computation requirements, a modification of the procedure is proposed for the case of a one-dimensional parameter space. An extension to higher-dimensional parameter spaces is straightforward, but may create disadvantages because of the exponential increase in complexity.

Since the equations (4.18)–(4.21) imply a nonlinear but continuous dependence of the controller matrices on θ, and a linear dependence on $\dot{\theta}$, one approach to save online computation power is a piecewise linear approximation of this dependence. The one-dimensional parameter interval is divided into $q-1$ uniform subintervals with boundary points

$$\underline{\theta} =: \theta_1 < \theta_2 < \cdots < \theta_q := \overline{\theta} \tag{4.22}$$

and interval lengths $\Delta\theta := \theta_2 - \theta_1 = \theta_3 - \theta_2 = \ldots$. Note that the indices do not denote different components of θ anymore, but rather enumerate the several boundary points. Due to linear dependence on $\dot{\theta}$, the parameter variation rate interval needs only to be bounded by the two points $\theta_{d1} := \underline{\nu}$ and $\theta_{d2} := \overline{\nu}$.

By offline computation, $2q$ controller matrices

$$\mathcal{K}_{i,j} := \left[\begin{array}{c|c} A_K(\theta_i, \theta_{dj}) & B_K(\theta_i, \theta_{dj}) \\ \hline C_K(\theta_i, \theta_{dj}) & D_K(\theta_i, \theta_{dj}) \end{array}\right], \quad i = 1, 2, \ldots, q, \quad j = 1, 2 \tag{4.23}$$

are generated via (4.17)–(4.21). Then the controller matrices of the gain-scheduled controller can be computed online by a two-dimensional interpolation. The following procedure has to be carried out at each time step instead of applying (4.17)–(4.21). First, the subinterval κ is located such that the current measurement $\theta(t) \in [\theta_\kappa, \theta_{\kappa+1})$:

$$\kappa = \left(\text{integer part of } \frac{\theta(t) - \underline{\theta}}{\Delta\theta}\right) + 1 \ . \tag{4.24}$$

The weight for θ-interpolation is then readily computed from $\theta(t)$ as

$$\eta = \frac{\theta(t) - \theta_\kappa}{\theta_{\kappa+1} - \theta_\kappa} \ . \tag{4.25}$$

From the current value of $\dot{\theta}(t)$, the weight for $\dot{\theta}$-interpolation is computed as

$$\eta_d = \frac{\dot{\theta}(t) - \theta_{d1}}{\theta_{d2} - \theta_{d1}} \ . \tag{4.26}$$

Note that $\eta \in [0,1)$ and $\eta_d \in [0,1)$. The controller matrices of (4.14) at each time-step,

$$\mathcal{K}\left(\theta(t), \dot{\theta}(t)\right) := \left[\begin{array}{c|c} A_K(\theta(t), \dot{\theta}(t)) & B_K(\theta(t), \dot{\theta}(t)) \\ \hline C_K(\theta(t), \dot{\theta}(t)) & D_K(\theta(t), \dot{\theta}(t)) \end{array}\right] , \tag{4.27}$$

are then obtained through a two-dimensional interpolation of the four corresponding pre-computed matrix structures with the formula

$$\mathcal{K}\left(\theta(t), \dot{\theta}(t)\right) = (1-\eta_d)\left((1-\eta)\mathcal{K}_{\kappa,1} + \eta\mathcal{K}_{\kappa+1,1}\right) + \eta_d\left((1-\eta)\mathcal{K}_{\kappa,2} + \eta\mathcal{K}_{\kappa+1,2}\right) \ . \tag{4.28}$$

According to this formula, there are only three matrix additions to be carried out at each time step besides some scalar multiplications. All other computations are done offline during controller construction. Of course, the piecewise linear approach yields only an approximation to the LPV controller with nonlinear parameter dependence, but by means of q, the number of interval boundary points, this approximation can be arbitrarily close. Moreover, discretization of the $2q$ LTI controllers is now also done offline, which means that no additional effort for discretization is necessary at run-time. If the parameter variation rate $\dot{\theta}$ is small or zero, the formula can be transformed to a one-dimensional interpolation by setting $\eta_d \equiv -\theta_{d1}/(\theta_{d2} - \theta_{d1})$.

For practical implementation, q may be determined heuristically as small as possible in order to still yield a satisfying approximation of the original nonlinear controller. Further refinement of the approximation could result from a non-uniformly spaced grid over the parameter range.

4.2.3 Design Methodology

As in the LTI H_∞ case, loop-shaping techniques as well as weights for vibration damping, disturbance attenuation and robustness considerations are applied. Several approaches to GS LPV H_∞ control are illustrated:

- GS design 1: Feedback of beam joint position error, feedforward of position reference command, use of a second-order weighting function for loop-shaping and inclusion of an integrator for zero steady-state error.
- GS design 2: Feedback of beam joint position error, feedforward of position reference command and use of a first-order weighting function for loop-shaping, resulting in a reduced-order controller.
- GS design 3: Feedback of beam joint and tip position errors, feedforward of position reference command and use of a first-order weighting function for loop-shaping.

Approaches which led to infeasible LMIs or bad performance included:

- Using error feedback only and not including the feedforward part.
- Assuming a polytopic θ-dependence of the beam model as in Yang [45].
- Applying multi-convexity concepts instead of gridding (Apkarian and Tuan [5]).

All controller tuning for the GS approach was performed as in the LTI H_∞ case.

GS Design 1

The first GS design investigated follows the ideas applied for LTI H_∞ control. The controller synthesis diagram is shown in Figure 4.7, where now the beam model and the controller depend on the head position. The integrator filter is defined as in (4.8), the weight W_{z1} as in (4.9). The external inputs and outputs of the control system are respectively combined into the vectors w and z as in (4.10), and the controller inputs into the vector y as in (4.11). With Figure 4.7, the control system can be transformed into the form (4.12). Only A and B_1 depend on the single parameter $\theta(t) = x_H(t)$.

For simulations and experiments, the design parameters were set to $\omega := 450$, $\zeta := 0.9$, $c_I := 1100$, $W_{d1} := 2000$, $W_{d2} := 0.3$, $W_{z3} := 5$. The output z_2 was finally not utilized because (i) robustness can be adjusted with W_{d2}, (ii) a reasonable choice of reference commands as in Section 3.6 results in a moderate control output, and (iii) use of z_2 results in bad performance due to early termination of the LMI optimization process.

Before applying the LMIs (4.15), a functional relationship for the solution matrices (4.16) has to be chosen. After experimenting with different possibilities, for example

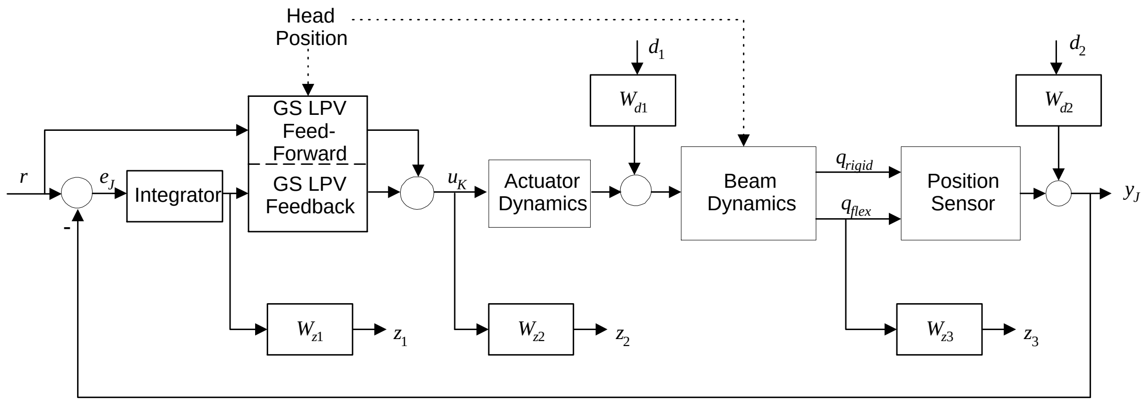

Figure 4.7: Synthesis diagram for GS design 1, with reference signal r, disturbances d_1, d_2, controller output u_K, generalized coordinates of rigid mode q_{rigid} and of flexible modes q_{flex}, joint position y_J, error signal e_J, and external outputs z_1, z_2, z_3.

using trigonometric functions to mirror the θ-dependence of the beam, a simple linear dependence was best suited to achieve the control objectives. Thus,

$$X(\theta) := X_0 + \theta X_1 \ , \tag{4.29}$$

where X_0 and X_1 are constant symmetric matrices. An analogous relationship was established for $Y(\theta)$, $\hat{A}_K(\theta)$, $\hat{B}_K(\theta)$ and $\hat{C}_K(\theta)$. D_K was set to be the zero matrix in advance, because the results improved considerably with this action. Since in the gantry robot application the derivative of the parameter can be easily obtained through a dynamic filter on the parameter value, the θ-dependence was kept for both X and Y.

A complication was experienced through the numerical properties of the solution matrices. Their condition numbers were very large, and virtually resulted in discontinuities of the controller matrix coefficients at the borders of the parameter range. The only effective bypass to this problem was an increase of the considered parameter range to $x_H \in [0.18\,\text{m},\, 0.65\,\text{m}]$ for the convex optimization, but still applying the resulting controller only to $x_H \in [0.2\,\text{m},\, 0.6\,\text{m}]$. The LMIs (4.15) on the grid $\Theta \times \Theta_d$ with

$$\Theta := \{0.18,\, 0.2,\, 0.3,\, 0.4,\, 0.5,\, 0.6,\, 0.65\}\ \text{m}\ , \quad \Theta_d := \{-3.5,\, 3.5\}\ \text{m/s} \tag{4.30}$$

were utilized for convex optimization, which yielded the solution matrices (4.16). The *LMI Toolbox* of *MATLAB* [24] was used for programming customized LMIs and for convex optimization. The LMIs were validated on a grid $\Theta \times \Theta_d$ with $\Theta := \{0.2, 0.201, \ldots, 0.6\}$ m and $\Theta_d := \{-3.5,\, 3.5\}$ m/s for $\gamma = 5.48$.

GS Design 2

The second GS design tries to achieve the same goals as GS design 1 with a reduced order controller. The controller synthesis diagram is shown in Figure 4.8. As a difference to the previous GS design, the integrator filter is not used. Furthermore the

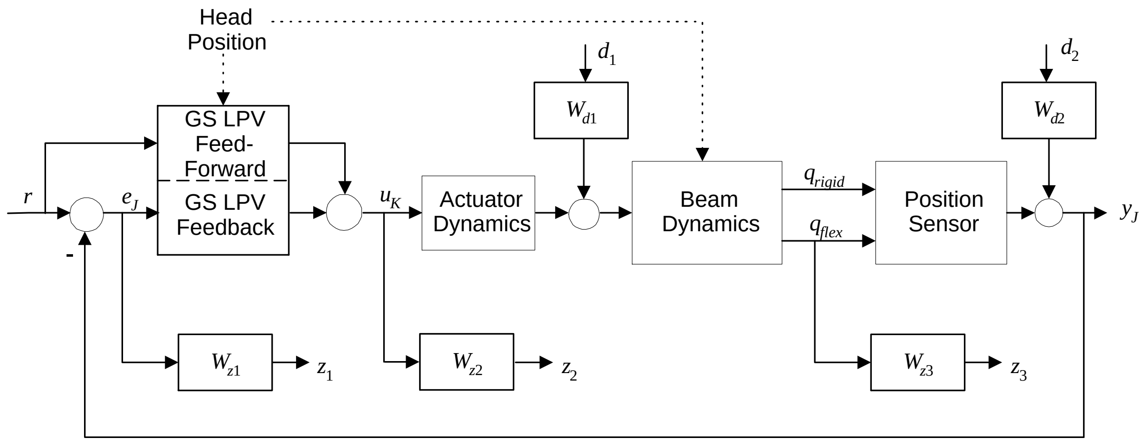

Figure 4.8: Synthesis diagram for GS design 2, with reference signal r, disturbances d_1, d_2, controller output u_K, generalized coordinates of rigid mode q_{rigid} and of flexible modes q_{flex}, measured output y_J, error signal e_J, and external outputs z_1, z_2, z_3.

weight W_{z1} is chosen to be the inverse of the desired sensitivity function

$$S_d(s) = \frac{s + 0.997475 \cdot 10^{-7}\omega}{s + 0.997475\omega}\ , \tag{4.31}$$

a first-order weight. This transfer function results in a closed-loop behavior with bandwidth $\approx \omega$, and steady-state error according to $S_d(0) = 10^{-7}$. A Bode magnitude plot of $S_d(s)$ is shown in Figure 4.9. The external inputs and outputs of the control system are respectively combined into the vectors w and z,

$$\begin{aligned} w &:= [r, d_1, d_2]^T \\ z &:= [z_1, z_2, z_3]^T = [W_{z1}(s)e_J(s), W_{z2}u_K(s), W_{z3}q_{flex}(s)]^T\ . \end{aligned} \tag{4.32}$$

The controller inputs and outputs are

$$y := [r, e_J]^T\ , \qquad u := u_K\ , \tag{4.33}$$

respectively, where the joint position error is defined as $e_J(t) = r(t) - y_J(t)$. With Figure 4.8, the control system can be transformed into the form (4.12). Again only A and B_1 depend on the single parameter $\theta(t) = x_H(t)$.

For simulations and experiments, the design parameters were set to $\omega := 400$, $W_{d1} := 2000$, $W_{d2} := 0.5$, $W_{z3} := 5$. As in the previous design, the output z_2 was not utilized. The structure of solution matrices was defined as a linear dependence on θ as in (4.29), and D_K was set to zero. Also as before, the LMIs (4.15) were applied with the gridding (4.30). The LMIs were validated on a grid $\Theta \times \Theta_d$ with $\Theta := \{0.2, 0.201, \ldots, 0.6\}$ m and $\Theta_d := \{-3.5,\ 3.5\}$ m/s for $\gamma = 9.52$.

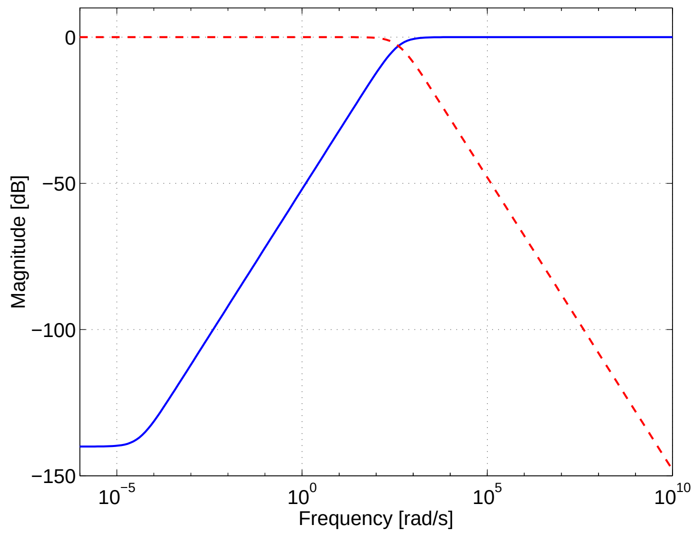

Figure 4.9: Desired first-order closed-loop behavior, expressed as Bode magnitude plots of sensitivity (–) and complimentary sensitivity (- -). The sensitivity is given by (4.31) with $\omega = 400$.

GS Design 3

The third approach to GS H_∞ control includes beam tip position as additional feedback. The tip sensor signal gives direct information about the possible bending of the beam and could increase control over structural vibrations further. Still, a force to the beam is only applied at the joint. The control system structure has strong similarities to GS design 2 from Figure 4.8. To include the tip position error, the feedback signal e_J is replaced by the vector

$$e := [e_J,\, e_T]^T = [r - y_J,\, r - y_T]\ .$$

Furthermore, the weight W_{z1} has to be adjusted. A direct approach would be to apply two separate weights $W_{z1,J}(s) := S_d^{-1}(s)$ and $W_{z1,T}(s) := S_d^{-1}(s)$ to the error signals e_J and e_T, respectively. This approach was not applicable for optimization, yielding values of $\gamma \approx 10^7$ for a variety of different choices for the design parameters. Instead, the weight W_{z1} is defined as

$$W_{z1} := S_d^{-1}(s) \cdot [0.75,\, 0.25]\ . \tag{4.34}$$

This results in a weighted sum of joint and tip position errors being filtered by the inverse desired sensitivity. A drawback of this approach is that one might expect non-zero steady-state errors of different sign for joint and tip. However, due to the weighting of the error signal sum, desired accuracies are still achieved. With Figure 4.8, the control system can be transformed into the form (4.12). Again only A and B_1 depend on the single parameter $\theta(t) = x_H(t)$.

For experimental implementation, the design parameters were set to $\omega := 450$, $W_{d1} := 2000$, $W_{d2} := 0.1$, $W_{z3} := 4$. Again, the output z_2 was not utilized. The structure of solution matrices was defined as a linear dependence on θ as in (4.29), and D_K was set to zero. The LMIs (4.15) were applied with the gridding (4.30). The solution was validated on a grid $\Theta \times \Theta_d$ with $\Theta := \{0.2, 0.201, \ldots, 0.6\}$ m and $\Theta_d := \{-3.5,\ 3.5\}$ m/s for $\gamma = 6.12$. As in the LTI case, robust stability with respect to higher bending modes could be shown with small-gain arguments for these three GS design approaches, but provided no valuable insights for the design and tuning process.

Controller Implementation

For all three GS designs, the controller matrices (4.23) are computed from the solution matrices (4.16) on a grid (q=41)

$$\{\theta_1 = 0.2\,\mathrm{m},\ 0.21\,\mathrm{m}, \ldots, 0.6\,\mathrm{m} = \theta_{41}\} \times \{\theta_{d1} = -3.5\,\mathrm{m/s},\ 3.5\,\mathrm{m/s} = \theta_{d2}\}\ .$$

These 82 LTI controllers are discretized with the zero-order hold method (3.14) and a sampling time of $T = 10^{-4}$ s to obtain (4.27). By means of formula (4.28), the actual controller matrices are computed depending on the current value of head position and velocity. Head position is obtained by a position sensor in real-time, whereas head velocity is estimated from the position signal by a filter according to (3.12). With this procedure, not only the online computation time for formulas (4.18)–(4.21) is saved, but also the online discretization with (3.14) has not to be carried out. Instead, only some scalar multiplications and three matrix additions are to be performed at every time step.

A controller discretization via trapezoidal approximation was applied for comparative reasons, and yielded the same performance as the ZOH discretization for this particular choice of sampling time T. The trapezoidal approximation method yielded better performance than the ZOH method in simulations at lower sampling rates, however. Initial conditions of the controllers are defined according to Section 4.1.2.

4.2.4 Experimental Results

In this section, experimental results for a beam motion of 0.5 m are presented. They give an indication of performance, strengths and weaknesses of the three GS H_∞ designs.

GS Design 1

Figure 4.10 shows the closed-loop response with simultaneous head movement for the smooth motion profile, including joint position, joint velocity estimation, applied current, and position error of joint and tip. As with the LTI H_∞ controller, a transient response is obtained instead of perfect tracking. Comparing the applied-current curve to the LTI case, one observes increased controller activity near the end of the motion due to gain-scheduling. This is also reflected in the position error plot. However, the maximum error is now about 2.2 cm.

A zoomed view of the position error, for fixed head at three locations as well as for the moving-head case, is shown in Figure 4.11. As in the LTI case, zero steady-state error up to measurement accuracy is achieved. Again, structural vibrations along the beam are well damped. In contrast to the LTI case, this is now also true even when applying the bang-bang motion command, as shown in Figure 4.12. For a comparison of settling times and vibration suppression see Section 4.3.

GS Design 2

Figure 4.13 shows the closed-loop response with simultaneous head movement for the smooth motion profile, including joint position, joint velocity estimation, applied current, and position error of joint and tip. Zoomed views of the position errors are shown in Figures 4.14 and 4.15 for smooth and bang-bang motions, respectively. The difference to GS design 1 is the occurrence of slight structural vibrations in the moving-head cases. However, these vibrations are of very low amplitude and degrade settling times only minimally. Settling times and vibration suppression are compared in Section 4.3.

GS Design 3

Figure 4.16 shows the closed-loop response with simultaneous head movement for the smooth motion profile, including joint position, joint velocity estimation, applied current, and position error of joint and tip. A zoomed view of the position error, for fixed head at three locations as well as for the moving-head case, is shown in Figure 4.17. Due to the particular design of joint plus tip position feedback, zero steady-state error is not achieved for GS design 3. However, in steady-state the error is inside the required ± 10 μm corridor always. Structural vibrations along the beam are well damped for the fixed head cases, but some vibration occurs with moving head. When using the bang-bang motion command (Figure 4.18), vibrations are well-damped only for the head being at $x_H = 0.2$ m. The achieved settling times are still within acceptable limits, though.

By using tip position feedback in addition to the joint position measurement, an improvement of settling times compared to the other GS designs may have been expected. The somewhat disappointing results are possibly due to punishment of a weighted sum of joint and tip position errors, instead of penalizing the two error signals separately. Settling times and vibration suppression in relation to the other control approaches are discussed in the following section.

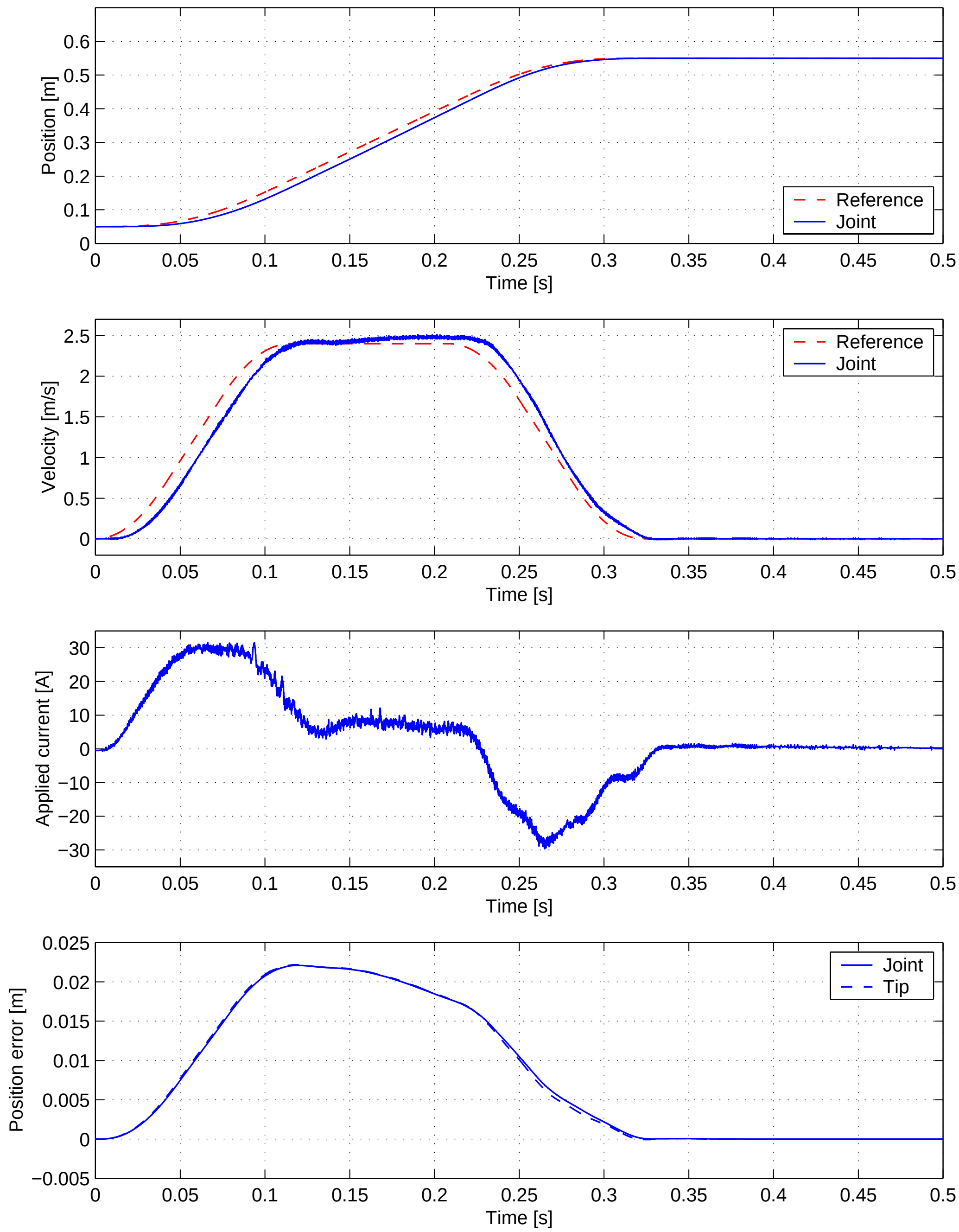

Figure 4.10: Experimental results of 0.5 m y-axis motion for GS H_∞ controller 1, moving head from x_H=0.2 $\rightarrow$ 0.6 m. The smooth motion profile is applied.

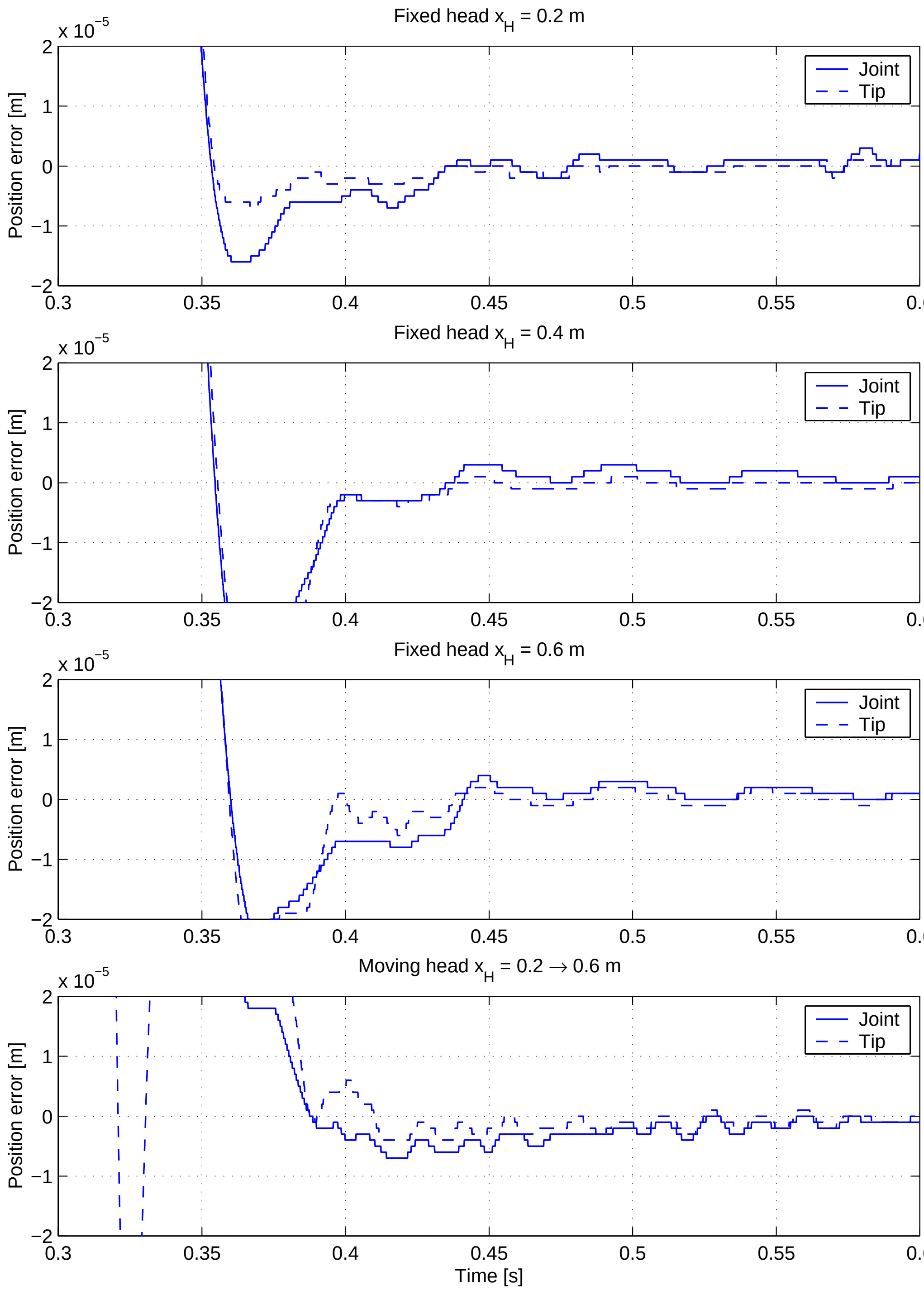

Figure 4.11: Position error of 0.5 m y-axis motion for GS H_∞ controller 1, with fixed head at different locations and moving head. The smooth motion profile is applied.

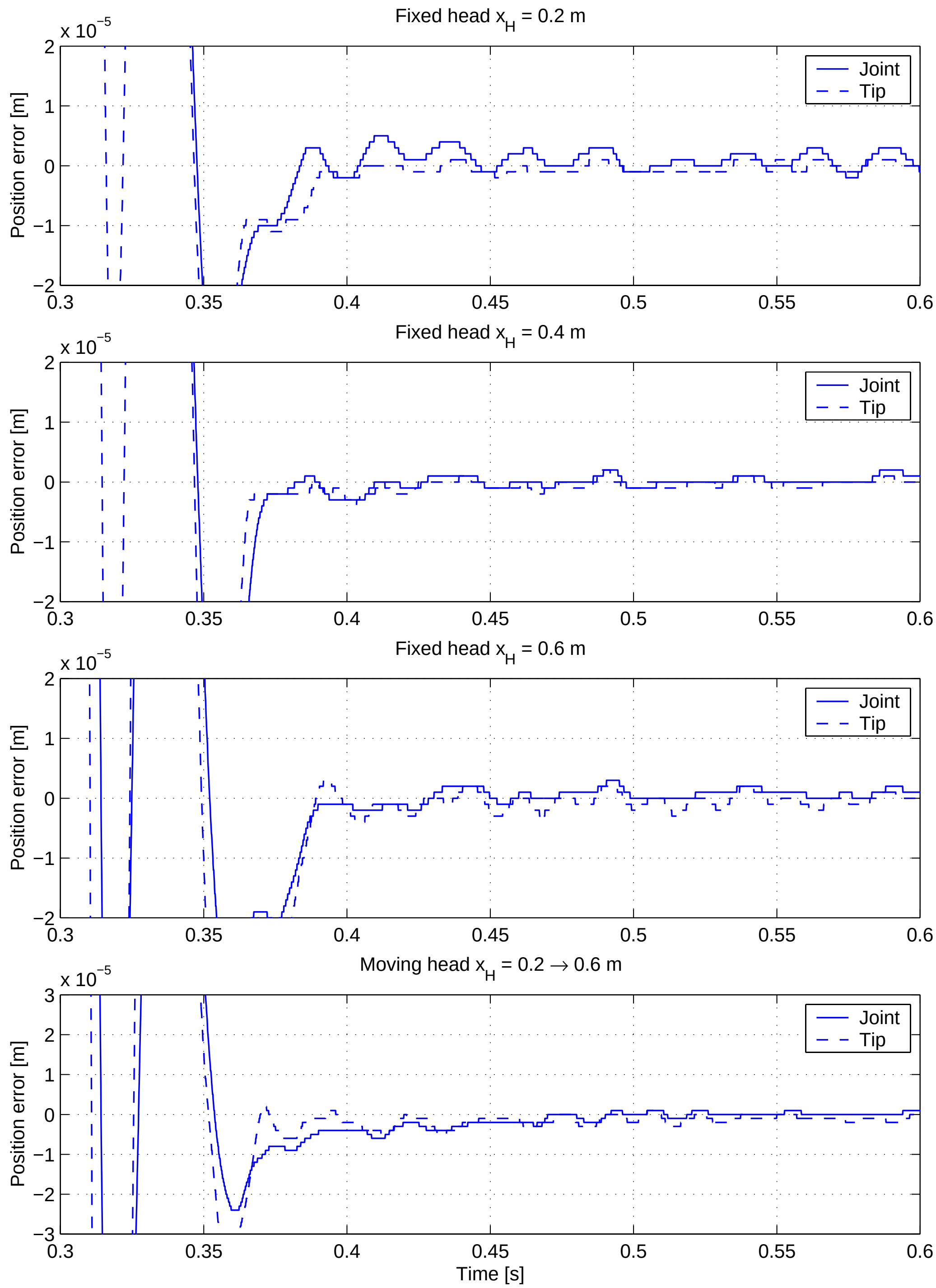

Figure 4.12: Position error of 0.5 m y-axis motion for GS H_∞ controller 1, with fixed head at different locations and moving head. The bang-bang motion profile is applied.

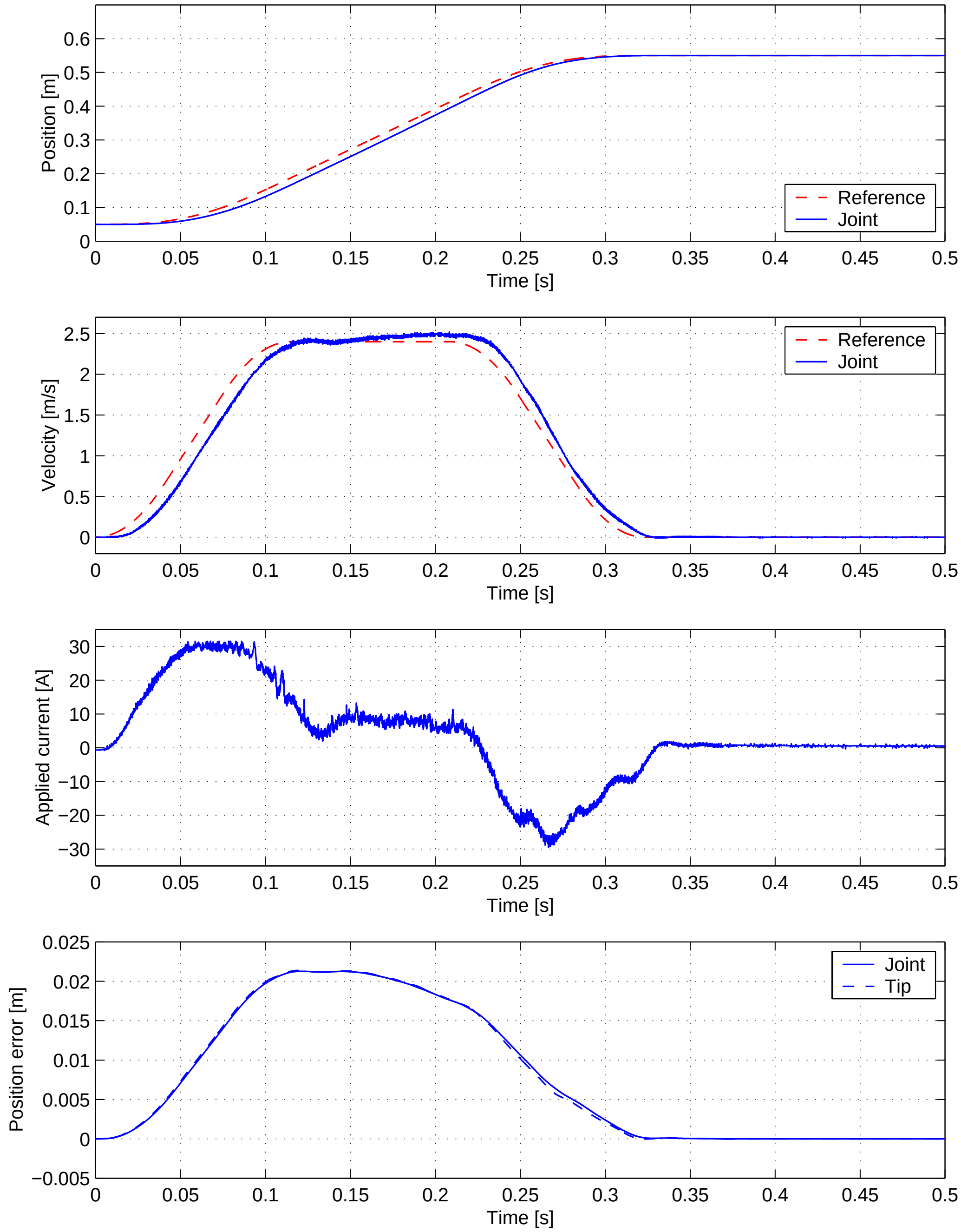

Figure 4.13: Experimental results of 0.5 m y-axis motion for GS H_∞ controller 2, moving head from x_H=0.2 $\rightarrow$ 0.6 m. The smooth motion profile is applied.

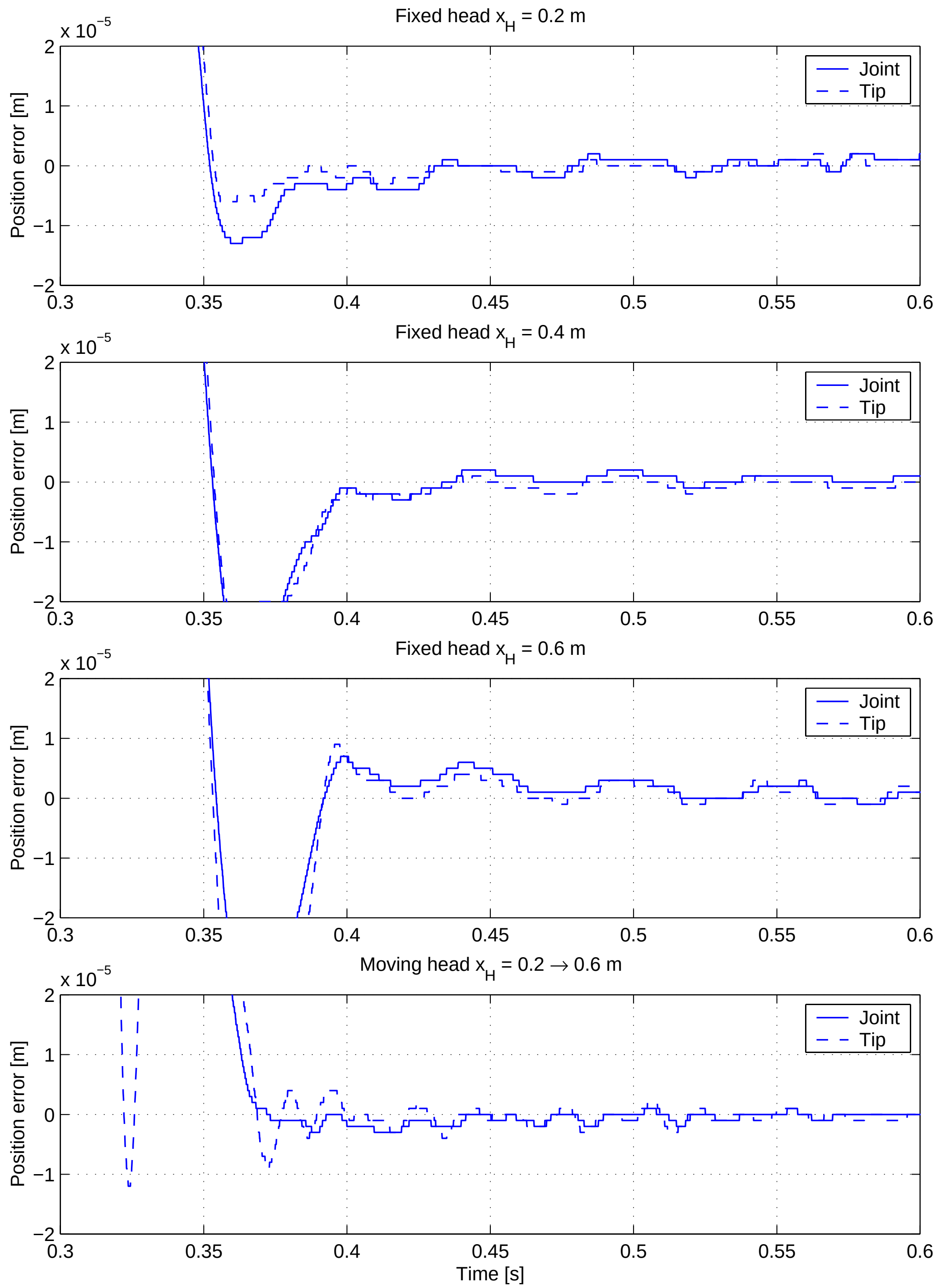

Figure 4.14: Position error of 0.5 m y-axis motion for GS H_∞ controller 2, with fixed head at different locations and moving head. The smooth motion profile is applied.

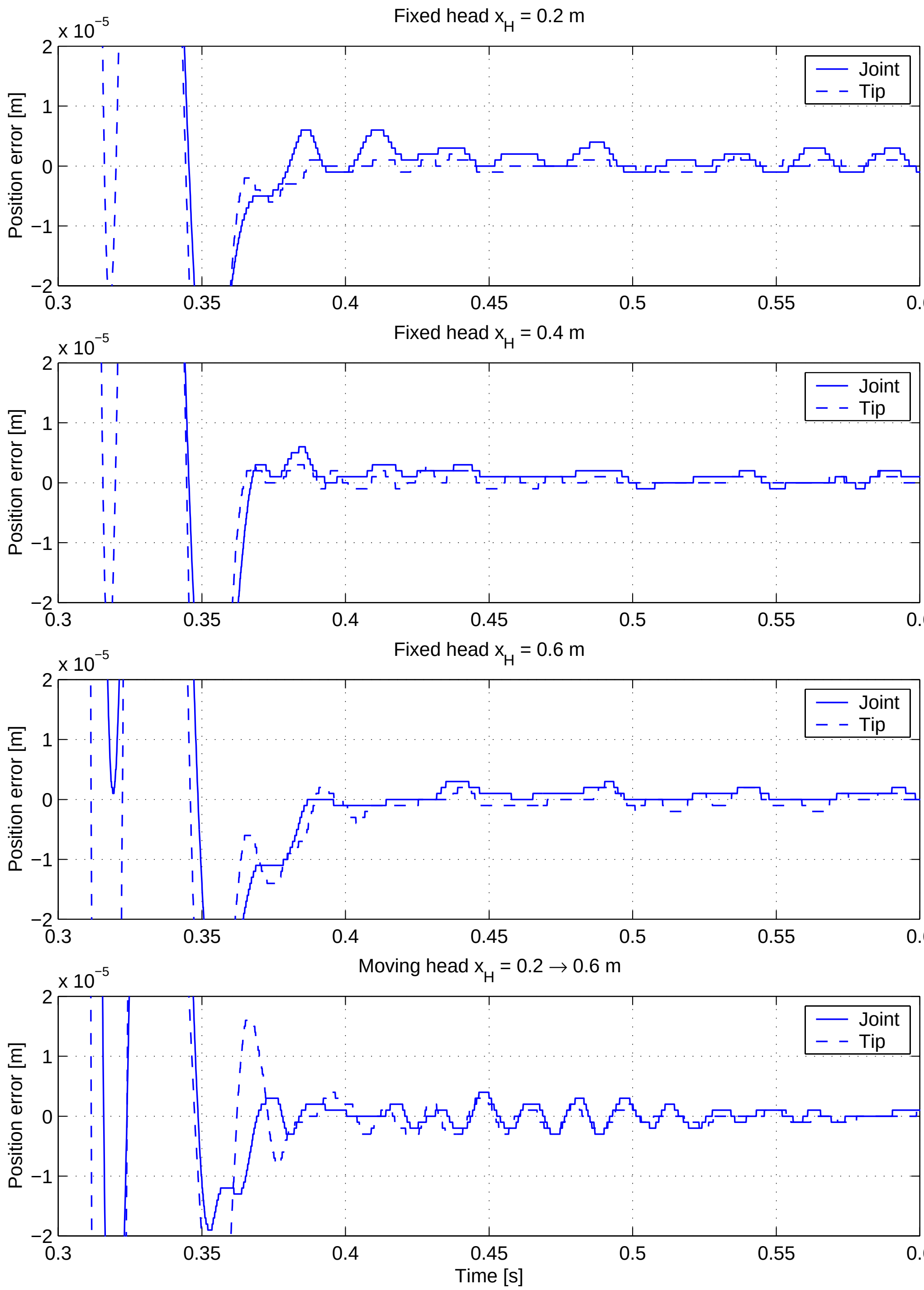

Figure 4.15: Position error of 0.5 m y-axis motion for GS H_∞ controller 2, with fixed head at different locations and moving head. The bang-bang motion profile is applied.

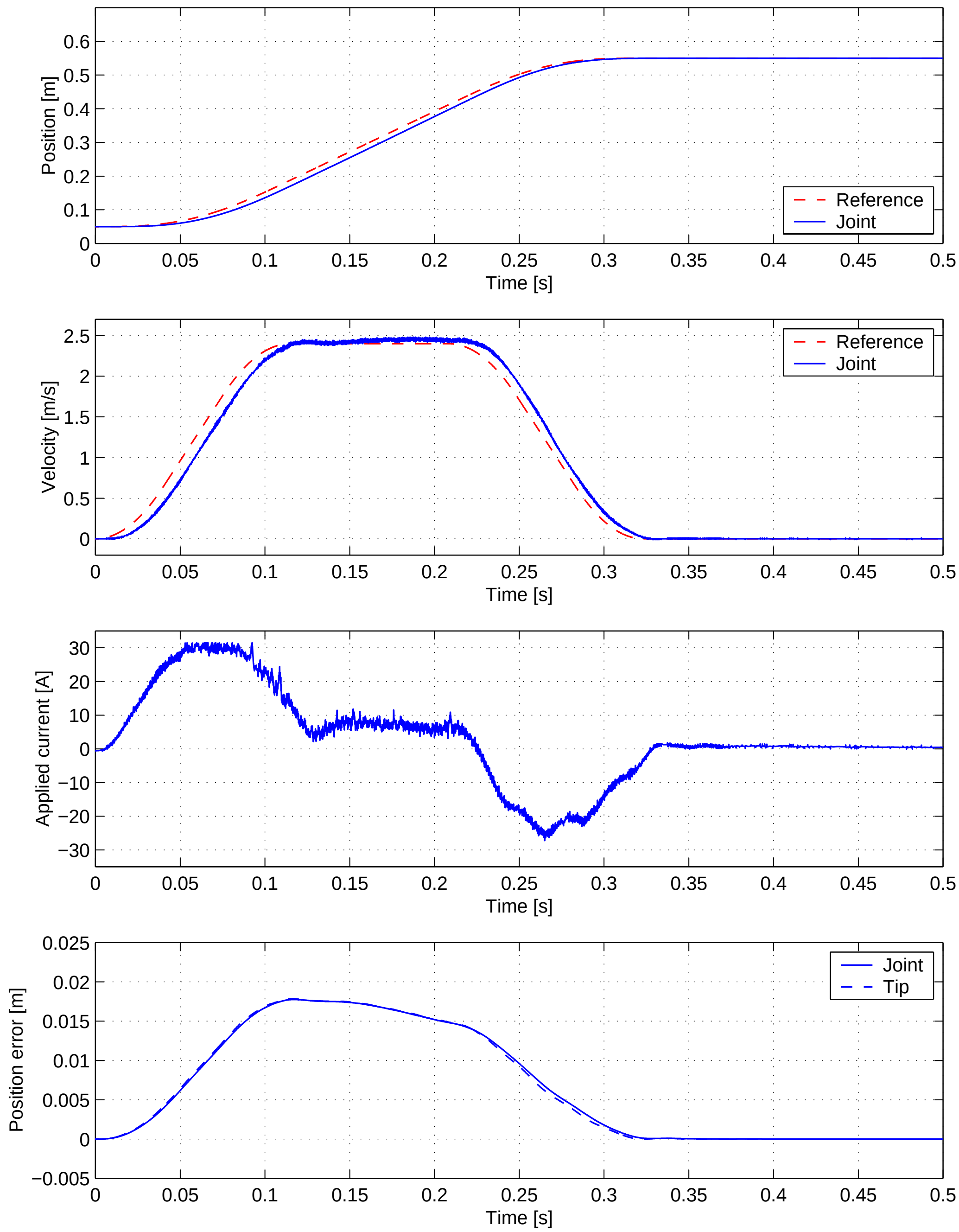

Figure 4.16: Experimental results of 0.5 m y-axis motion for GS H_∞ controller 3, moving head from x_H=0.2 → 0.6 m. The smooth motion profile is applied.

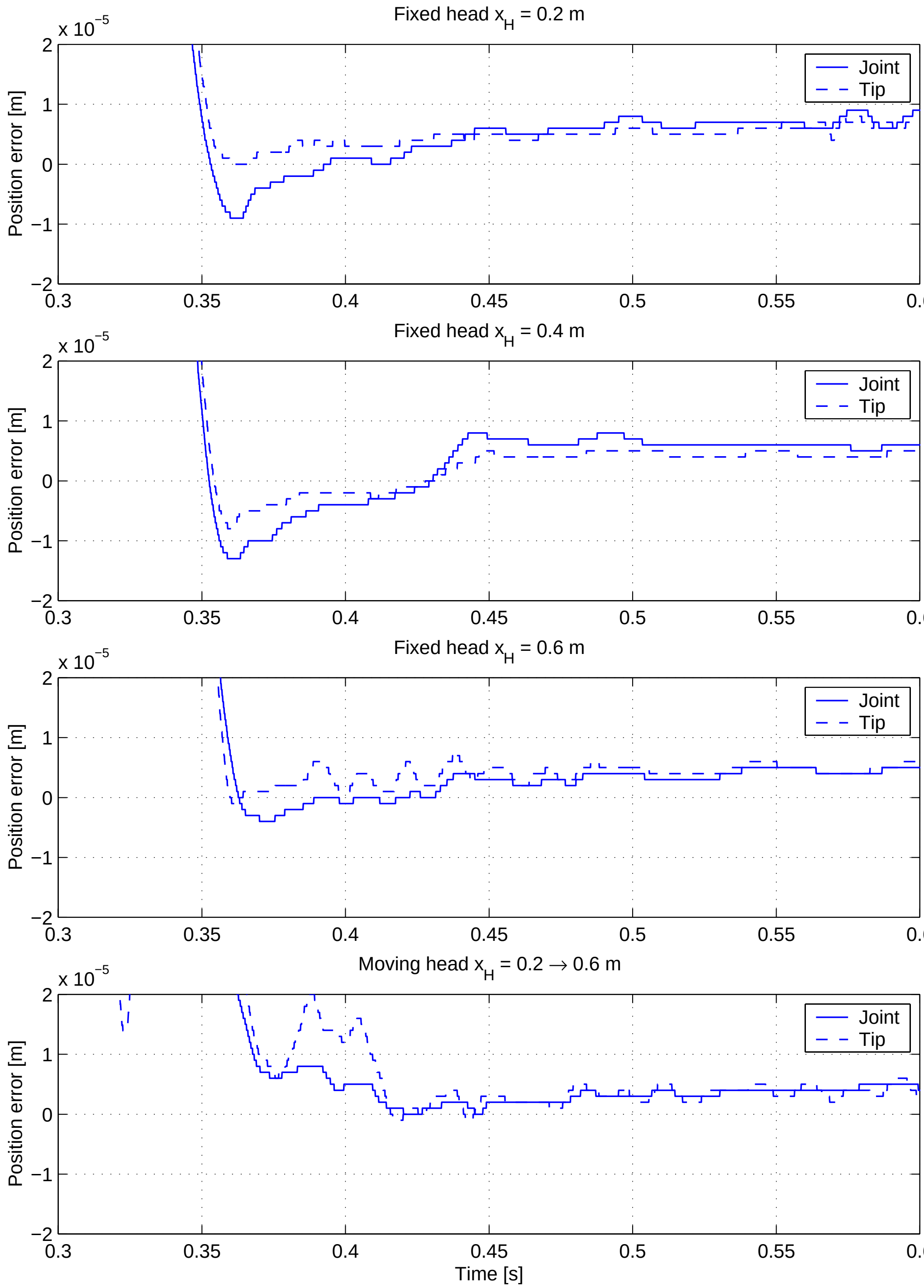

Figure 4.17: Position error of 0.5 m y-axis motion for GS H_∞ controller 3, with fixed head at different locations and moving head. The smooth motion profile is applied.

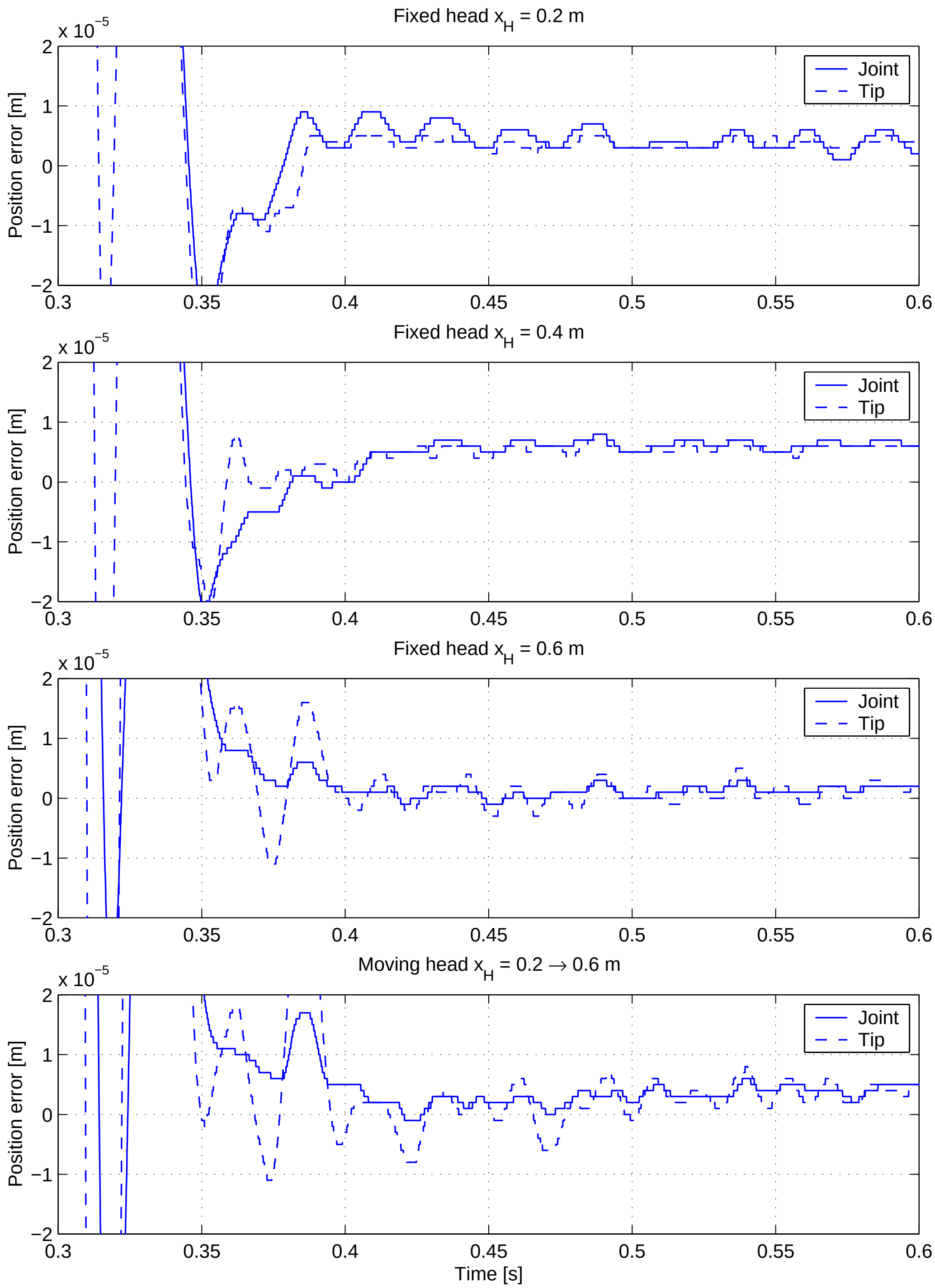

Figure 4.18: Position error of 0.5 m y-axis motion for GS H_∞ controller 3, with fixed head at different locations and moving head. The bang-bang motion profile is applied.

4.3 Comparison of Different Approaches

In this section, the different controllers' ability to achieve fast positioning of the beam as well as good suppression of structural bending vibrations is discussed. Closed-loop performance is evaluated with respect to the smooth and the bang-bang reference commands. In order to get a more complete view of the controllers' strengths and weaknesses, motions of different distance are investigated. A perspective on the shape of a favorable motion profile can also be obtained from these results.

Due to the high stiffness of the prototype beam, structural vibrations are not easily excited by smooth and relatively non-aggressive motions. Instead, motion profiles with (nearly) bang-bang behavior for acceleration have to be applied in order to fully test vibration damping capabilities of controllers. From the results of these aggressive motions, controller performance for more flexible beams is "extrapolated" to a certain extent. Therefore, two kinds of conclusions can be obtained by comparison of the experimental results: statements about control of this particular prototype gantry robot, and statements about a more general class of gantry robots with beams of possibly lower stiffness.

Settling Times of 0.5 m Beam Motion

From Figures 4.3 to 4.5 and 4.10 to 4.18, ± 10 μm settling times are summarized in Tables 4.1 (smooth motion) and 4.2 (bang-bang motion). Several trends and conclusions are revealed by these data. Considering the smooth motion, all controllers achieve good conformance of joint and tip settling times for fixed head, whereas GS design 3 has slight advantages over the others. In the practically more relevant case of moving head, the tip settling times differ by 1 % or less from the joint settling times for all controllers except for GS design 3, where the margin is 11 %. This means that with GS design 3, structural bending vibrations have a large degrading effect on performance. GS design 2 shows the best performance for simultaneously moving head, although LTI H_∞ is quite close.

With respect to bang-bang motion, LTI H_∞ shows decent performance for fixed head, whereas in the moving-head case performance degrades heavily. The tip settling time is increased by 21 % compared to joint settling time. The GS controllers on the other hand have margins of less than 1.5 % between joint and tip settling times. Especially the numbers of GS design 2 consistently differ by less than 6 ms. In both the smooth and the bang-bang motion cases, no controller shows large sensitivity of settling times with respect to head position for fixed head, although there is a general tendency for increased settling time when the head position is increased.

The settling times of LTI H_∞ and GS design 2 (apparently the best GS approach) are visualized in Figure 4.19. For each bar the worse number of joint or tip settling time is taken. The LTI H_∞ has a slight advantage for fixed head, whereas in the practically more relevant case of moving head, GS design 2 has an edge over LTI H_∞. But their performance is close to each other. In contrast, the bang-bang motion experiments show problems of the LTI H_∞ controller with structural vibrations in the moving-head case, the settling time being about 18 % larger than for GS design. The GS controller has constantly low settling times throughout the figure on the other hand. From Figure 4.6, the ± 10 μm settling time for 0.4 m head motion is 342 ms, which is below all of the settling times for 0.5 m beam motion. Since the head reaches its destination first with respect to its x-coordinate, the whole effort of obtaining a low settling time with respect to its y-coordinate becomes significant at all.

Two conclusions may be derived from these observations. First, for a 0.5 m motion on this particular gantry robot with its very stiff beam, the LTI H_∞ controller might be most appropriate due to its performance and relative simplicity compared to GS H_∞ controllers. Second, the GS H_∞ approach may provide more uniform behavior and enhanced vibration damping even for aggressive trajectories and/or beams of lower stiffness than the prototype beam. As mentioned before, such a statement is "extrapolated" from the obtained results, and still has to be verified via experiments with a re-engineered beam.

± 10 μm settling times [ms] for smooth 0.5 m beam/head motion								
Head	0.2 m		0.4 m		0.6 m		0.2 m $\to$ 0.6 m	
Measurement	Joint	Tip	Joint	Tip	Joint	Tip	Joint	Tip
LTI H_∞	352	354	365	351	379	381	372	371
GS LPV H_∞ 1	376	352	391	390	393	391	380	384
GS LPV H_∞ 2	372	352	385	388	387	389	363	366
GS LPV H_∞ 3	349	351	366	352	359	357	368	409

Table 4.1: Settling times of joint and tip positions for 0.5 m motion, for different fixed head positions and moving head. The smooth motion profile is applied.

± 10 μm settling times [ms] for bang-bang 0.5 m beam/head motion								
Head	0.2 m		0.4 m		0.6 m		0.2 m $\to$ 0.6 m	
Measurement	Joint	Tip	Joint	Tip	Joint	Tip	Joint	Tip
LTI H_∞	377	357	361	356	363	360	363	438
GS LPV H_∞ 1	369	378	368	364	383	384	370	367
GS LPV H_∞ 2	364	362	365	362	378	379	365	370
GS LPV H_∞ 3	361	374	360	356	356	391	391	393

Table 4.2: Settling times of joint and tip positions for 0.5 m motion, for different fixed head positions and moving head. The bang-bang motion profile is applied.

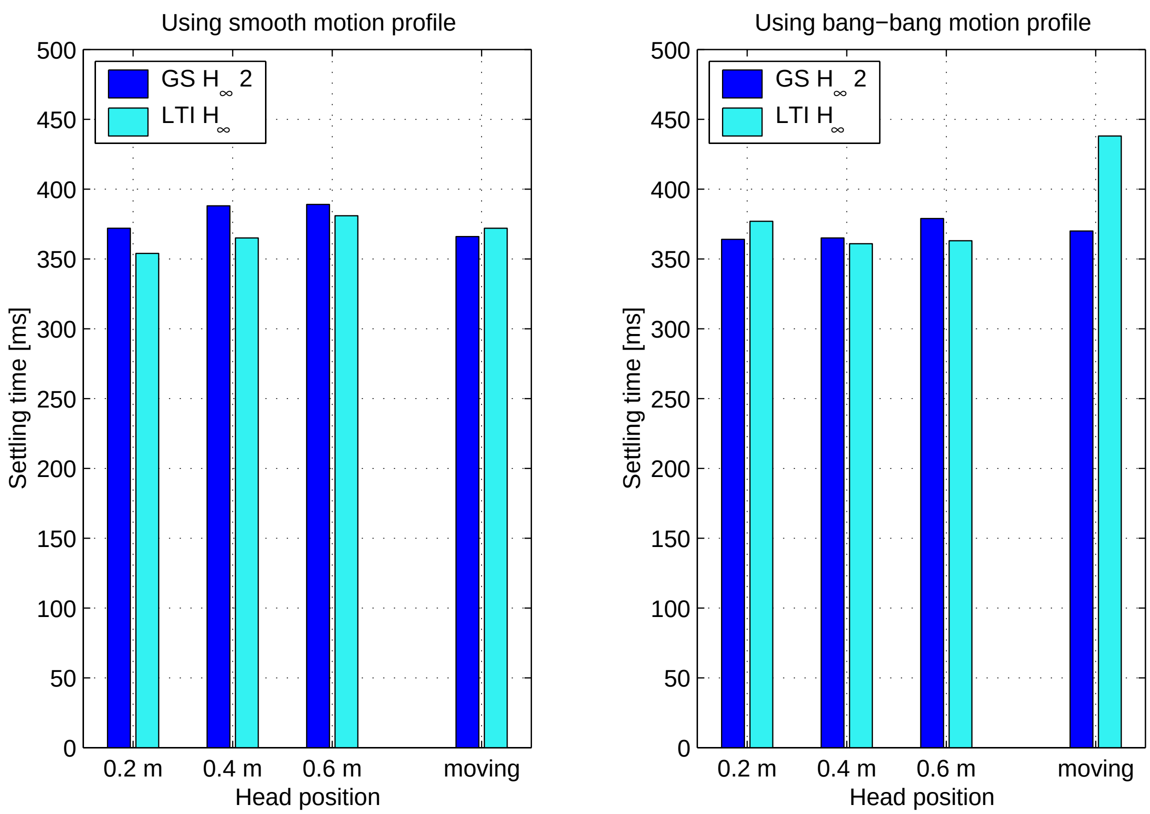

Figure 4.19: Comparison of settling times for 0.5 m motion, for different fixed head positions and moving head. The values are the worse number of joint or tip settling time each, taken from Tables 4.1 and 4.2.

Settling Times of Beam Motions of Varying Distance

According to the common tasks of the considered gantry robot, as described in Section 2.1, small movements of placement head and beam are of equal or greater importance to a 0.5 m motion. This encouraged an investigation of closed-loop performance for several beam motions from 10 mm to 0.5 m traveling distance. Reference commands for these motions are defined in Table 3.1. The head performs a simultaneous motion along the x-axis of equal length as the beam motion, starting from $x_{H,0} = 0.2$ m. For the 0.5 m beam motion, the head covers its full range of 0.4 m.

Settling times for smooth and bang-bang reference commands are summarized in Tables 4.3 and 4.4, respectively, for LTI H_∞ design and GS design 2. These numbers are visualized in Figure 4.20, where again the worse number of joint or tip settling time is shown. Both controllers exhibit nearly identical performance for smooth reference trajectories. In the bang-bang case, both controllers show severely degraded performance for small beam movements of 100 mm or below, compared to the application of a smooth reference command. An increase of 16 % to 97 % occurs in settling time, where the degradation is more severe for the GS H_∞ controller. For large beam movements (larger than 100 mm), only the LTI H_∞ controller degrades compared to smooth motion.

More importantly, Figure 4.20 gives suggestions about the favorable shape of commanded motion. One possible interpretation of the numbers would suggest that a smooth reference command is more appropriate at least for small movements. This is supported by the fact that, during experiments with small movements and bang-bang reference command, the beam joint motion was very jerky and noisy, unlike in the other cases with smooth reference command and/or large movements. It has to be remarked that the results reported in this chapter were obtained via controllers tuned for the 0.5 m beam motion on the experimental setup. Numbers may look (slightly) different if the tuning process was carried out with respect to small movements.

These observations are summarized in two conclusions. On the one hand, smooth reference commands may give significant advantages in settling time for the practically important case of small beam movements, even with a very stiff beam. On the other hand, the GS H_∞ design has virtually no disadvantages to the LTI H_∞ design, but may perform much better for large beam movements, especially when carried out with a very flexible beam. Again, this second statement comes from an “extrapolation” of results obtained with a very stiff beam to results obtainable with a more flexible one.

± 10 μm settling times [ms] for smooth beam/head motions						
Motion length [mm]	10		25		50	
Measurement	Joint	Tip	Joint	Tip	Joint	Tip
LTI H_∞	142	145	143	128	189	165
GS LPV H_∞ 2	143	144	153	130	196	198
Motion length [mm]	100		250		500	
Measurement	Joint	Tip	Joint	Tip	Joint	Tip
LTI H_∞	206	207	252	256	372	371
GS LPV H_∞ 2	209	208	252	254	363	366

Table 4.3: Settling times of joint and tip positions for beam motions of varying distance, with moving head each. The smooth motion profile is applied.

± 10 μm settling times [ms] for bang-bang beam/head motions						
Motion length [mm]	10		25		50	
Measurement	Joint	Tip	Joint	Tip	Joint	Tip
LTI H_∞	229	248	228	254	200	220
GS LPV H_∞ 2	285	285	282	301	222	238
Motion length [mm]	100		250		500	
Measurement	Joint	Tip	Joint	Tip	Joint	Tip
LTI H_∞	231	248	381	415	363	438
GS LPV H_∞ 2	245	231	231	231	365	370

Table 4.4: Settling times of joint and tip positions for beam motions of varying distance, with moving head each. The bang-bang motion profile is applied.

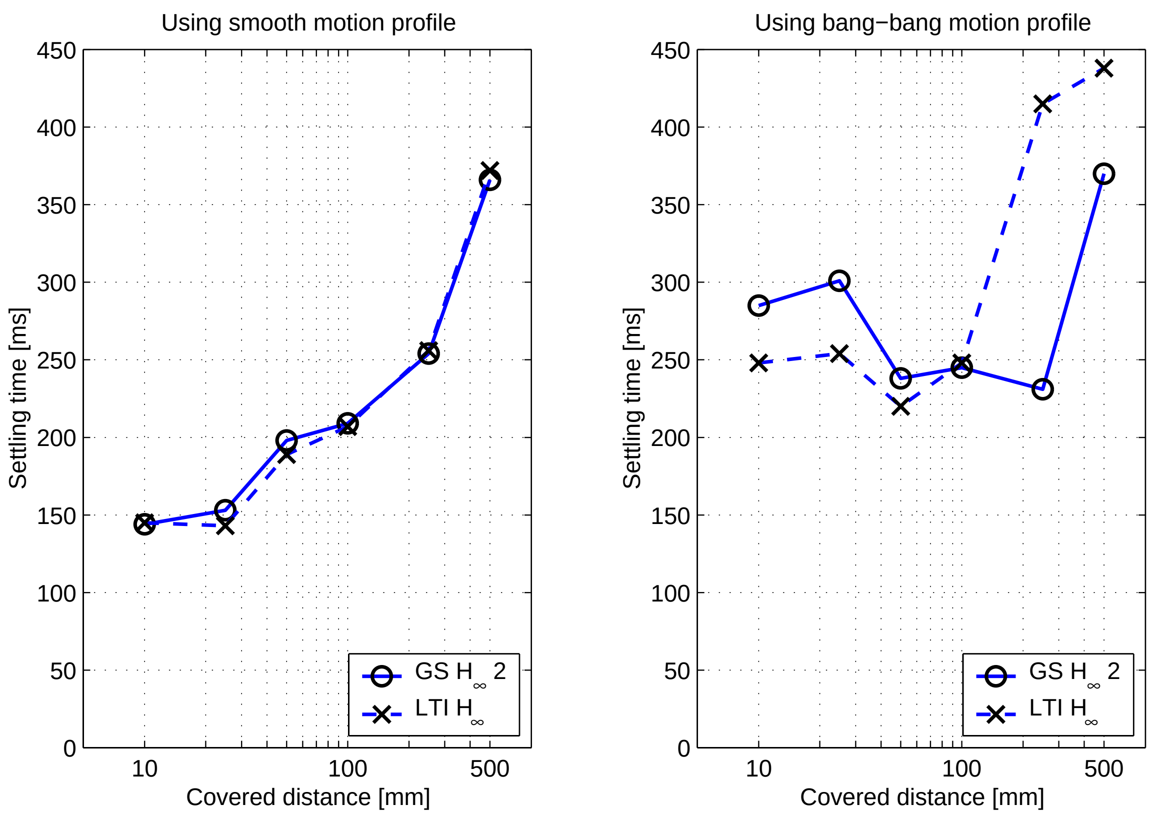

Figure 4.20: Comparison of settling times for beam motions of varying distance, with moving head each. The values are the worse number of joint or tip settling time each, taken from Tables 4.3 and 4.4.

Comparison with Previous Work

The previous considerations allow a judgement about favorable reference commands and appropriate control design methods, not only for the particular prototype gantry robot but also for a class of gantry robots with possibly more flexible beams.

A comparison with the previous work by Yang [45] can furthermore reveal the achievements of these experimental results. One difference to Yang's results is the decent performance and robust stability with respect to head position of the LTI H_∞ controller, even for the moving-head case. Comparing the GS H_∞ controllers, one can see from Table 4.2 that Yang's settling times are 3 % to 6 % smaller than the ones reported here, for the case of fixed head. In the practically more relevant moving-head case, performance is identical. However, the achievement of this work is that decent performance can now be obtained even for high head accelerations of up to 25 m/s^2, whereas in Yang's results controller performance degraded for head accelerations over 15 m/s^2. The major advantage of higher head acceleration is the possibility of placing the head into its ± 10 μm corridor with respect to x-axis *before* reaching the corridor with respect to y-axis. Only in that case does the much-debated y-axis settling time become important at all. From this perspective, the moving-head test results in Yang [45] may overstate the quality of the GS controller proposed there.

Chapter 5

Influence of Beam Design Modifications

The fast and accurate beam positioning is a difficult task because of two major problems. First, the long slender beam has a finite stiffness and is therefore subject to structure vibrations caused by strong accelerations and decelerations. Second, the beam dynamics have a nonlinear dependence on the placement head position and thus pose challenging demands to a high performance controller.

To cope with these problems, one usually designs a beam with very high stiffness. Such a beam basically behaves like a rigid body, and vibrations and dependence on head position can be neglected. In order to keep the beam cross section dimensions in a reasonable region, the beam mass will also be very high. The main drawback of this approach is the need to use very powerful motors for achieving a decent performance with respect to positioning time.

Another approach would be the restriction to a certain beam mass and accepting a possibly lower stiffness. Provided there is an appropriate control system design which can handle structure vibrations and changing beam dynamics, then the use of increased acceleration and velocity, and thus faster beam positioning, would be possible even when keeping the motor power constant. Conversely, less powerful motors could be used for achieving the same performance as for a massive beam. The potential of this idea, namely the interaction of control system design and beam design and their mutual benefits, is more closely investigated in this chapter. A treatment related to this topic can be found in Book and Majette [10].

5.1 Potential of Beam Mass Reduction

In this section, the subject under investigation is how beam mass reduction can potentially result in improved performance. The beam is viewed as a rigid body subject to a driving force, so the effects of vibrations and time-varying dynamics are neglected. For

$M_B/M_{B,0}$	M/M_0	a_{max} [m/s^2]	v_{max} [m/s]	T_s [ms]	$T_s/T_{s,0}$
100 %	100.0 %	24.0	2.8	305	100.0 %
75 %	90.8 %	26.0	2.9	293	96.1 %
60 %	85.3 %	27.0	3.0	287	94.1 %
50 %	81.6 %	28.0	3.1	282	92.5 %
40 %	77.9 %	29.5	3.1	276	90.5 %
30 %	74.2 %	30.0	3.2	270	88.5 %
20 %	70.6 %	32.0	3.2	266	87.2 %
10 %	66.9 %	33.0	3.3	261	85.6 %

Table 5.1: Ideal positioning times for reduced beam mass. $M_{B,0}$ and M_0 denote the nominal beam mass and nominal total moving mass, respectively. Acceleration rise time is set to t_r=0.01 s throughout. $T_{s,0}$ = 305 ms is the nominal positioning time.

such a rigid body, the best motion trajectory under certain restrictions is designed. This simplified investigation leads to an ideal bound on achievable performance for the flexible system.

The following assumptions are made: the rigid body with mass M performs a linear motion of distance 0.5 m. It is driven by a force F_y with the constraint $|F_y| \leq F_{y,max} =$ 890 N. No motor effects such as change of gear ratios are considered, but rather an ideal force source is assumed. The body is subject to mechanical friction with a viscous friction coefficient of F_v = 100 Ns/m and a Coulomb friction level of F_c = 50 N. The considered motion profile with limited jerk is shown in Figure 3.2 and can be defined by three parameters: acceleration rise time t_r, maximum acceleration a_{max} and maximum velocity v_{max}. These parameters have to be chosen such that the absolute value of the applied force, i.e. the force needed for acceleration and overcoming of friction, does not exceed the maximum force according to

$$|F_y(t)| = |Ma(t) + F_v v(t) + F_c \mathrm{sgn}(v(t))| \leq F_{y,max} \;. \tag{5.1}$$

As mentioned in Section 2.3, the beam of the prototype gantry robot, called nominal beam, has the mass $M_{B,0}$ = 8.72 kg. Only this mass is subject to reduction in the following. In contrast, the joint mass M_J = 7.41 kg and the head mass M_H = 7.57 kg are not changed. Thus, the total nominal moving mass is $M_0 = M_{B,0} + M_J + M_H =$ 23.7 kg. Positioning times are optimized via the motion profile Fig. 3.2, subject to the constraint (5.1), for different beam masses between 10 % and 100 % of $M_{B,0}$. The results are summarized in Table 5.1 as ± 10 μm positioning times. It can be seen that, by reducing beam mass, not only is material saved, but a considerable improvement of positioning time could be made as well. This is especially beneficial when many repeated motions have to be made.

Based on this observation, the main potential advantages of beam mass reduction are:

- Reduced positioning time (with same actuators)
- Use of smaller actuators (for same performance)
- Material and energy savings
- Increased safety due to lower inertia

The disadvantage however is a potential for higher excitation of bending vibrations due to reduced stiffness and higher acceleration. An appropriate control system design has to be invoked in order to deal with this problem.

5.2 Modification of Beam Design

Before dealing with appropriate control systems, some modifications of beam design from the prototype beam, as well as limitations thereof, are discussed. A "family" of beams with decreasing mass and rigidity is created, on which the further investigations are based.

The two determining factors in beam design for dynamic modeling are mass M_B and moment of inertia of the cross-sectional area I_z, see Section 2.2.1. Since it is the purpose of this study to investigate potential benefits of combining control system design and beam design, and not to design a "perfect" beam for this gantry robot, simplifying assumptions have been made such that design variations do not become too complex. The beam cross section is considered to be a hollow square with outer and inner widths b and b_i, respectively, as shown in Figure 5.1. Furthermore this cross section is assumed constant over the whole beam length. Design specialities such as asymmetric mass distribution, varying cross section, holes in the beam wall, or struts inside the beam or at the beam joint, are not considered. The beam length $l = 0.8$ m is kept constant, since the overall purpose of using the beam in a configuration as in the prototype setup is still valid.

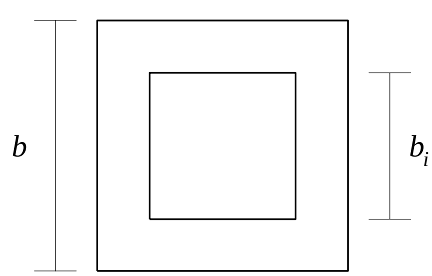

Figure 5.1: Hollow square beam cross section with outer width b and inner width b_i.

Beam Dimensions

The cross section area

$$A_{cs} = b^2 - b_i^2 \tag{5.2}$$

is in direct relation to the beam mass by

$$M_B = \varrho A_{cs} l = \varrho (b^2 - b_i^2) l \ , \tag{5.3}$$

where ϱ is the density of the beam material. The moment of inertia for a hollow square cross section is given by

$$I_z = I_y = \frac{1}{12}(b^4 - b_i^4) \ . \tag{5.4}$$

Nominal values for mass and moment of inertia are $M_{B,0} = 8.72$ kg and $I_{z,0} = 3.868 \cdot 10^{-7}$ m^4. The so-called stiffness of the beam increases in proportion to I_z.

The relationships for mass, cross section area and moment of inertia suggest the possibility of achieving arbitrary stiffness for any given mass, since b and b_i can be chosen independently. Large values for I_z are obtained by taking large values for b and b_i which are very close to each other. Arising problems in this case are of course the big dimension of the resulting cross section, but more importantly the effect of local buckling as with a tin can. To prevent this, a constraint

$$\frac{b_i}{b} < 0.9 \tag{5.5}$$

has been imposed. This constraint ensures a wall thickness $b - b_i$ of at least some millimeters in this application, and is chosen more intuitively rather than by rigorous calculations. With the constraints (5.3)–(5.5), valid values of b and b_i can be determined for a given beam mass M_B.

Beam Stresses

Due to the linear elastic behavior of the beam, certain limits for stiffness reduction have to be considered. In particular these are the maximum bending stress due to the bending moment and the maximum shear stress due to shearing forces or due to torsion. Of these only the bending stress imposed an important limitation to stiffness reduction and will be dealt with further on. A more detailed discussion is carried out in Appendix A.

The maximum stresses occur for bending in the horizontal plane, because accelerations of more than 30 m/s^2 can occur in beam movement, whereas in vertical direction only acceleration by gravity takes place. Hence, the following considerations are furthermore restricted to the horizontal plane. The maximum bending stress in the considered cross section is (Gere and Timoshenko [25])

$$\sigma_{max} = \frac{M_{b,max} c}{I_z} , \tag{5.6}$$

where $c = b/2$ denotes the maximum distance to the neutral axis and $M_{b,max}$ represents the maximum bending moment in z-direction. The bending moment in a cantilever beam of length l with distributed load per unit length $q(x,t)$ and concentrated load $F_H(t)$ at $x = x_H$ is (Pilkey [34])

$$M_b(x,t) = F_H(t)(x - x_H)h(x_H - x) - \frac{1}{2}q(x,t)(l^2 - 2lx + x^2) , \tag{5.7}$$

where $h(\cdot)$ represents the Heaviside step function defined as

$$h(\xi) := \begin{cases} 1 & \text{if } \xi > 0 \\ 0 & \text{if } \xi < 0 \end{cases} .$$

The distributed load $q(x,t) = M_B a(x,t)/l$ is imposed by the acceleration $a(x,t)$ in y-direction, the concentrated load $F_H(t) = M_H a(x_H,t)$ by the moving head with mass M_H and acceleration $a(x_H,t)$. The maximum bending moment occurs at $x = 0$ with the head being at $x = l$ under maximum acceleration a_{max}, and its absolute value follows from (5.7) as

$$M_{b,max} = M_H a_{max} l + \frac{1}{2} M_B a_{max} l .$$

With this result and (5.4), the maximum bending stress follows from (5.6) as

$$\sigma_{max} = \frac{3 a_{max} b l (2M_H + M_B)}{b^4 - b_i^4} . \tag{5.8}$$

In order to ensure validity of the linear elastic assumption, the maximum beam stress calculated by (5.8) has to be less than the so-called yield stress σ_y. Typical values of yield stress for steel are between 200 MPa and 700 MPa. Values of a_{max} are taken from Table 5.1.

Summary of Modified Beam Designs

A summary of the chosen values for cross section dimensions as well as of the calculated maximum bending stresses is given in Table 5.2. The beam with 10 % nominal mass is close to the yield stress limit of 200 MPa. Considering that the acceleration for small beam movements could even be about 30 % larger than the values considered here, which from (5.8) implies a proportional increase of the maximum stress, this 10 % beam doesn't fulfill the requirements from a strength of materials point of view.

$M_B/M_{B,0}$	$I_z/I_{z,0}$	b [cm]	b_i [cm]	b/b_i	a_{max} [m/s^2]	σ_{max} [MPa]
100 %	100.0 %	4.87	3.13	0.64	24	14.3
75 %	100.0 %	5.25	4.14	0.78	26	15.2
60 %	92.8 %	5.48	4.66	0.85	27	16.8
50 %	64.5 %	5.00	4.25	0.85	28	21.9
40 %	52.3 %	4.96	4.37	0.88	29	26.4
30 %	35.6 %	4.68	4.21	0.90	30	36.1
20 %	15.8 %	3.82	3.44	0.90	32	67.9
10 %	4.0 %	2.70	2.43	0.90	33	187.3

Table 5.2: Modified beam designs. For each considered beam mass M_B, the values for moment of inertia I_z, cross section dimensions b and b_i, maximum acceleration a_{max} and maximum bending stress σ_{max} are shown.

But up to 80 % mass reduction is feasible in this simplified framework. Note that the ratio b_i/b is smaller than 0.9 for beams with relatively large mass, and therefore the moment of inertia I_z is smaller than it could be with $b_i/b = 0.9$. Small values for I_z were chosen by intention, since the study should reveal the benefits and limitations of compensating for increased structural vibrations by control technology.

5.3 Performance for Modified Beams

For each of the valid hypothetical beams designed in the previous section, a gain-scheduled H_∞ controller has been created according to GS design 2 presented in Section 4.2, and has been tuned for desired behavior. Simulations of the closed loop were carried out using a detailed model with five flexible bending modes in addition to the rigid mode, see (2.22). Viscous and Coulomb friction were modeled according to (2.16). The 0.5 m motion trajectories computed in Section 5.1 were used as reference commands to the controller. A simultaneous head motion with maximum velocity of 3 m/s, maximum acceleration of 30 m/s^2 and acceleration rise time of 0.01 s was commanded.

Figure 5.2 shows the achievable ± 10 μm settling times for the family of beams with different mass and flexibility defined in the previous section. Settling times improve until $M_B = 50$ % of $M_{B,0}$. The time to be gained corresponds roughly to the time that can be gained because of choosing a reference trajectory with lower positioning time. This means that actually a good job of vibration suppression is done for these cases. But higher vibration excitation occurs for low mass/low stiffness beams. The flexibility in these cases is so large that the controller cannot compensate for it. Therefore settling times increase for beams with M_B below 50 % of $M_{B,0}$.

So an optimal trade-off between mass reduction and settling time can be found

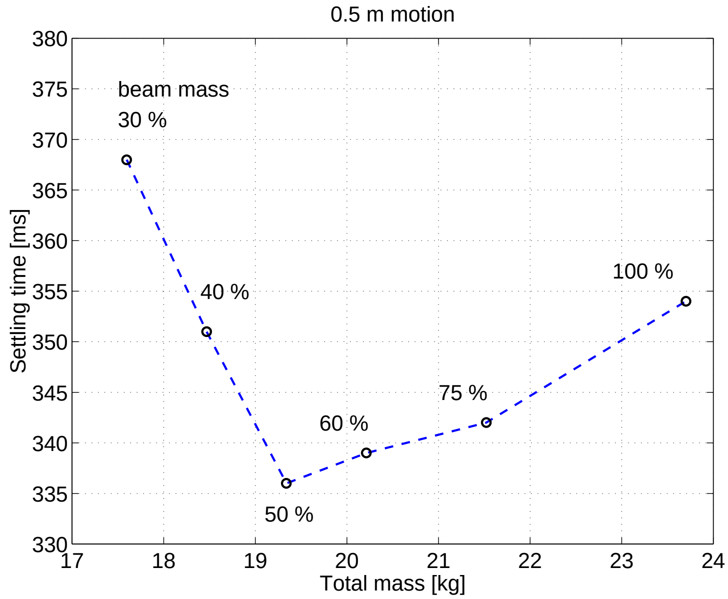

Figure 5.2: Achievable ± 10 μm head settling times for design study. A beam motion of 0.5 m and a simultaneous head motion of 0.4 m are commanded.

at around 50 % beam mass compared to the nominal beam. This result provides valuable insight for improvement of the nominal beam design. A more detailed study for many different but reasonable combinations of beam mass and moment of inertia could further refine the achievable minimum settling time. An incorporation of tip sensor feedback as in GS design 3 might further improve positioning times for beams with low stiffness, and show more significant advantages over GS design 2 than in the nominal case.

As an example, simulation results for the case $M_B = 0.5 \cdot M_{B,0}$ are presented. The beam position response, with fixed head at different head positions, is shown in Figure 5.3, along with head position errors with respect to y-position and corresponding applied forces. Note the practically zero steady-state error and quite uniform convergence to the ± 10 μm corridor regardless of head position. The beam position errors with respect to the y-coordinate for joint, head and tip, with moving head from x_H=0.2 m to x_H=0.6 m, are shown in Figure 5.4, as well as the corresponding applied force. The maximum head acceleration was 30 m/s^2, the maximum head velocity 3 m/s. Again we have practically zero steady-state error. Also one can see good suppression of structural vibration, since the curves for joint, head and tip enter the ± 10 μm corridor within about 10 ms of each other, even for this beam with relatively low stiffness and for a relatively aggressive position command. Note the increased controller activity due to head acceleration, deceleration and stopping.

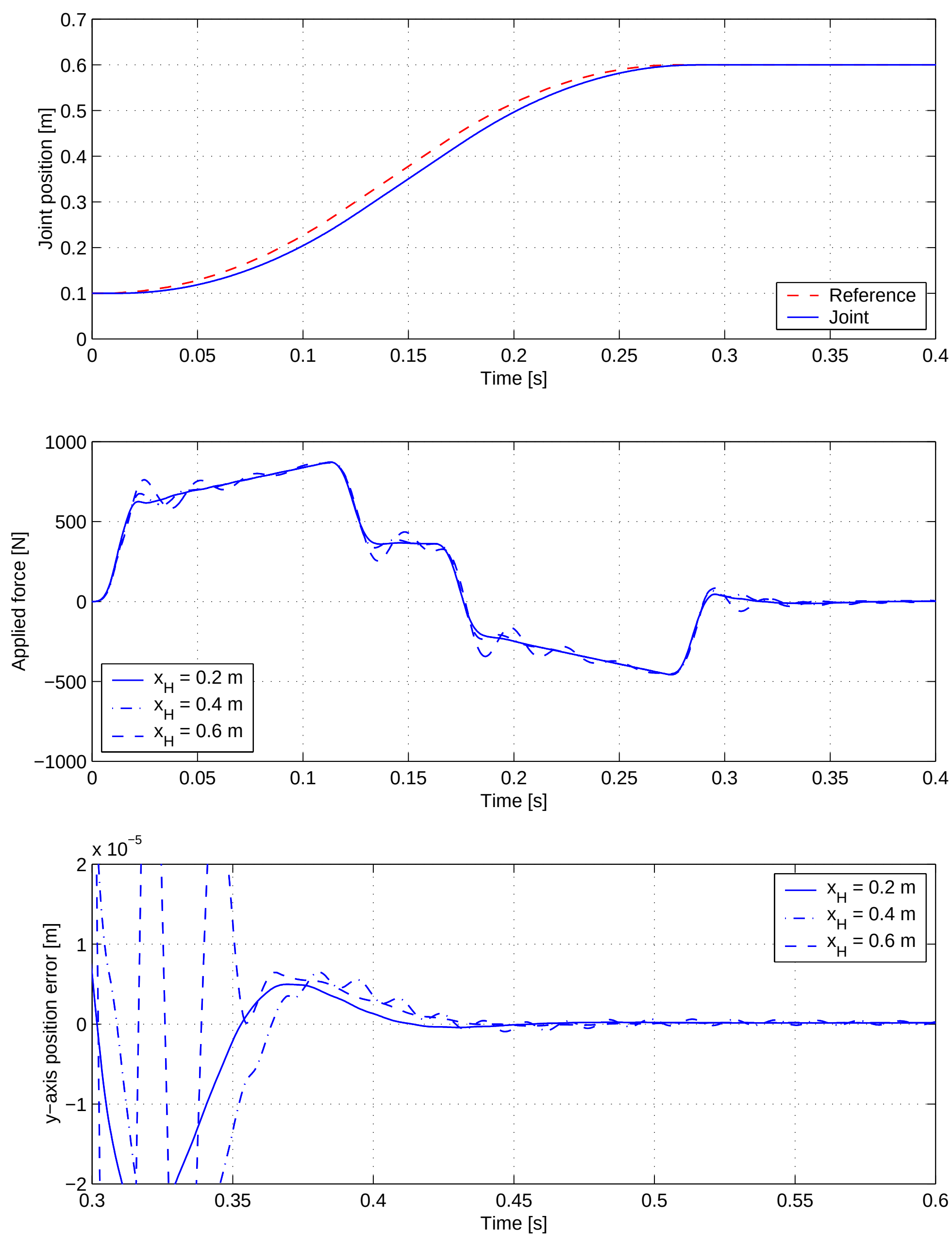

Figure 5.3: Simulation results of closed-loop response for 0.5 m motion of 50 % mass beam, with fixed head.

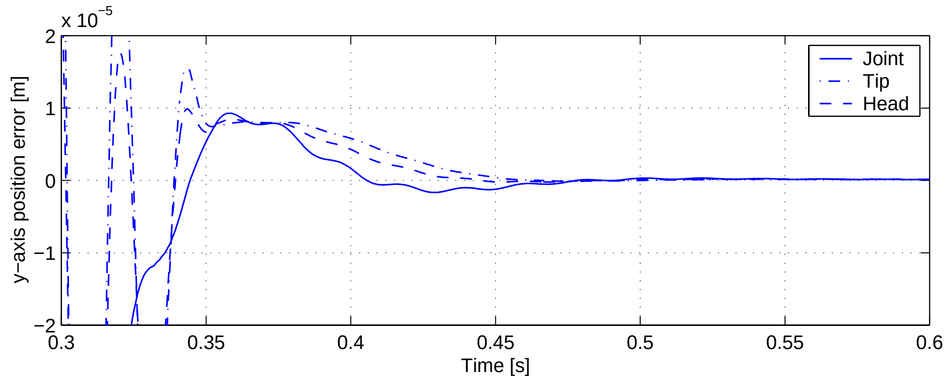

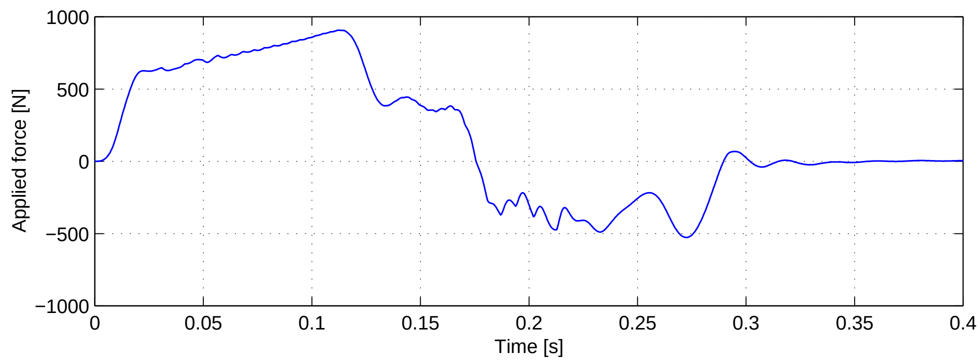

Figure 5.4: Simulation results of closed-loop response for 0.5 m motion of 50 % mass beam, with moving head from x_H=0.2 $\rightarrow$ 0.6 m.

Conclusion of Simulation Study

As shown by this simulation study, the combination of control system design and mechanical design can have valuable benefits. Instead of giving a ready-made part to the control engineer with the desire for a good controller, iterations can take place to improve, in this case, the mechanical design and raise overall performance. If advanced control technology is available and applicable, the controlled components may be designed in a more simple, cost-saving and performance enhancing way .

Chapter 6

Conclusions

Contributions of this Thesis

This thesis has addressed motion control of a class of two-axis belt-drive gantry robots exhibiting flexible and compliant behavior. This industry-motivated project poses high-level requirements on accuracy and speed. These criteria formed the basis for performance evaluation and can be translated into expectations on uniformity and numerical value of ± 10 μm beam joint and beam tip settling times.

Based on a flexible beam model, L_2-gain based control design methods were utilized to develop motion controllers. In doing so, a two-loop control structure with an inner loop for compensation of transmission compliance, and an outer loop for motion control, was employed. The controller performance was determined through experiments on a prototype gantry robot. Effects of "smooth" as well as vibration exciting, more "aggressive" motion reference commands were investigated. The beam was commanded with accelerations of up to 32 m/s^2 and velocities of up to 2.4 m/s. The maximum head accelerations and velocities were 25 m/s^2 and 2.5 m/s, respectively.

A single linear time-invariant H_∞ controller showed robust stability and excellent performance for smooth motions, with fixed or moving placement head. For the particular prototype gantry robot, a settling time of 372 ms for a 0.5 m motion could be achieved in the practically relevant case of moving head. Structural vibrations of the beam and disturbances due to mechanical friction were largely attenuated. However, for a more aggressive reference command with bang-bang-like acceleration, bending vibrations occurred and degraded the performance to 438 ms. With the use of advanced gain-scheduling H_∞ techniques, which incorporate the change of beam dynamics explicitly by scheduling on the head position, uniformly good performance could be achieved for different head positions and moving head. In the moving-head case, a settling time of 366 ms was obtained for a smooth 0.5 m motion, which degraded minimally to 370 ms for the aggressive reference command. Furthermore, controller performance was measured for beam movements of different length, ranging from 10 mm to 0.5 m. It was observed that, for smooth reference commands, both linear-time invariant and gain-scheduled controllers perform equally well on this particular gantry robot with its quite stiff beam. However, experiments with more aggressive motion commands imply a degradation of the linear-time invariant H_∞ controller performance. Bang-bang reference commands should not be applied for motions of only several millimeters due to resulting jerky beam motion.

An investigation on the trade-off between settling times and beam mass showed that performance of the prototype gantry robot may be increased by design modifications of the beam. A re-design of the beam, yielding reduced mass and therefore possibly reduced stiffness, would be necessary. It is believed that an appropriate control system design, incorporating head position variations and variation rates as well as the flexible nature of the beam, needs to be applied for motion control of such a re-engineered beam.

In order to speed up online computations of the gain-scheduled control algorithm, modifications to the existing procedures were proposed, using piecewise linear approximation of nonlinear functions and two-dimensional interpolation.

Suggestions for Future Research

In the course of this research, various opportunities for future investigation have become apparent. The first category of open problems comprises details of the currently achieved solutions. The closed-loop positioning performance still exhibits some sensitivity to belt tension of the belt-drive transmission, although an inner-loop compensation is applied. To add performance robustness to the compensation poses a highly challenging problem by itself. Another major impact on positioning performance is given by viscous and Coulomb friction during motion. In this thesis, friction was treated as an unknown disturbance. More direct approaches for rejecting friction effects deal with disturbance observers as in Kempf and Kobayashi [30], or with model-based friction compensation, see Armstrong-Helouvry et al. [6], Canudas de Wit et al. [13]. It would also be very interesting to use head-mounted accelerometer feedback to augment the controller with direct vibration sensing. Furthermore, an investigation into approximation qualities of different controller discretization schemes, especially for lower sampling rates, may reveal further implementability aspects of the proposed control algorithms.

A second category of worthwhile investigations to be done include modified or new approaches to control system design. The application of gain-scheduled controllers has shown many promising aspects in this research, especially when beams of low stiffness and/or aggressive motion profiles are to be considered. An extension in this direction could be made with different LMI schemes, as in Dussy and El Ghaoui [18], Scorletti and El Ghaoui [41]. A completely new approach would be the application of nonlinear H_∞ theory, perhaps even as an integrated design of beam and head motion control. Basic literature on this subject includes van der Schaft [38], Ball et al. [7], Isidori and Astolfi [27]. A point for improvement certainly is the relatively large position error during motion. In Taylor and Li [43], stable inversions of the beam model are described. In combination with methods for disturbance attenuation and for robustness considerations, these stable inverse models could be used for an approach to approximating perfect tracking of the (filtered) reference command.

The generation of suitable reference commands for beam and head motion also is a task of its own. Its success depends on proper understanding of the underlying system dynamics, unmodeled effects, actuator limits, and controller capabilities. Therefore, command shaping is a difficult problem which needs to be carried out consistently with controller design. It is believed that performance can still be enhanced by investigation on this subject. Some basic references were given in Section 3.6.

Finally, a last category of possible future research directions comprises new concepts on gantry robot design. Obvious alternatives to belt-drive systems are linear direct-drive systems. They may reduce the friction influence, improve accuracy, and increase possible motion speed. The re-design of the beam, as roughly sketched in Chapter 5, may also contribute to performance enhancement. It still has to be shown experimentally, perhaps with a new prototype beam, that available control technology can compensate for increased structural vibrations of beams with lower stiffness.

Appendix A

Further Investigations on Beam Stresses

In this appendix, a more thorough discussion on stresses in the gantry robot beam is given, in addition to Section 5.2. In particular it is shown that shear stresses due to shear forces and torsion do not impose important limits on the choice of cross section dimensions and moment of inertia for this application. They can therefore be neglected compared to the stress caused by the bending moment.

Shear Stress due to Shear Force

First, the shear stress due to shear forces is derived. Here shear forces caused by bending in the horizontal plane are considered. Bending in the vertical plane can be neglected because loads caused by gravity are much smaller than the loads caused by beam acceleration in the horizontal plane. The maximum shear stress in the considered cross section is (Gere and Timoshenko [25])

$$\tau_{max} = \frac{V_{b,max} Q}{I_z b} \;, \tag{A.1}$$

where Q denotes the first moment of the cross sectional area on one side of the neutral axis, and $V_{b,max}$ represents the maximum shear force due to bending. The first moment Q can be obtained by

$$Q = \int_0^{b/2} y \, dA_1 - \int_0^{b_i/2} y \, dA_2 = \int_0^{b/2} yb \, dy - \int_0^{b_i/2} yb_i \, dy = \frac{1}{8}(b^3 - b_i^3) \;. \tag{A.2}$$

The maximum shear force in a cantilever beam of length l with distributed load per unit length $q(x,t)$ and concentrated load $F_H(t)$ at $x = x_H$ occurs at $x = 0$. Its absolute value is (Pilkey [34])

$$V_{b,max} = q_{max} l + F_{H,max} \;,$$

where $q_{max} = M_B a_{max}/l$ and $F_{H,max} = M_H a_{max}$ are imposed by beam mass M_B, head mass M_H and maximum acceleration a_{max}. This leads to the following relation for maximum shear force:

$$V_{b,max} = (M_B + M_H)a_{max} \ . \tag{A.3}$$

Thus the maximum shear stress follows from (A.1) together with (5.4), (A.2) and (A.3) as

$$\tau_{max} = \frac{3a_{max}(M_H + M_B)(b^3 - b_i^3)}{2b(b^4 - b_i^4)} \ . \tag{A.4}$$

In order to ensure validity of the linear elastic assumption, the maximum shear stress calculated by (A.4) has to be less than half the yield stress σ_y. In this application τ_{max} should be less than 100 MPa. Maximum shear stress values computed from (A.4) are given in Table A.1 in the column $\tau_{max,1}$.

Shear Stress due to Torsion

Another source for shear stress is torsion, caused by the alignment of the placement head. The z-coordinate of the head center of gravity has a distance to the beam neutral axis of $z_H = -0.058$ m. Therefore a maximum torque or twisting moment with absolute value

$$M_{t,max} = |F_{H,max} z_H| = M_H a_{max} |z_H| \tag{A.5}$$

acts on the beam in x-direction. From this, the maximum shear stress due to torsion could be obtained. However, for a non-circular cross section, the torsional stress analysis is usually done numerically, since no appropriate formulas are available for this case. Hence, an estimation of torsional stress is carried out here using the theory of thin-walled tubes, see Gere and Timoshenko [25]. For some of the considered cross sections the assumption of a thin wall may not be completely justified, but will nevertheless give a rough approximation in order to see expected magnitudes of shear stress. For a thin-walled tube with wall thickness t and area A_m enclosed by the median line, the maximum shear stress is given by

$$\tau_{max} = \frac{M_{t,max}}{2tA_m} \ . \tag{A.6}$$

In the case of a hollow square cross section with median width $b_m = (b + b_i)/2$, one obtains $t = b - b_i$ and $A_m = b_m^2 = (b + b_i)^2/4$. Thus, together with (A.5) the maximum shear stress becomes

$$\tau_{max} = \frac{2M_H a_{max} |z_H|}{(b - b_i)(b + b_i)^2} \ . \tag{A.7}$$

As in the previous paragraph, the maximum shear stress calculated by (A.7) has to be less than 100 MPa. Maximum shear stress values computed from (A.7) are given in Table A.1 in the column $\tau_{max,2}$.

$M_B/M_{B,0}$	$I_z/I_{z,0}$	b [cm]	b_i [cm]	b/b_i	a_{max} [m/s^2]	σ_{max} [MPa]	$\tau_{max,1}$ [MPa]	$\tau_{max,2}$ [MPa]
100 %	100.0 %	4.87	3.13	0.64	24	14.3	0.219	0.189
75 %	100.0 %	5.25	4.14	0.78	26	15.2	0.167	0.233
60 %	92.8 %	5.48	4.66	0.85	27	16.8	0.140	0.281
50 %	64.5 %	5.00	4.25	0.85	28	21.9	0.162	0.383
40 %	52.3 %	4.96	4.37	0.88	29	26.4	0.155	0.496
30 %	35.6 %	4.68	4.21	0.90	30	36.1	0.165	0.709
20 %	15.8 %	3.82	3.44	0.90	32	67.9	0.242	1.403
10 %	4.0 %	2.70	2.43	0.90	33	187.3	0.452	4.079

Table A.1: Modified beam designs, extended. For each considered beam mass M_B, the values for moment of inertia I_z, cross section dimensions b and b_i, maximum acceleration a_{max}, maximum bending stress σ_{max}, maximum shear stress due to shear force $\tau_{max,1}$ and maximum shear stress due to torsion $\tau_{max,2}$ are shown.

Summary

A summary of the chosen values for cross section dimensions as well as maximum bending and shear stresses is given in Table A.1, an augmented version of Table 5.2. It is clear that values for shear stress are far from their limit of 100 MPa. In contrast, the bending stress values get close to their limit of 200 MPa in the considered cases.

Bibliography

[1] P. Apkarian, "On the discretization of LMI-synthesized linear parameter-varying controllers," *Automatica*, vol. 33, no. 4, pp. 655–661, 1997.

[2] P. Apkarian and R. J. Adams, "Advanced gain-scheduling techniques for uncertain systems," *IEEE Transactions on Control Systems Technology*, vol. 6, no. 1, pp. 21–32, 1998.

[3] P. Apkarian and P. Gahinet, "A convex characterization of gain-scheduled H_∞ controllers," *IEEE Transactions on Automatic Control*, vol. 40, no. 5, pp. 853–864, 1995.

[4] P. Apkarian, P. Gahinet and G. Becker, "Self-scheduled H_∞ control of linear parameter-varying systems: a design example," *Automatica*, vol. 31, no. 9, pp. 1251–1261, 1995.

[5] P. Apkarian and H. D. Tuan, "Parametrized LMIs in control theory," *SIAM Journal on Control and Optimization*, vol. 38, no. 4, pp. 1241–1264, 2000.

[6] B. Armstrong-Helouvry, P. DuPont and C. Canudas de Wit, "A survey of models, analysis tools and compensation methods for the control of machines with friction," *Automatica*, vol. 30, no. 7, pp. 1083–1138, 1994.

[7] J. A. Ball, J. W. Helton and M. L. Walker, "H_∞ control for nonlinear systems with output feedback," *IEEE Transactions on Automatic Control*, vol. 38, no. 4, pp. 546–559, 1993.

[8] G. Becker and A. Packard, "Robust performance of linear parametrically varying systems using parametrically dependent linear feedback," *Systems and Control Letters*, vol. 23, no. 3, pp. 205–215, 1994.

[9] W. J. Book, D. P. Magee and S. Rhim, "Time-delay command shaping filters: robust and/or adaptive," *Journal of the Robotics Society of Japan*, vol. 17, no. 6, pp. 761–769, 1999.

[10] W. J. Book and M. Majette, "Controller design for flexible distributed parameter mechanical arms via combined state space and frequency domain techniques," *ASME Journal of Dynamic Systems, Measurement and Control*, vol. 105, no. 4, pp. 245–254, 1983.

[11] S. Boyd, L. El Ghaoui, E. Feron and V. Balakrishnan, *Linear Matrix Inequalities in System and Control Theory*. Philadelphia, PA: SIAM, 1994.

[12] R. H. Brown, S. C. Schneider and M. G. Mulligan, "Analysis of algorithms for velocity estimation from discrete position versus time data," *IEEE Transactions on Industrial Electronics*, vol. 39, no. 1, pp. 11–19, 1992.

[13] C. Canudas de Wit, H. Olsson, K. J. Astrom and P. Lischinsky, "A new model for control of systems with friction," *IEEE Transactions on Automatic Control*, vol. 40, no. 3, pp. 419–425, 1995.

[14] M. Chilali and P. Gahinet, "H_∞ design with pole placement constraints: an LMI approach," *IEEE Transactions on Automatic Control*, vol. 41, no. 3, pp. 358–367, 1996.

[15] B. G. Dijkstra, N. J. Rambaratsingh, C. Scherer, O. H. Bosgra, M. Steinbuch and S. Kerssemakers, "Input design for optimal discrete time point-to-point motion of an industrial XY-positioning table," *Proceedings of the 39th IEEE Conference on Decision and Control*, Sydney, Australia, pp. 901–906, December 2000.

[16] J. C. Doyle, B. A. Francis and A. R. Tannenbaum, *Feedback Control Theory*. New York, NY: Macmillan, 1992.

[17] J. C. Doyle, K. Glover, P. P. Khargonekar and B. A. Francis, "State-space solutions to standard H_2 and H_∞ control problems," *IEEE Transactions on Automatic Control*, vol. 34, no. 8, pp. 831–847, 1989.

[18] S. Dussy and L. El Ghaoui, "Measurement-scheduled control for the RTAC problem: an LMI approach," *International Journal of Robust and Nonlinear Control*, vol. 8, no. 4–5, pp. 377–400, 1998.

[19] E. Feron, P. Apkarian and P. Gahinet, "Analysis and synthesis of robust control systems via parameter-dependent Lyapunov functions," *IEEE Transactions on Automatic Control*, vol. 41, no. 7, pp. 1041–1046, 1996.

[20] G. F. Franklin, J. D. Powell and M. Workman, *Feedback Control of Dynamic Systems*, Third Edition. Menlo Park, CA: Addison-Wesley, 1997.

[21] P. Gahinet, "Explicit controller formulas for LMI-based H_∞ synthesis," *Automatica*, vol. 32, no. 7, pp. 1007–1014, 1996.

[22] P. Gahinet and P. Apkarian, "A linear matrix inequality approach to H_∞ control," *International Journal on Robust and Nonlinear Control*, vol. 4, no. 4, pp. 421–448, 1994.

[23] P. Gahinet, P. Apkarian and M. Chilali, "Affine parameter-dependent Lyapunov functions and real parametric uncertainty," *IEEE Transactions on Automatic Control*, vol. 41, no. 3, pp. 436–442, 1996.

[24] P. Gahinet, A. Nemirovski, A. J. Laub and M. Chilali, *LMI Control Toolbox User's Guide*. Natick, MA: The MathWorks Inc., 1995.

[25] J. M. Gere and S. P. Timoshenko, *Mechanics of Materials*, Fourth Edition. Boston, MA: PWS Publishing Company, 1997.

[26] A. Helmersson, *Methods for robust gain-scheduling*, PhD. Thesis, Linköping University, Linköping, Sweden, November 1995.

[27] A. Isidori and A. Astolfi, "Disturbance attenuation and H_∞ control via measurement feedback in nonlinear systems," *IEEE Transactions on Automatic Control*, vol. 37, no. 9, pp. 1283–1293, 1992.

[28] T. Iwasaki and R. E. Skelton, "All controllers for the general H_∞ control problem: LMI existence conditions and state-space formulas," *Automatica*, vol. 30, no. 8, pp. 1307–1317, 1994.

[29] H. Kajiwara, P. Apkarian and P. Gahinet, "LPV techniques for control of an inverted pendulum," *IEEE Control Systems Magazine*, vol. 19, no. 1, pp. 44–54, 1999.

[30] C. J. Kempf and S. Kobayashi, "Disturbance observer and feedforward design for a high-speed direct-drive positioning table," *IEEE Transactions on Control Systems Technology*, vol. 7, no. 5, pp. 513–526, 1999.

[31] H. K. Khalil, *Nonlinear Systems*, Second Edition. Upper Saddle River, NJ: Prentice Hall, 1996.

[32] P. H. Meckl and W. P. Seering, "Experimental evaluation of shaped inputs to reduce vibration for a Cartesian robot," *ASME Journal of Dynamic Systems, Measurement and Control*, vol. 112, no. 2, pp. 159–165, 1990.

[33] Y. Nesterov and A. Nemirovski, *Interior Point Polynomial Methods in Convex Programming: Theory and Applications*. Philadelphia, PA: SIAM, 1994.

[34] W. D. Pilkey, *Formulas for Stress, Strain, and Structural Matrices*. New York, NY: Wiley & Sons, 1994.

[35] A. Rehm and F. Allgöwer, “Self-scheduled H_∞ output feedback control of descriptor systems,” *Computers and Chemical Engineering*, vol. 24, no. 2–7, pp. 279–284, 2000.

[36] J. M. Rieber and D. G. Taylor, “Combined control and design of a flexible parameter-varying robot link,” *Proceedings of the 8th International Conference on Advances in Communications and Control*, Rethymnon, Greece, to appear September 2001.

[37] J. M. Rieber and D. G. Taylor, “Gain-scheduled L_2-gain based control of a flexible parameter-varying robot link,” *Proceedings of the 27th Annual Conference of the IEEE Industrial Electronics Society*, Denver, Colorado, to appear December 2001.

[38] A. J. van der Schaft, “L_2-gain analysis of nonlinear systems and nonlinear state-feedback H_∞ control,” *IEEE Transactions on Automatic Control*, vol. 37, no. 6, pp. 770-784, 1992.

[39] C. W. Scherer, “Mixed H_2/H_∞ control for linear parametrically varying systems,” *Proceedings of the 34th IEEE Conference on Decision & Control*, New Orleans, Louisiana, pp. 3182–3187, December 1995.

[40] C. Scherer, P. Gahinet and M. Chilali, “Multiobjective output-feedback control via LMI optimization,” *IEEE Transactions on Automatic Control*, vol. 42, no. 7, pp. 896–911, 1997.

[41] G. Scorletti and L. El Ghaoui, “Improved LMI conditions for gain scheduling and related control problems,” *International Journal of Robust and Nonlinear Control*, vol. 8, no. 10, pp. 845–877, 1998.

[42] N. C. Singer and W. P. Seering, “Preshaping command inputs to reduce system vibration,” *ASME Journal of Dynamic Systems, Measurement and Control*, vol. 112, no. 1, pp. 76–82, 1990.

[43] D. G. Taylor and S. Li, “Feedforward compensation for gantry robots with structural flexibility,” *Proceedings of the 7th Mechatronics Forum International Conference*, Atlanta, Georgia, September 2000 (on CD-ROM).

[44] F. Wu, X. H. Yang, A. Packard and G. Becker, “Induced L_2-norm control for LPV system with bounded parameter variation rates,” *Proceedings of the 1995 American Control Conference*, Seattle, Washington, pp. 2379–2383, June 1995.

[45] X. Yang, *Modeling and control of two-axis belt-drive gantry robots*, PhD. Thesis, Georgia Institute of Technology, Atlanta, Georgia, November 2000.

[46] X. Yang and D. G. Taylor, "H_∞ control design for positioning performance of gantry robots," *Proceedings of the 2000 American Control Conference*, Chicago, Illinois, pp. 3038–3042, June 2000.

[47] X. Yang and D. G. Taylor, "Reduced-order model matching control design for gantry robots," *Proceedings of the 8th IEEE Mediterranean Conference on Control and Automation*, Patras, Greece, July 2000 (on CD-ROM).

[48] X. Yang and D. G. Taylor, "Design of gain-scheduled H_∞ controllers for gantry robots," *Proceedings of the 7th Mechatronics Forum International Conference*, Atlanta, Georgia, September 2000 (on CD-ROM).

[49] X. Yang, D. G. Taylor, N. Nahm and M. Lauzi, "Simulation models for gantry subsystems of SMT placement machines," *Proceedings of the 3rd International Symposium on Advanced Electromechanical Motion Systems*, Patras, Greece, pp. 971–976, July 1999.

[50] K. Zhou, J. C. Doyle and K. Glover, *Robust and Optimal Control*. Englewood Cliffs, NJ: Prentice Hall, 1996.

[51] K. Zhou and P. P. Khargonekar, "An algebraic Riccati equation approach to H_∞ optimization," *Systems and Control Letters*, vol. 11, no. 2, pp. 85–91, 1988.